Politecnico di Torino · Facoltà di Ingegneria

Development of Intentional Mistuning Technologies applied to Aircraft Engines' Turbines Rotors aiming at Reducing Aeromechanical Instabilities

A Major Qualifying Project Report
Submitted to the Faculty
of the
POLITECNICO DI TORINO
in partial fulfilment of the requirements for the
Degree of Master of Science in
Mechanical Engineering

Tutor:
Prof.Christian Maria Firrone
Prof.ssa Daniela Misul
Ing. Marco Moletta

Candidate:
Gianluca Mosiello

A.A. 2017 - 2018

Some men see things as they are, and ask why.
I dream of things that never were, and ask why not.
Robert Francis Kennedy

Dedicated to my whole family
Dedicated to Matteo

Abstract

The trend to an increasingly globalized world, together with the continuous development of new technologies, is rapidly allowing the aviation market to grow at unprecedented rates in its whole history. The high demand coming from passengers leads to a high demand of new aircrafts, capable of improving comfort and, most importantly, cut down the environmental impact of air travel. The innovative projects the two leading manufacturers, Boeing and Airbus, are working on are perfectly inserted in the mainframe of a shifting aviation model, from hub-and-spoke to point-to-point. The future airliners require next generation engines to achieve these ambitious goals, and General Electric is investing great resources in developing new machines that feature all the great technology achievements in recent aviation history and allow a strong decrease in both fuel burn and polluting emissions. The performance improvements come from the optimization of key engine components from different engineering points of view. Low Pressure Turbines are crucial modules in the overall architecture and play a fundamental role in the overall performance. If considering the series of improvements turbine rotors are due to get, aeromechanical stabilization is among the top priorities. The need of decreasing the overall system mass leads to critical engineering issues. When dealing with the optimization of turbine blades, flutter instabilities are among the top priorities to work on. Flutter stabilization not only allows the reduction of dangerous vibration phenomena, that may lead to anticipated structural failures, but also allows a more efficient gas-flow throughout the module. The work herein presented, carried out in collaboration with Avio Aero, a GE Aviation business, deals with the concept development of aeromechanically stable turbine rotors through “Mistuning”, a technology characterized by mass alternated patterns in the blades row. Despite the mistuning technology flutter stabilizing effect is widely covered by state-of-the-art studies, the aim of this project is attempting the introduction of mistuning in aviation engines modules with the development of little-mass asymmetries within Low Pressure Turbines. The target of verifying the flutter stabilizing effects in an aircraft engine is accompanied by a look at the various issues in the product life-cycle this technology introduction may involve.

Contents

List of Figures

List of Tables

Chapter 1

The G2020 Project

1.1 A Greener Commercial Aviation

This report takes full part of a big project named after as G2020, which stands for GReen Engine for Air Traffic control 2020 [39] [10]. Several big and medium sized engineering companies take part in the project, and they all share the characteristic of being Piemonte-based. Moreover, several public institutions take part in the project, including Regione Piemonte and Politecnico di Torino.
The project was born in 2009, following the indications coming from European Commission and ACARe(Advisory Council for Aviation Research and Innovation in Europe), that suggested a drastic reduction of aviation engines' polluting emissions and the provision of a more efficient service to the final aviation customer: the passenger. With this basics, the G2020 projects aims at drastically reducing polluting emissions and acoustic radiation by the year 2020. More in details, the ultimate goal is providing new engine technology being able of providing a greener commercial aviation, with respect to year 2000 [39]

- Reduction by 50 % of all CO_2 emissions
- Reduction by 80 % of all NO_x emissions
- Redcution by 10 dB of the engine's acoustic emissions

Despite the ambitious target, the project has been able to attract various entities, ranging from public institutions, to advanced research laboratories, to medium and big sized companies. The leading role of the project is certainly covered by Avio Aero (a GE Aviation Business) that has played a crucial part in the development of cutting edge technology in the aviation market in the past decades. The reach of these ambitious targets is only possible by a deep analysis of each engine component from an aerothermal and dynamic point of view, with the aim of reducing, or even eliminating, all sources of energy waste or assembly instabilities.

1.2 GreatLAB and TAL

Avio Aero, which is now fully part of the General Electric Conglomerate, has been investing substantial human and financial resources in the project, allowing the creation of various research poles, that are leading the way in the definition of tomorrow's aircraft engine. The two major examples of this investment campain can be found in the two reasearch labs that have been jointly created with Politecnico di Torino: GreatLab and TAL.
The GreatLab (GReen Engine for Air Traffic control LABoratory) is off-sote located Avio research lab where new engine architecture solutions are investigated and new dynamic technologies are tested before the real implementation on engine components. It is located with Politecnico di Torino walls, which enables a strong connection between the university research world and the complex aviation company market.
On the other hand, the TAL (Turin Additive Lab), located just next to the GreatLab, is the perfect example of how the aviation industry is trying to reimagine the way engine components should be manufactured, by allowing the expansion of Additive Manufacturing technologies in the aviation world. Within the TAL, new additive solutions are developed, which enable Avio Aero to be a front-runner among the aviation companies that investing in the field, also thanks to the close collaboration with the newly born business GE Additive.
The project that is presened within this report has been conducted in the G2020 mainframe, and its activity have been partly developed within the GreatLab environment.

Chapter 2

Aircraft Engine Architecture

2.1 Aircraft Engine Types

Among all the engineering systems, the aircraft is definetly one of the most complex ones and one of those that has seen the most substantial development from its birth, back in 1903 [29].

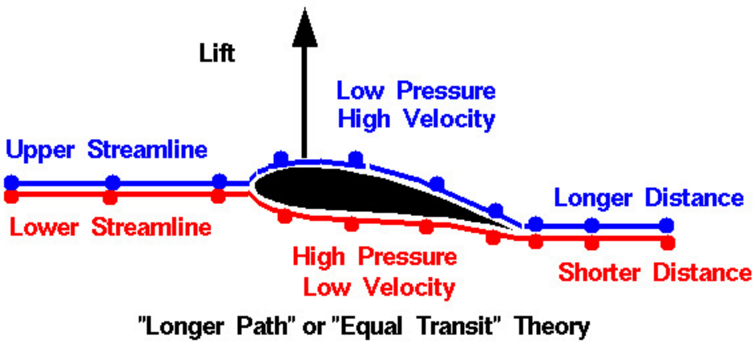

Figure 2.1: Lift Force scheme based on Airflow - Source [5]

Despite an aircraft may be classified from various points of view [43], from application (civil or military), size (narrow body or wide body) or propulsion system, their basic working principle is identical among all types. With reference to Figure 2.1 [30], when air particles hit the wing of the aircraft, their stream gets split between the upper side and the lower side of the airfoil. Despite being the upper track and the lower track unequally long, the particles need to make their way in exactly the same time [29]. The latter implies a different velocity between the particles following in the upper part (being the upper part of the airfoil longer, they will feature a higher velocity) and the lower part (being the lower part of the airfoil shorter, they will feature a lower velocity). Based on Newtwon's Law [29], the counterpart of a lower velocity is a greater static pressure, pushing the airfoil upwards. This is what we generally name as "Lift Force".

Even though the lift force may take place despite the velocities in action, the great aircraft's mass implies that in order to generate the sufficient lift, engines have to provide great acceleration and cruise speed. The latter implies that engines are required to provide enough thrust so that a sufficient acceleration may be provided, especially during take off operations, when the most lift is needed. Nowadays, despite various variants have been developed throught the aviation history, aircraft engines may be categorized [35] into three main types:

- Turboprop Engines, mainly used in small-sized aircrafts. They are capable of reaching low speeds, usually up to 300 mph [8]. For a scheme of how Turboprops are set, you may refer to Figure 2.1

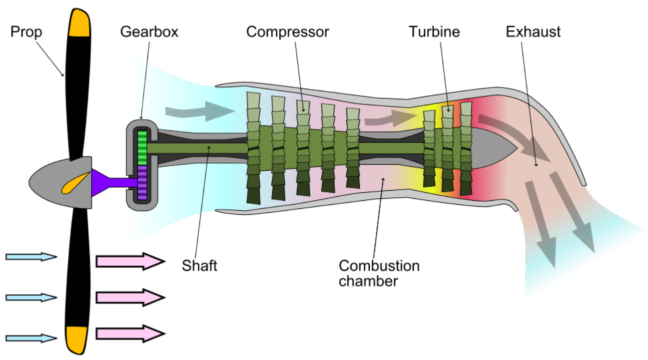

Figure 2.2: Scheme of Turboprop main components - Source [8]

- Turbofan Engines, used in the majority of civil aircrafts. They feature a double air-flow: the engine core flow and the by-pass flow. They are capable of reaching speeds up to 550 mph, but are not suitable for supersonic travel [47]. This type of aircraft engines will be dealt with more in depth within Section 2.2.

- Turbojet Engines, even called zero-bypass Turbofan Engines, are widely used in military jets [7]. They are capable of reaching supersonic speeds, even though this implies very high fuel consumption [12], which makes them little suitable for civil aviation exploitation. The classic example of their use in civil aviation is represented by the Rolls Royce®Snecma®Olympus 593, designed to power the iconic Concorde. The high consumption the engines used to imply made the use of the aircraft limited to limited market segments, and can be definitely considered one of the reasons why the aircraft stopped flying in 2003 [1]. A scheme of the main

[1]Source: Wendover Productions - "Why Planes don't Fly Faster"

Turbojet structure can be found in Figure 2.1.

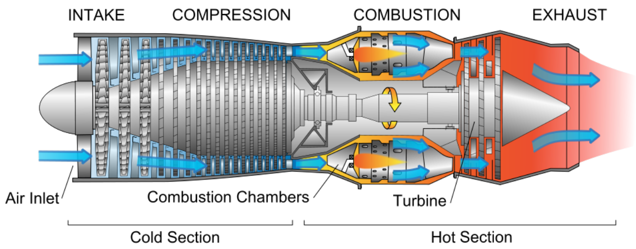

Figure 2.3: Scheme of Turbojet Main Components - Source [7]

2.2 Turbofan Engines

Among the three main variants that have been shown in Section 2.1, the Turbofan engine covers a major role within the aviation market, especially from the commercial market point of view [6] [47]. Nowadays the majority of medium-sized and large-sized commercial planes are powered by turbofan engines. The reason this type of engines has been widely preferred over Turboprops and Turbojets can be accounted to their increased reliability in terms of safety and their more competitive fuel economy.
As far as the engine reliability is concerned [9], Turbofan engines offer much lower IFSD[2] Rates than Turboprop engines. This translates in higher safety standards that can be guaranteed on commercial flights. To provide an example, based on GE's press release[3] and ICAO[4] EDTO Considerations [5], the GE90 (one of the best commercial success among Turbofan engines, set on Boeing®777 jets) is rated with "one IFSD engine failure per million flight hours". On the contrary, Turboprops are historically more related to aircraft incidents than Turbofans. A 2017 AOPA[6] study showed that turboprop powered aircraft are much more affected by incidents (both fatal and non-fatal) than turbofan powered ones. Results of the study are shown in Figure 2.2

On the other hand, as far as the fuel economy is concerned [17], there are various reasons why commercial aircrafts are usually powered by Turbofans rather than Turboprops or Turbojets. By taking into account all forces acting on the Aircraft system, drag plays a major role in determining the efficiency of the aircraft itself.

[2]Source: In-Flight ShutDown
[3]GE Aviation GE90 Press Release Dated March 13th, 2016
[4]International Civil Aviation Organization, a United Nations Agency
[5]EDTO Workshop - Module 4: Aircraft certification considerations
[6]Aircraft Owners and Pilot Organization

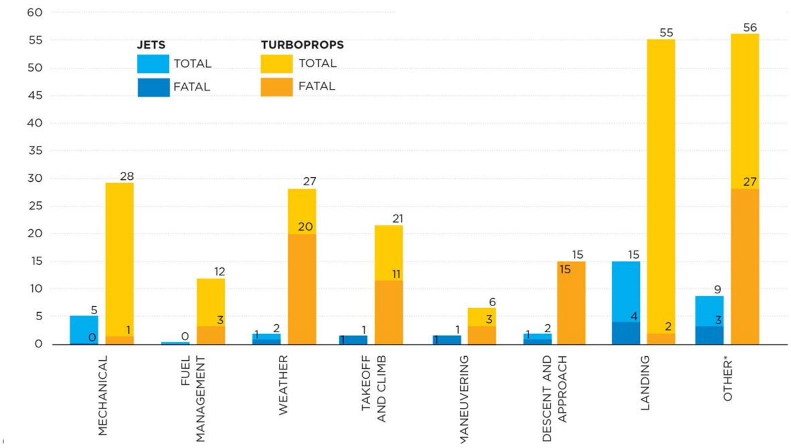

Figure 2.4: 2005 - 2014 Engine incidents reports based on the type of engine powering the aircraft - Source: AOPA

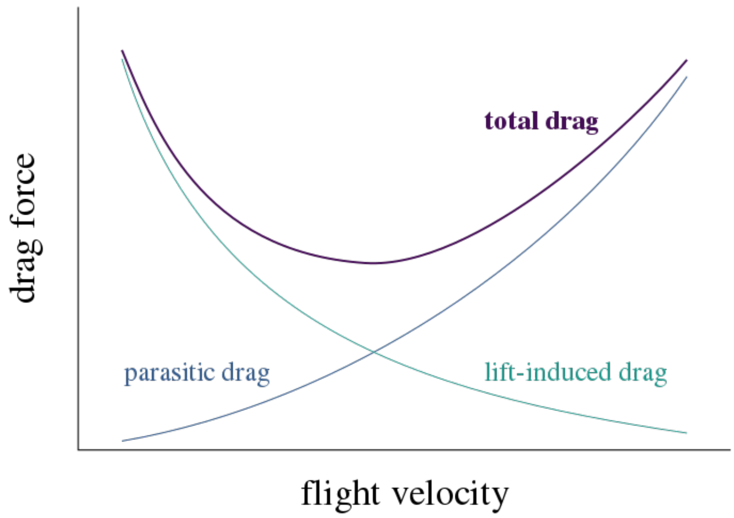

Figure 2.5: Relationship between Drag Force and Speed in a generic Aircraft - Source [3]

Drag force [30], as shown by Figure 2.2, is closely correlated to the speed the aircraft is travelling at. There is a clear minimum on the graph showing that the best efficiency can be found by travelling within a specific speed range, so that the drag effects can be reduced as much as possible. Provided the architecture of today's commercial aircrafts, the range the drag force is minimum at falls within the range where turbofan engines are more fuel efficient.

One key point that should be highlighted is that the fuel economy in aviation can be

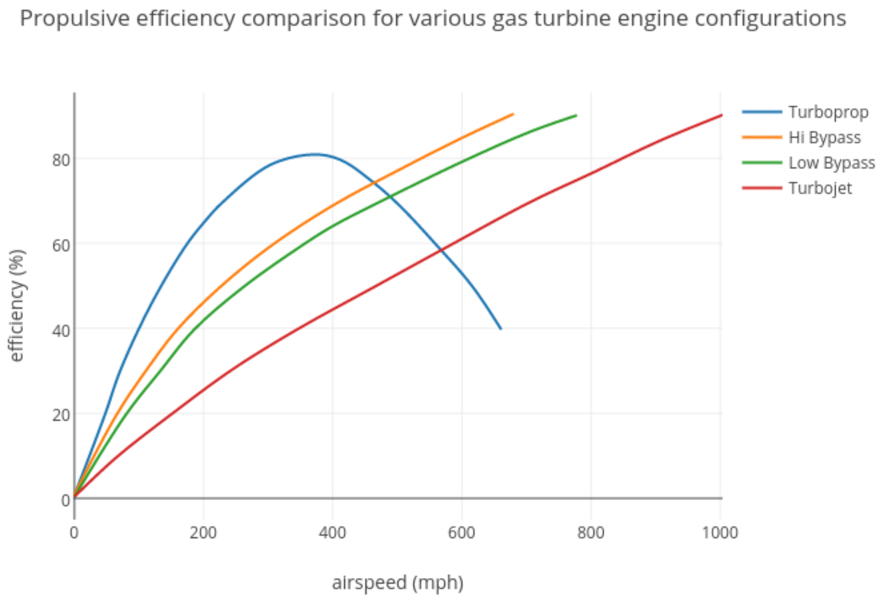

Figure 2.6: Fuel Efficiency based on the type of engine and ground speed - Source [3]

either computed in terms of **Lb per flown mile** or **Miles per gallon per passenger** [3]. When the latter definition is concerned, the comparison between aircraft engines is even clear. By taking into account two iconic aricraft engines, the GEnX (a very efficient turbofan engine) and the Rolls Royce®Snecma®Olympus 593 (a turbojet engine), we can classify the **Miles per gallon per passenger** rating as shown in Table 2.2.

Aircraft	Engine	Aircraft FE [lb/mile]	Passenger FE [mpg]
Concorde	Olympus 593	46.85	14
787 - 9	GEnX	18.7	103

Table 2.1: Fuel economy comparison between Boeing 787 - 9 and Concorde - Source [6]

Despite the clear age difference between the two aircrafts and the two engines (GEnX and Boeing®787 are more modern), the provided data gives an evident proof of the success of Turbofans over Turboprops.

2.3 Turbofan Architecture

Although the engine, being a very complex system, is composed by various kinds of mechanical, hydraulic and electronic components [40], and although significantly different

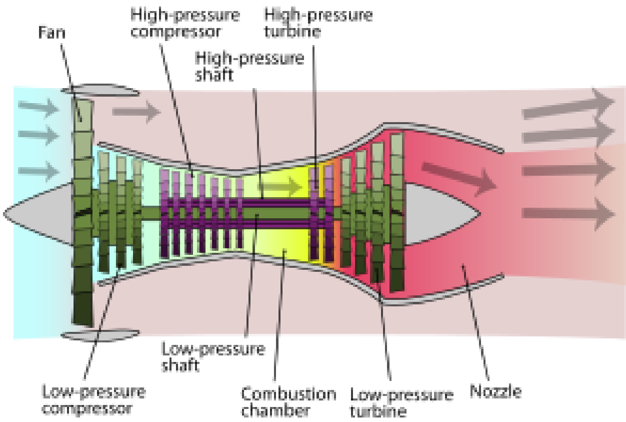

Figure 2.7: Turbofan main components' structure - Source [6]

architecture variants have been developed throughout history, a turbofan may be divided into four major sections, shown in Figure 2.3

- Fan: speeding up the inlet air and providing the most of the thrust. It is driven by the main shaft
- Compressor: the first stage of the engine core, driven by the main shaft, compresses the air by the engine pressure ratio
- Combustor: the compressed air, after having mixed with sprayed fuel, ignites and experiences combustion
- Turbine: the exhaust gases flow through the turbine, allowing the main shaft to spin in rotate with the power needed by both the fan and the compressor

With reference to Figure 2.3, the architecture of the engine is characterized by what is called the **ByPass Duct**, being the duct that by-passes the engine core, composed by compressor, combustor and turbine. This feature leads to the definition of a very important index for a turbofan engine: the **ByPass Ratio (BPR)** [40] [47].

$$BPR = \frac{\dot{m_{bypass}}}{\dot{m_{core}}} \tag{2.1}$$

where $\dot{m}$ stands for the mass-flow rate flowing through either the engine core or the by-pass duct. Both Figure 2.3 and Eq. 2.1 provide a relevant differentiation of the air coming in into two major flows:

- By-pass Flow, being the air that bypasses the engine core after having been sped up by the fan

- Core Flow (or Combustion Chamber flow), being the air that passes through all three engine core sections after having been sped up by the fan

As a matter of fact, the BPR is a relevant factor [47] in order to determine the efficientcy of a turbofan engine. In fact, given a unitary $\dot{m_{core}}$, the higher the BPR the more thrust can be obetained, with the same amount of fuel. Spinning a larger fan requires relatively less fuel than running a larger engine core. Therefore, as a general rule [47], the higher the BPR, the higher the engine efficiency.

$$Efficiency \propto BPR \tag{2.2}$$

As highlighted in Section 2.1, a Turbojet engine can be rated as a zero-BPR Turbofan Engine.
Table 2.3 provides some examples of BPR values for commercial aricraft engines.

Engine	**Aircraft**	**BPR**
P& W JT8D	DC-9, 727, 737	0.96:1
CF6-50	A300, DC-10, DC-30	4.26:1
P & W 4000	A300, A310, 767, 747-400	4.85:1
CF6-80C2	MD-11, A300-600, A310, 747-400	4.97:1
Trent 700	A330	5.00:1
Trent 500	A340	7.6:1
Trent 900	A380	8.7:1
GE90	777	9:1
Trent XWB	A350 XWB	9.3:1
GEnX	747-8 - 787 Dreamliner	9.6:1
Trent 7000	A330neo	10:1
P & W 1000G	A220 - A320neo	12:1

Table 2.2: BPR comparison between common engines Source [6]

Thrust is provided as an effect of action-reaction principle [35] for a given action there is an equal and opposite reaction. In the case of aircraft engines, the action is the high-speed air exhaust caused by the fan and the turbine. As mentioned above, despite the exhaust from the turbine provides some thrust, the most of it comes from the fan that accelerates the inlet air through the ByPass Duct. In order to provide an example of this comparison, ®Safran [4] has stated that 90% of its ®LEAP[7] engine comes from the fan operation, while only a 10% comes from the turbine exhaust air.

[7] LEAP engine is produced by the ®CFM consortium, which is a joint venture between the french engine company ®Safran and ®GE Aviation

2.3.1 Thermodynamic Cycle

Given that, as explained through Section 2.3, the flow path is divided in two main flows, it is important to highlight how the fluid develops along the Engine Core. The Thermodynamic Cycle an engine is based on is the Brayton Cycle, which is a more modern development of Joule's thermodynamic cycle [19] [18].

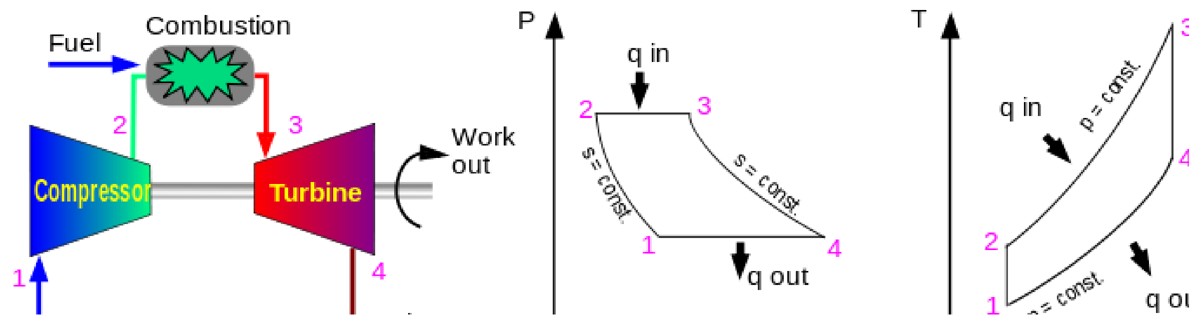

Figure 2.8: Left: Schematic Representation of the components involved in the cycle. Center: Ideal Cycle representation on a p-V Diagram. Right: Ideal Cycle representation on a T-S Diagram - Source [6]

As represented by Figure 2.3.1, the cycle is composed by four main stages[19] [18]:

- Stage 1: compression of atmospheric air, from T1 (P1) to T2 (P2). This phase takes place in the axial compressor of the turbofan engine, usually composed by various stages. It is important to notice that the compression ratio being namely:

$$\beta = \frac{P2}{P1} \tag{2.3}$$

  is a key factor to determine the efficiency of an engine. The higher pressures the engine is capable of reaching by the end of the compression phase, the more thermodynamic energy will be exploitable by the turbine. Modern engine architecture features the division of the compressor in two major units, being the Low Pressure Compressor (LPC) and the High Compression Compressor (HPC), highlighted in Figure 2.3.1 . Despite numerous different variants are being developed, the engine compressor is driven by the main engine shaft, thanks to the Turbine rotation.

- Stage 2: combustion of compressed air. This stage takes ideally place at constant pressure $P2 = P3$, even though some pressure losses are present in reality. The purpose of combustion is increasing the temperature of gases from T2 to T3, in

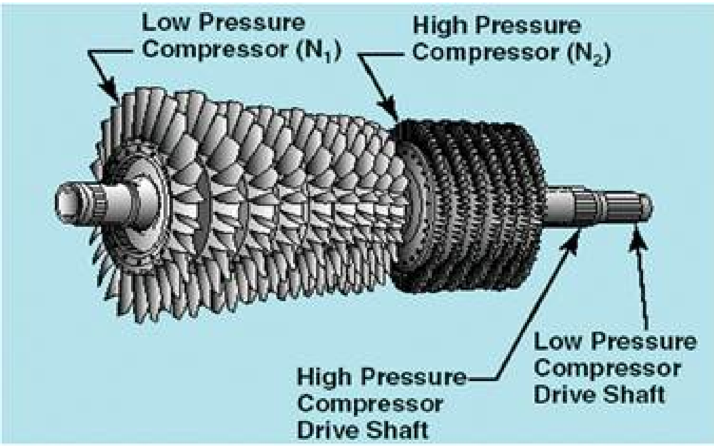

Figure 2.9: Division of an axial compressor in LPC and HPC - Source: American Journal of Mechanical and Industrial Engineering

order to increase the thermodynamic energy content of gases that will have to expand through the turbine. The combustion stage takes place into a combustion chamber (or combustor), represented in Figure 2.3.1

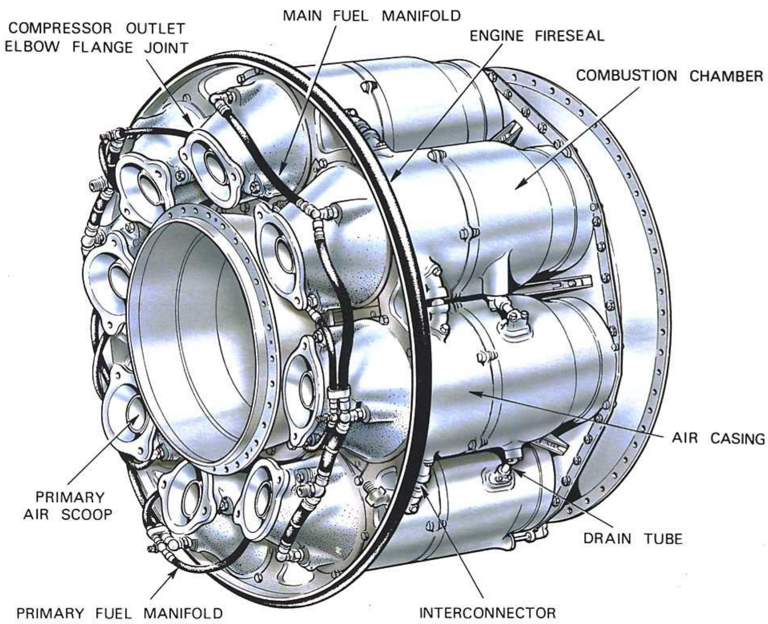

Figure 2.10: Schematic representation of a combustor - Source: [2]

More in details [34], just before the combustion process starts, the compressed air is mixed with fuel droplets, sprayed by fuel nozzles. The more homogeneous the mixture, the more efficient the combustion process is. This is why modern engine architecture have adopted an air-fuel mixture configuration that takes place before enterin the actual combustion chamber. It is worth mentioning that, in the case of commercial aircraft engines, Kerosene is the most commonly used fuel. During phase 2, the actual combustion process takes place in the combustion chambers, represented in 2.3.1, where the mixture gets ignited and reaches the targeted T3, which is the Turbine Entry Temperature. This value is one more important factor for engine efficiency: the use of more thermo-resistant materials in modern engine architecture aims at allowing engine components (such as in combustor or in turbine first stages) to handle higher temperatures, which translates into an overall higher efficiency.

- Phase 3: combustion exhaust gases expansion through the turbine stages. Starting at T3, the exhaust gases begin their expansion process that involves an energy exchange between the gases themselves and the turbine blades. This exchange is what drives the main engine shaft, thus making the fan and compressor spinning possible. Despite being usually divided in two major modules (being, namely, the High Pressure Turbine, HPT, and the Low Pressure Turbine, LPT), the functioning of a turbine remains the same throughout its stages. Each stage is composed by a statoric component row, named after as **Vane** and a rotoric component row, composed by a set of **Blades**.

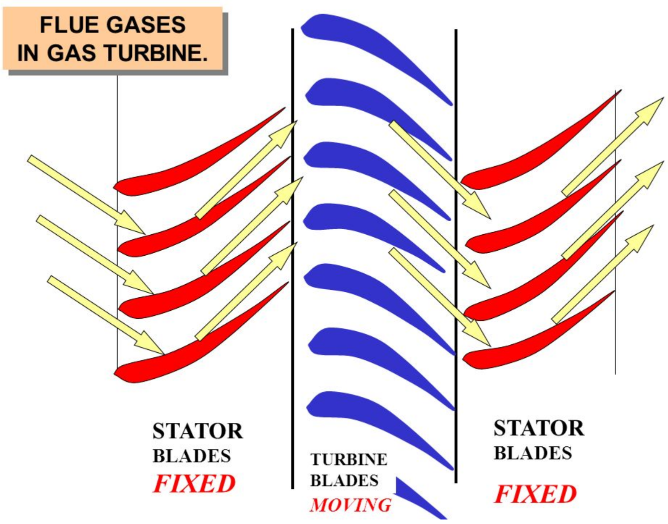

Figure 2.11: Schematic Representation of a Turbine Stage - Source: [2]

At the beginning of each stage, the gases enter the Vane cross section, where they experience a pressure drop and an increase in mean velocity. At the end of this phase, gases will feature high velocity (which may be described with a high total enthalpy content), useful to allow a high speed rotor spinning. Turbine blade cross sections, can be described by an airfoil shape. This causes, as explained in 2.1, produces a pressure difference between **Pressure Side** and **Suction Side**, thus causing the rotor motion and the shaft spinning. During this process, work is exchanged between the gases and the turbine components, meaning that at the end of each stage the energy content of the exhaust gases gets diminished. This concept stresses the importance of reaching a high pressure P2 at the end Phase 1 and a high temperature T3 at the end of phase 2, according to which a higher energy exchange may be obtained through the turbine stages.

- Phase 4: at the end of the expansion process, gases get exhausted from engine. This process usually takes place through an exhaust nozzle, after $\dot{m}_{bypass}$ and $\dot{m}_{core}$ have mixed up back together. The nozzle ensures an increase in velocity of exhaust gases which will cause an increase in reaction force the atmosphere will act on the aircraft.

Figure 2.12: Chevron Nozzle Nacelle of a GEnX Engine Mounted on a B787 Dreamliner - Source: [1]

Chapter 3

Engine Rotors Dynamics

As far as the physics of aircraft turbines is concerned, it is very important to understand what is the dynamic behaviour of Bladed Disks is. In the following chapter, an insight of the basics aspect of modal analysis will be provided. Moreover, several tool and methods will be explained in order to better understand the way the validation process works from a dynamics point of view. Moreover, as it will be explained in the next sections, the modal behaviour of the components is a key factor to evaluate the aeromechanical instability of the system.

3.1 Bladed Disks Sectors

Turbines are engine sub-assemblies that, as explained in Chapter 2, are composed by a series of stages, each one divided in the statoric component (from now on called as **Vane** or **V**) and the rotoric component [44]. By taking into account the rotor of the turbine stage, it is usually composed by a set of multiple blades, assembled on a rotating disk, which is the component connecting the shaft to the rest of the module. Since the number **N** of blades, the computational cost of analysing a complete stage would be too high, even with current technology. Therefore, it is convenient to take advantage of the cyclic symmetry [39] each i-th blade sector features with respect to the rest of the stage (**N-1**): the sector will be hence composed by only one i-th blade (see Figure 3.2).
In order to obtain a further simplification of the model, only the blade and the disk are typically included in the studied model. When these two components are included, the model will be named after as **Blade Disk** or **BD**, while in the case only the blade is considered, with model will be named after as **Blade Only** or **BO**.

As far as an all tuned rotor is concerned, the BD sector will be considered as a single sector. As it will be explained in the following sections, the application of cyclic symmetry, not only allows a drastic reduction in computational power, but does not compromise the precision of results from a dynamic point of view.

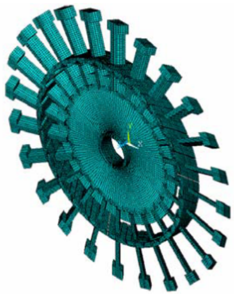

Figure 3.1: Complete Rotor Assembly Source [36]

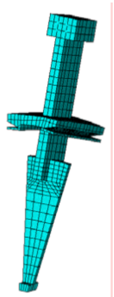

Figure 3.2: Simple Bladed Disk Source [36]

3.2 The role of modal analysis in the validation process

Aircraft engines are very complex systems, where components interact from many points of view (thermal interaction, mechanical interaction, fluid-dynamic interaction). The validation process needs to take into account the integrity of the components, and its good performance, by both looking at the single discipline and by looking at the different multi-physics interaction within the system (e.g. teh thermal strain the thermal field creates).
The dynamic behaviour of the BD covers a very important role in terms of interaction with other engineering disciplines. In the current report, the use of modal analysis will be expolited from two different points of view:

- Aeroelastic Validation: the modal behaviour is a key ingredient (together with the aerodynamics) in the evaluation of flutter instabilities

- Fatigue Validation: Vibrations cause the creation of alternate stress that may cause the rupture of the component by fatigue at a certain number of working cycles. The evaluation of either frequencies and vibration amplitudes is important to certify the component will be able to cover its life-cycle without reaching the rupture conditions.

The structural validation of a rotor component from a fatigue point of view follows a specific set of simulations and tests that end with the Goodman Plot evaluation. The scheme shown in Figure 3.3 provides an insight of the methodology used for fatigue evaulation during the current study.

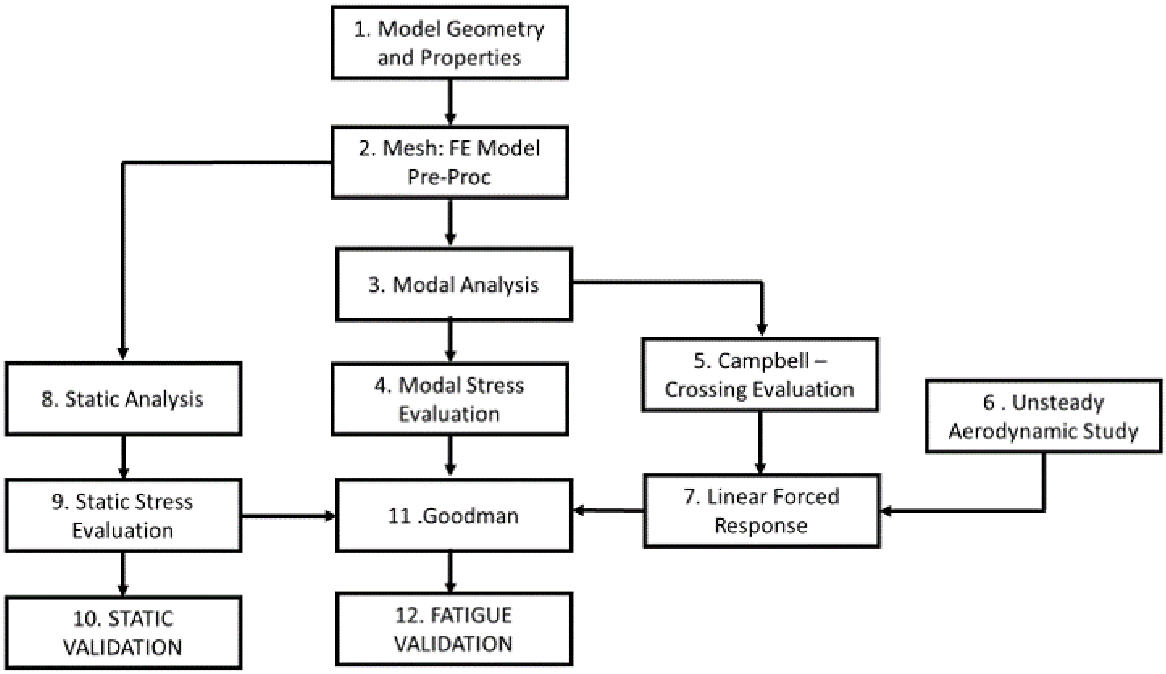

Figure 3.3: Fatigue Validation Process

1. The component geometry is defined and modelled through a CAD Software tool (®Siemens NX is the used tool). Moreover, its properties, such as materials of surface coatings, are defined

2. The component is meshed to create the FE model. The model is defined through TETRA10 Elements, formatted in ®Nastran language. Areas where higher stresses are expected (i.e. blends, cavities, etc...) should be mesh more finely, to allow a higher resolution of stress computation.

3. A modal analysis is performed for the required Harmonic values to evaluate the resonance frequencies (eigenvalues) and modal shapes (eigenvectors). Usually, in order to simplify the problem and to reduce the number of simulations, the modal analysis is launched at three different conditions:
    - Take Off (**TO**)
    - Crusise (**CR**)
    - Cold (**CO**)
4. For each mode of interest, dynamic stresses are evaluated at each FE model node. These values will be input data for the Goodman Plot Evaluation
5. By taking into account the Enegine Orders (**EO**) of interest, the Campbell Diagram is evaluated and the major crossings within the engine operative range are found
6. The unsteady aerodynamic study results are used to evaluate the gas flow forcing term acting on the blades
7. The data coming from 6. are used to compute the linear response function between each mode and the gas flow forcing term. These data are useful to evaluate the "weight" each mode has. More in details, this analysis provides a scale factor for the dynamic stresses during the Goodman polit computation.
8. By using the same FE model (i.e. the same mesh), a static analysis is launched by taking into account the following loads:
    - Gas Load on Airfoil PS and SS
    - Centrifugal Load
    - Thermal Load (i.e. thermal stress effect computation)
    - Interference between adjacent surfaces at the interlocking region
9. Static Stresses are evaluated at each node of the mesh. These values will input data for the Goodman Plot computation
10. By considering the material property, the component can be validated from a static point of view, by making sure there a certain Safety Factor between the maximum equivalent stress that is experienced and the yield stress of the material
11. By using the data coming from 4. - 7. - 9. the Goodman plot can be evaluated. The computation is performed for each node contained in the mesh.

12. If all the mesh nodes fall respect a specific safety factor target, the component is validated from a fatigue point of view. More in details, material curves are provided for a specific number of cycles: therefore, the Goodman plot will provide the fatigue validation for the number of cycles the material curves are rated for.

3.3 Modal Analysis of a BD in Cyclic Symmetry

As explained in 3.1, the simplification the model can be done by considering only the blade (**BO** model) or the blade and the disk together (**BD** model). Despite the **BO** analysis covers a very important role in the validation process, especially during preliminary studies, the current report will focus its attention on **BD** models, unless where differently stated. Moreover, as long as this chapter is considered, only single sectors will be treated (i.e. sectors with only one blade). More complex systems will be introduced in the following chapters.
The **BD** model that has been defined, as stated in 3.1, features cyclic symmetry with respect to the engine main axis, noted **z**. The geometric model needs to be discretized into a Finite Elements (**FE**) model by means of a meshing tool (in the current study ®Altair Hypermesh has been used). The discretization created a FE model with **m** DOFs. The motion of the entire system can be described by the equation of motion, written in matricial form [10]:

$$[M] \cdot \{\ddot{x}\} + [C] \cdot \{\dot{x}\} + [K] \cdot \{x\} = \{F\} \tag{3.1}$$

Where:

- $[M]$ represents the mass matrix
- $[C]$ represents the damping matrix
- $[K]$ represents the stiffness matrix
- $\{\ddot{x}\}$ represents the acceleration vector
- $\{\dot{x}\}$ represents the velocity vector
- $\{x\}$ represents the displacement vector
- $\{F\}$ represents the forcing term vector

The set of equation contained in 3.1 represents the **Eigenroblem** of the system with **m** equations and **m** solutions.
In order to compute the eigenvalues and eigenvectors of the system, the homogeneous form of 3.1 needs to be solved. It will be written in the form [10]:

$$([K] - \omega^2 \cdot [M]) \cdot \{\psi\} = \{0\} \tag{3.2}$$

Where:

- ω represents the eigenvalue (or natural frequency) of the system
- $\{\psi\}$ represents the eigenvector (or modeshape) of the system

The reduction of the DOFs of the system by taking into account only a single **BD** sector and the imposition of the right boundary conditions allows the computation of the solution that is cylindrically periodic through the stage row. The nodes contained **BD** sector (named after as fundamental representative sector) shown in Figure 3.4 can be divided into three categories:

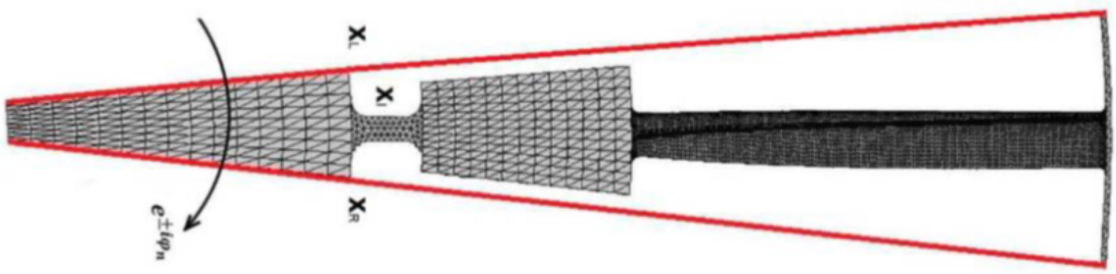

Figure 3.4: FE Model of a Fundamental Representative Single Sector - Source [10]

- Right-hand side nodes (with subscript **R**), being the connection nodes with the adjacent sector and where the boundary conditions will be applied
- Left-hand side nodes (with subscript **L**), being the connection nodes with the adjacent sector and where the boundary conditions will be applied
- Inner nodes (with subscript **I**, where no boundary condition is applied

The cyclic symmetry condition will be applied between the **R** and **L** nodes with respect to the **z** axis. The three type of system nodes represent even the type of DOF the sector feature: the solution vector $\{x^s\}$ (here indicated with superscript **s**) can be written as [10]:

$$\{x^s\} = \left\{ \begin{array}{c} \{x_R^s\} \\ \{x_L^s\} \\ \{x_I^s\} \end{array} \right\} \tag{3.3}$$

Similarly, even the forcing vector $\{F\}$ highlighted in 3.1 can be written as:

$$\{F\} = \left\{ \begin{array}{c} \{F_R\} \\ \{F_L\} \\ \{F_I\} \end{array} \right\} \tag{3.4}$$

Both Eq. 3.3 and Eq. 3.4 allow to rewrite the solution of the non-homogeneous solution for the fundamental sector as [10]:

$$([K^s] - \omega^2 \cdot [M^s]) \cdot \{x^s\} = \{F\} \tag{3.5}$$

The solution found for one sector is still valid in terms of amplitude for all the remaining sectors. However, the solution results phased by an angle ϕ that is commonly known as **IBPA**(InterBlade Phase Angle). This angle can be expressed as [20] [28]:

$$IBPA = \phi = \frac{2\pi \cdot n}{N} \tag{3.6}$$

Where:

- N represents the number of blade in the row
- n represents the number of nodal diameters ND (see Section 3.4.1

This allows a further simplification of the solution vector, as the nodes that feature cyclic symmetry property (i.e. $\{x_R^s\}$ and $\{x_L^s\}$) have an eigenproblem solution that can be written as [10]:

$$\{x_R^s\} = \{x_L^s\} \cdot e^{j\phi} \tag{3.7}$$

The complete solution vector $\{x^s\}$ can be, therefore, written as:

$$\{x^s\} = \left\{ \begin{array}{c} \{x_R^s\} \\ \{x_R^s\} \cdot e^{j\phi} \\ \{x_I^s\} \end{array} \right\} \tag{3.8}$$

Further considerations over the **IBPA** can be done by writing Eq. 3.7 with Euler notation:

$$\{x_R^s\} = \{x_L^s\} \cdot e^{j\phi} = \{x_L^s\} \cdot \left(cos\left(\frac{2\pi \cdot n}{N}\right) + jsin\left(\frac{2\pi \cdot n}{N}\right)\right) \tag{3.9}$$

By looking at Eq. 3.9 we can notice that for certain values of **IBPA** (i.e. when $n = 0, N$) the Imaginary part of the solution is null. Hence, in this case the eigenproblem allows only real modes as solution. For all other cases, the eigenproblem has complex modes as solution vectors.

3.4 Solutions of a BD modal analysis

In Section 3.3 the Eigenproblem of **BD** Sector has been presented. In the current section different solution analysis methods will be presented. These methodologies are key factors to fully understand the dynamic behaviour of a turbine rotor.

3.4.1 Nodal Diameters

The solution of the eigenproblem, explained in Section 3.3, provides the eigenvalues (frequencies) and eigenvectors (modal shapes) of the system according to specific loads ($\{F\}$) and boundary conditions (cyclic symmetry applied to the R-nodes and L-nodes). However, the description of the vibration phenomena for a **BD** is not satisfying when providing only these data. In order to fully understand the phenomena, the description should be taking into account even what happens at the entire row level.

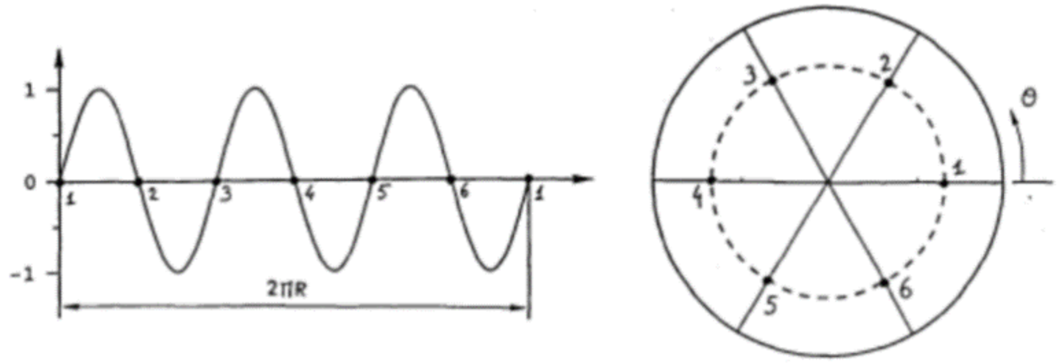

Figure 3.5: $ND = 3$ Configuration - Source [11]

When looking at the displacement of the **BD** systems, particular configurations can be found, such as **Nodal Diameters** and **Nodal Circumferences**. When dealing with **Nodal Diameters**, they represent segments passing through the center of the disk where a null displacement is experienced. The value is usually indicated with **ND** Mode-shapes (or eigenvectors) can always be represented as a linear combination of harmonic functions such as $cos(ND\theta)$ and $sin(ND\theta)$. When looking at the displacement of the harmonic function along angle θ , specific angular locations where displacement is nulla can be found. As an example, let's take a **ND** = 3 configuration, represented in Figure 3.5: there will be 6 different θ coordinates where the displacement is null.

A similar definition can be provided for **Nodal Circumferences**: they represetn concentric circumferences where a null displacement can be found.

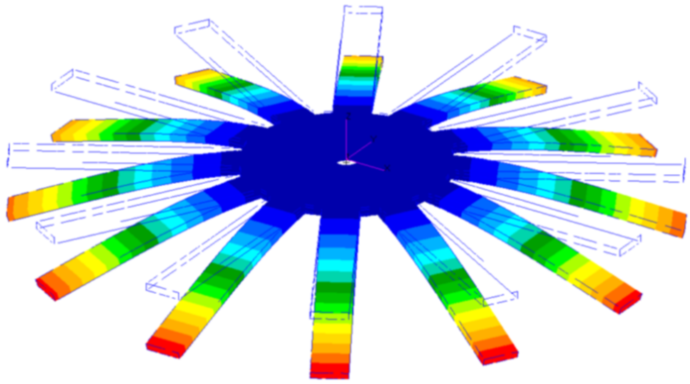

Figure 3.6: Configuration with ND=0 and NC=0 [10]

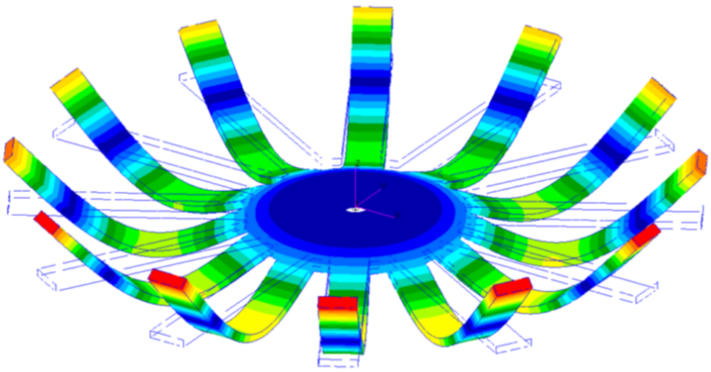

Figure 3.7: Configuration with ND=0 and NC=1 [10]

The maximum value of **ND** is directly correlated to the number of blades present in the row [10]:

$$\begin{cases} 0 \leq ND \leq \frac{N}{2} & \text{if N is even} \\ 0 \leq ND \leq \frac{N}{2} - 1 & \text{if N is odd} \end{cases} \tag{3.10}$$

In the modal analysis of **BD** systems, the concept of **Nodal Diameter**, covers a very important role, sicne it helps to uniquely identify vibration modes. When complex vibrating systems, such as **BD**s, are taken into account a single frequency value does not identify a single mode. In fact, for a specific value of frequency, multiple modeshapes may coexist. However, it is possible to freeze the deformed configuration of the system in time and divide it into multiple harmonics, representing the **ND** value. In this case, by looking at both the frequency and **ND** configuration, the identified mode is unique. As explained in Section 3.3, the **IBPA** value is an other important factor to identify a vibrating mode. By recalling Eq. 3.6, the angle value represent the phase angle the modes are vibrating at between nodes where cyclic symmetry is experienced.

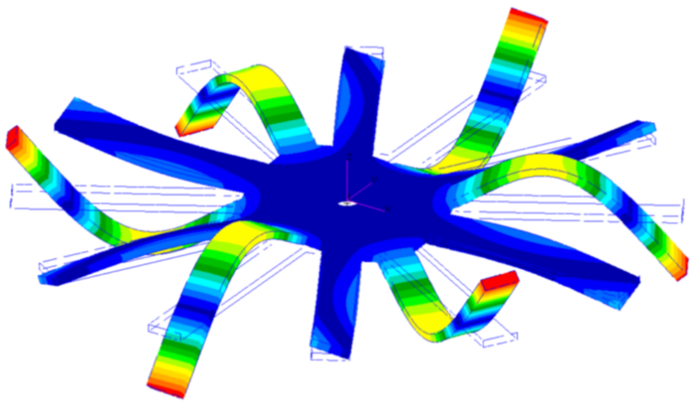

Figure 3.8: Configuration with ND=3 and NC=1 [10]

By taking advantage of the **ND** and **IBPA** concepts, vibration modes can be classified as follows:

- Stationary Modes: they take place only for $ND = 0$ or $ND = \frac{N}{2}$. In this case the mode can be described by a static wave, where all sectors vibrate according to the same amplitude and phase angle. Therefore, only one eigenvector is necessary to descrobe the modeshape.

- Rotating Modes: They take place for all other values of **BD**. They can be described with a couple of rotating waves travelling in opposite directions. The first travelling, travelling in the same rotational direction of the system, will be named after as **Forward** travelling wave. On the other hand, the second wave, travelling counter-direction with respect to the system, will be named after as **Backward** travelling wave. All modes are here phased by the **IBPA** angle. Therefore, the sign of the **IBPA** values is directly correlated to the travelling wave: a positive sign accounts for a forward travelling wave, while a negative sign accounts for a backward travelling wave. By taking into account the mode belonging to the two waves, they can be represented by two real eigenvectors, whose scalar product is null: they result modally orthogonal.

3.4.2 Modal Families

Even by considering a single value of **ND** the modes of a **BD** system as almost infinite. This is because the discretization during the meshing process creates a very

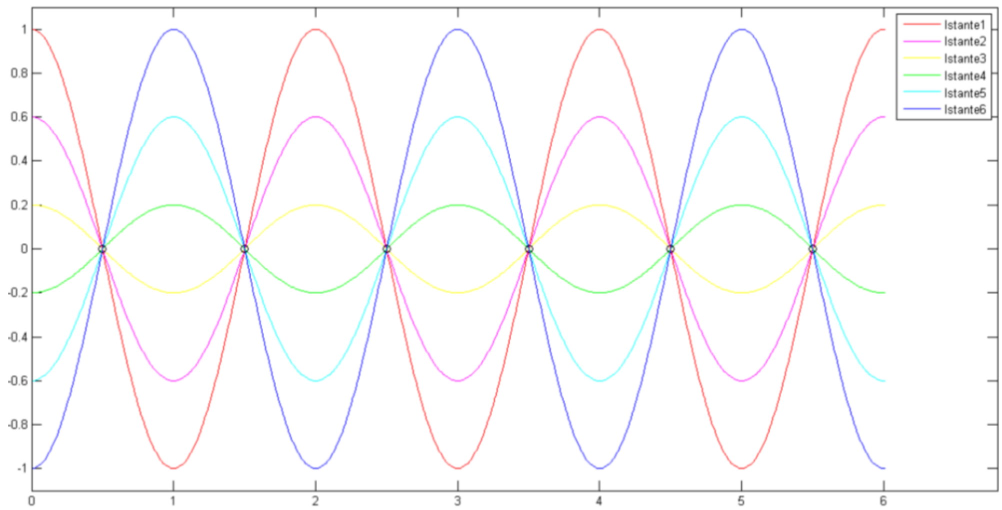

Figure 3.9: Representation of a Stationary Wave - Source [10]

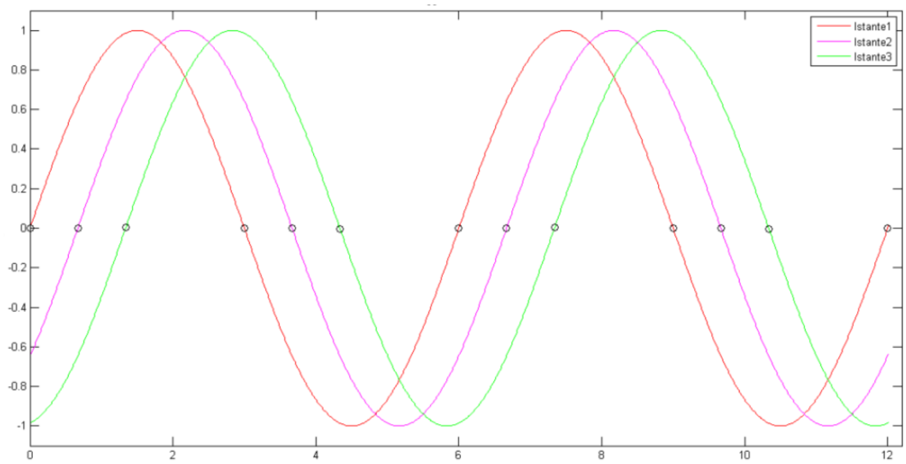

Figure 3.10: Representation of a Rotating Wave - Source [10]

high value of DOFs. Hence, the natural frequencies may reach very high values that are hard to analyse. However, the modal study of turbine rotors may be reduced to the analysis of the modes that occur only a t lower frequencies. This simplification is sufficient to evaluate the overall system dynamic behaviour since the first modes are those that carry the cause the higher amount of energy dissipation, while reaching higher frequency modes are less dissipative.
As far as this report is concerned, the attention will be focussed on first order modes. When considering the lower frequency modes, modeshapes can be classified in a set of *Modal Families*. The most common *Modal Families* that can be found in **BD** deformed configurations are:

- Flapwise (**Flap**)

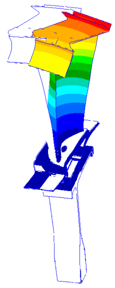

Figure 3.11: 1Flap Mode - Source [23] [38]

- Edgewise (**EW**)

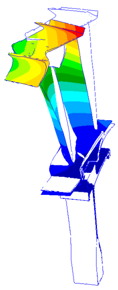

Figure 3.12: 1EW Mode - Source [23] [38]

- Twist (**Twist**)
- Flexural (**F**)

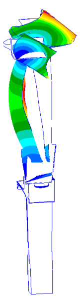

Figure 3.13: 1F Mode - Source [23] [38]

- Tortional (**T**)

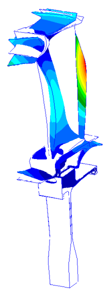

Figure 3.14: 1T Mode - Source [23] [38]

- Stripe (**1-2S**)

The modal classification of modes is a key part of the post processing: it allows to follow the evolution of modeshapes according to frequency and **ND** values. This is the aim of *FREND* (FREquency Nodal Diameter) diagrams.

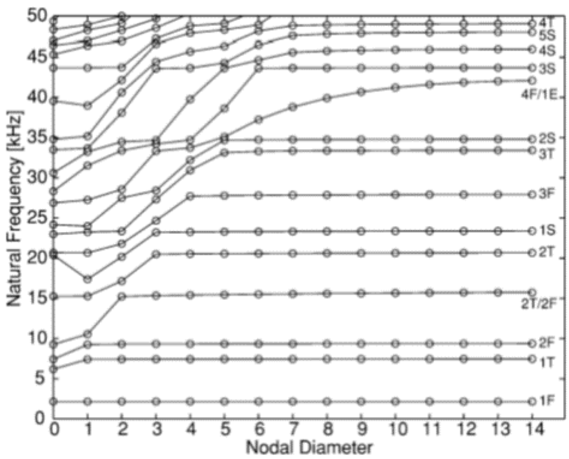

Figure 3.15: Example of FREND Diagram - [16]

FREND diagrams set the **ND** value on the x-axis, whereas the y-axis reports the frequency value a certain mode takes place at. It can be seen from the example reported in Figure 3.15 that modeshapes tend to be more frequency-unstable at lower **ND** values. This is because lower harmonics hold the highest energetic amount. By increasing the **ND** configuration, modeshapes tend to stabilize and occur at almost constant Frequency values. When complex systems are concerned, some modeshapes tend to get close to each other. This phenomenon, occurring at lower **ND** values, is known as *Veering*. When the *veering* phenomenon occurs, it is important to set investigate modal classification in terms of modeshape [10], instead of frequency. By doing so, modal families on the

FREND diagram are allowed to cross, while this is not possible when a frequency-based classification is acted.

3.5 Forcing Term

The model that has been presented in Section 3.3 has not further developed the forcing term $\vec{F}$. However, this term covers a very important role in dynamics of a **BD**. The system begin part of an aircraft engine is continously subject to aerodynamic forces acting on the airfoil of the blades. This forcing term, being represented by a pressure acting on the Pressure Side and Suction Side surfaces, is characterized by a specific amplitude and frequency. The frequency of the forcing term, labeled with letter Ω needs to be related to the rotational velocity of the rotor, labeled with letter ω. In any scenario where the resonance frequency is a multiple of the rotational velocity, resonance phenomenon may take place. This is why it is very important to express the ratio between forcing term frequency and rotational velocity of the rotor. This ratio take the name of *Engine Order* or **EO**, defined as:

$$EO = \frac{\omega}{\Omega} \tag{3.11}$$

Hardly ever forcing term can be expressed as a single harmonic function. In most cases forcing term functions are very complex functions that can be express by exploiting Fourier Series. In such cases, multiple frequencies, multiple of the fundamental one, will characterize the forcing term function. For this reason, multiple EOs may lead to a resonance condition [13].
By looking at the rotating system it is possible to consider the forcing term in two possible ways:

- By considering a fixed reference frame
- By considering a rotating reference frame, spinning by velocity Ω

When considering the second option, the system gets excited by two different harmonic forces.This situation is clarified when looking at Figure 3.5. More in details, two forcing terms can be encountered. The first one will have a the same rotational versus of the rotor while the second one will be counterwise.

In the rotating Reference Frame Case the forcing term can be expressed as follows:

$$\begin{cases} f_{\theta^{\star}}(t) = F_0 cos(\omega t) = F_0 cos(N_b \Omega t) \\ f_{\theta^{\star} \neq \theta}(t) = 0 \end{cases} \tag{3.12}$$

Where:

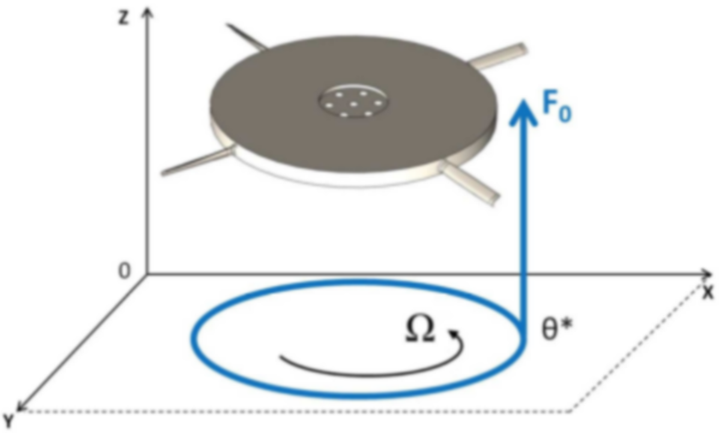

Figure 3.16: Example of rotating forcing term - Source [10]

- N_b represents the number of blades the rotor is composed by

By applying the Fourier series definition, the forcing term can be decomposed as follows:

$$f_\theta(t) = \frac{F_0}{\pi} = \sum_{n=1}^{\infty} cos[n(\theta - \theta^\star)]cos(\omega t) \tag{3.13}$$

Where:

- n represents the harmonic index

When considering $f_\theta(t)$ in a rotating reference frame, Eq. 3.13 can be written as follows [10]:

$$f_\theta(t) = \frac{F_0}{\pi} = \sum_{n=1}^{\infty} cos[(\omega - n\Omega)t]cos(n\theta_R) + sin[(\omega - n\Omega)t]sin(n\theta_R) + cos[(\omega + n\Omega)t]cos(n\theta_R) - sin[(\omega \tag{3.14}$$

Where:

- The variable change $\theta_R = \theta + \Omega t$ has been applied

With reference to Eq.3.5 two different rotating forcing terms can be identified, namely:

- A forward rotating forcing term, with frequency

$$\omega_f = \omega - n\Omega \tag{3.15}$$

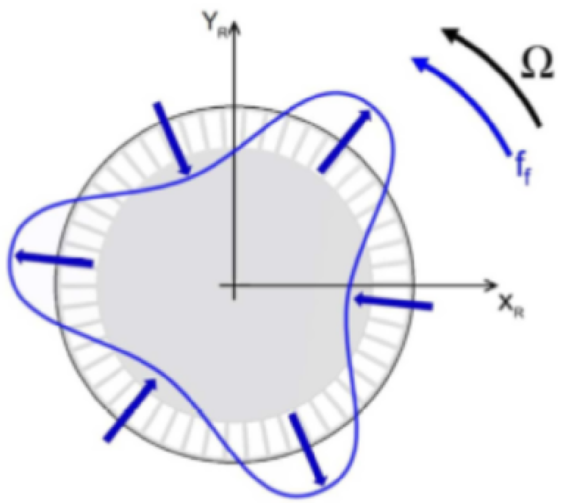

Figure 3.17: Representation of Forward Forcing Term [10]

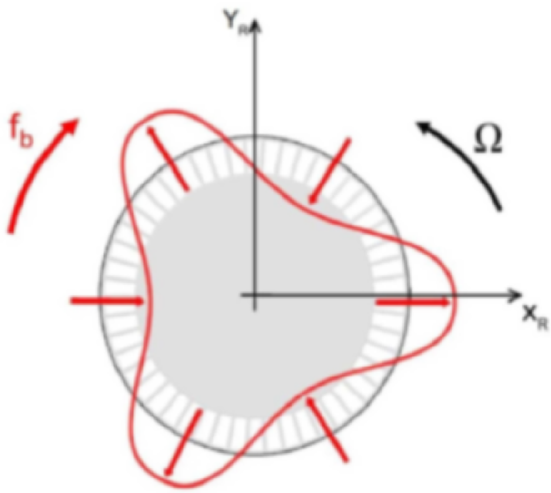

Figure 3.18: Representation of Backward Forcing Term [10]

- A backward rotating forcing term, with frequency

$$\omega_b = \omega + n\Omega \tag{3.16}$$

By setting $n = 1$ and $N_b = 4$, as represented in Figure 3.5, the frequencies of the rotating forcing terms turn [10]:

$$\begin{cases} \omega_f = \omega - n\Omega = \Omega(N_b - n) = 3\Omega = EO_f\Omega \\ \omega_b = \omega + n\Omega = \Omega(N_b + n) = 5\Omega = EO_f\Omega \end{cases} \tag{3.17}$$

The terms $EO_f = 3$ and $EO_b = 5$ are the Engine Orders representing the resonance excitation for the rotor in Figure 3.5 in a rotating Reference Frame.

3.6 Campbell Diagram

As explained through Section 3.5, correlating the rotational speed of the rotor and the frequency of the aerodynamic forcing term is a key part of the dynamic analysis of a **BD** system in order to determine the setting of resonance phenomena within the system. However, both the $\vec{F}$ term and the ω cannot be considered as constant values. More in details:

- The operating point of aircraft engine is defined through a series of key parameters, including the flight stage and various aircraft power needs. For this reason the aircraft engine spins at variable speed within its operating range, bounded by a lower value, usually named after as *Min. Cruise Speed*, a higher value, usually named after as *Red Line*.

- The aerodynamic forcing term $\vec{F}$ is composed by various is hardly composed by a single harmonic term. By recalling the expression used in 3.13, the forcing term can be expressed as the sum of various harmonic components, each one characterized by its own frequency Ω_n. This means that the forcing term will be deriving by the exciting actions of specific components and this adds new non-linearity effects in the modal analysis problem.

The Campbell Diagram is a useful diagram that correlates the frequency (expressed in [Hz])of the forcing term with the rotational speed of the rotor (expressed in [RPM]). Various **EOs** will be plotted as lines with different slopes on the graph and, by recalling the definition given in 3.11, each **EO** will represent the exciting action of a specific engine component. Together with the Engine Orders, the Campbell Diagram plots the natural frequency various modeshapes occur at based on both the nodal diameter (or harmonic index) of the system and the rotational speed of the rotor. The connection between the points the modeshapes occur at forms a curve that describes the behaviour of the modeshapes in the operative range of the engine. The point where, within the engine operative range, the **EO** lines and the modes lines cross each other, is called *Campbell Crossing* and identifies the possible setting of dangerous resonance phenomena. CAMBELL CROSSINGS identify a condition that requires further investigation. More specifically, the structural validation process, presented in Figure 3.3, needs to focus its attention on the *Campbell crossings* since they are more likely to harm the structural integrity of the component.

3.7 Engine Orders and Nodal Diameters

As explained through section 3.6 it is important to highlight the crossing between **EOs** and the modes of a excited rotor. Moreover, by recalling what has been explained in section 3.4.1, different modeshapes take place at different nodal diameters configurations, which means that, for most cases, each mode can be found at each **ND** value respecting Eq. 3.10. However, there is a strict correlation between **EO** and **ND** values, that can be expressed through [10]: :

$$\begin{cases} EO = ND \\ EO = N_b \pm ND \end{cases} \tag{3.18}$$

that can be written more in general as:

$$EO = mN_b \pm ND, \forall m \in N \tag{3.19}$$

where:

- ND stands for the Nodal Diameter value
- N_b stands for the stage number of blades

Eq. 3.19 (or Eq. 3.18) means that for a specific nodal Diameter configuration, when the forcing term frequency of a specific **EO** is equal to the natural frequency of a vibration mode, a resonance condition can be found. The consequence of this is that a specific Engine Order has the most effect on vibration modes having the same harmonic index. On the other hand, the effect of all different Nodal Diameter configurations will be different: for a specific **EO** value, the focing term shape will be orthogonal to all other **ND** configurations. The orthogonality property can be read even the other way around, meaning that all modes related to a specific **ND** configuration are orthogonal to all forcing terms having $EO \neq ND$.

3.7.1 Aliaing Phenomenon

By recalling Eq. 3.10, the maximum value of Nodal Diameter configuration is set by the stage number of blades. However, this does not mean that blades cannot be excited with a forcing term having $EO > ND_{max}$, as defined in Eq. 3.10. Any EO with value defined by the second term of Eq. 3.18 is capable of exciting a blades' row thanks to the *Aliasing* phenomenon. As the blade along a rotor do not represent a continuous system but a discrete one, they sample the forcing term with a finite number of points.

As shown by Figure 3.7.1, the wave representing the $EO = 24$ is seen by the row of blades as a wave been represented by a $EO = 8$. This important mathematical phenomenon allows the correlation of high **EOs** to the right Nodal Diameter configurations, even when they exceed the maximum value set by Eq. 3.10.

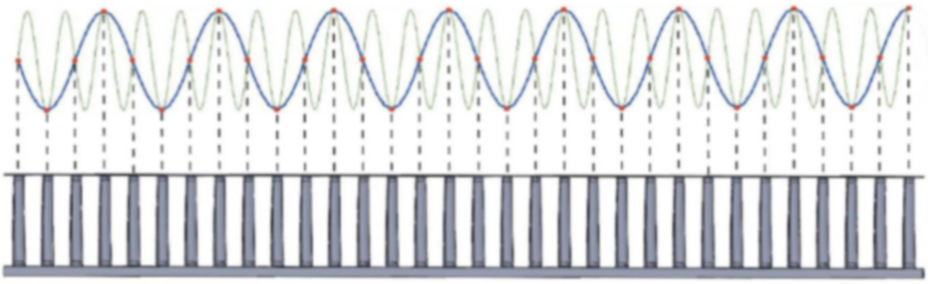

Figure 3.19: Schematic Representation of the *Aliasing* phenomenon of a blades' row Source [10]

Chapter 4

Aeromechanical Instabilities

Among the various phenomena that take place in a engine rotor system, the aeromechanical instability takes a very high importance for various reasons: the instauration of the so called *Flutter* phenomenon allows the blade vibration to turn auto-excited, where the gas flow operates a "negative" damping over the blade. This means that the gas flow does not dissipate the vibrations but rather enhances the amplitude. This instability is to be carefully studied as it may lead to unexpected fatigue rupture phenomena.

4.1 Fluid Flow - Vibration Modes Interaction

The Aeromechanical instability named as *Flutter* is a phenomenon [22] taking place in various components where the aerodynamic interaction with an elastic structure covers an important role. Flutter occurs when, subsequential to an initial structure displacement the fluid enhances the vibration rather than dissipating the vibration mode. the vibration amplitude enhancement may take to the structure rupture even before the fatigue classical analysis had predicted. The discipline that studies the interaction between modal behaviour of a structure with the fluid flow is called *Aeromechanics* or *Aeroelasticity*. In order to better visualize the different components the Aeromechanics is composed by it is useful to have a look at the graphical visualization Collar proposed in 1946 [21] [32].

The so called *Collar Diagaram*, shown in Figure 4.1, highlights the various interaction between differe engineering disciplines, each one covers an important role for the understanding of the Flutter phenomenon. The diagram, even called *Collar Triangle*, sees the main discipline actors being placed at the triangle vertices, whereas the intersection identifies the identifies the interaction between the disciplines. More in details:

- Aerodynamics: this is the discipline studying the static and dynamic behaviour of the gas flow

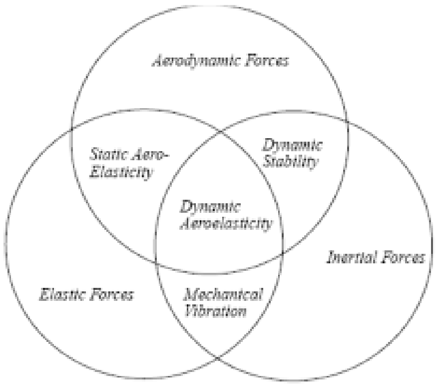

Figure 4.1: Collar Diagram [46]

- Elasticity: this is the discipline studying the reaction forces an excited structure creates when a load is applied on its surface
- Inertia: this is the discipline where the inertial effects of the applied loads are studied

As far as the intersection are concerned:

- Mechanical vibration, as explained in Chapter 3, deals with the modal simulation problem. A structure, when excited, produces vibration phenomena according to the nature of the exciting term and to its material properties
- Dynamic Stability is the study of the interaction between inertia forces and aerodynamic flow
- Static Stability is the study of how elastic forces and aerodynamic flow interact
- Finally, Aeroelasticity is the field where all the previously explained components merge. The interaction between the elastic forces, the inertial forces and the aerodynamic forces may lead to the instauration of the Flutter physical phenomenon.

Among the interactions that have been itemized above, a few particular categories can be identified:

1. Static problems category, where inertia forces are not involved
2. Dynamic problems category, where inertia forces are involved

Each one of the above mentioned category can be further divided in:

1. Aeroelastic Stability is the specific sub-category where no external forces are taken into account

2. Aeroelastic Response is the specific sub-category where external forces are applied on the system

The Flutter phenomenon is identified within the dynamic aeroelastic stability sub-category. The origin of this phenomenon may be due to the detach of the fluid flow from the airfoil or the detach of the Wake Vortex from the **LE** that cause auto-excited vibrations. In the first case *Stall Flutter* is taken into account, whereas in the second case the nature of the phenomenon depends on the **Re** number value (*Vortex Shading*, *Galopping* or *Transonic buffering*). As far as turbine rotor blades are concerned, the Stall Flutter is the most dangerous one, whereas the other types do not usually create structural problems. Despite the Stall Flutter may be described in may forms, according to the specific nature, and according to various physical models, the current report will focus its attention on the *Classic Flutter* semi-stationary model, whose details will be provided through Section 4.2.

4.2 Classic Flutter Model

As stated in Section 4.1, despite the Flutter phenomenon occurs in various forms, the Classic Flutter model is the one the identifies the most the aeromechanical instability issues within turbomachines.
As described in Section 4.1, the aeroelastic issues take origin from the interaction among various forces and according to the studies carried out by Y.C. Fung [27], these interactions can be represented by functional diagrams. By taking into account a simple aerodynamic structure, i.e. the airfoil structure represented in Figure 4.2, it may withstand three major actions:

1. Aerodynamic Function. The aifroil shape the strucutre is characterized by, together with the stagger angle α that geometrically connects with the fluid flow direction, allows the generation of two major forces. The first one, identified with letter **L**, is the lift force, allowing the rotor to spin or the aircraft to take off. The second one, identified with lettr **M**, is the moment whose properties depend on the boundary conditions the structure is subject to.

2. Elastic Function. Provided the elastic property of the material (identified by Elastic Modulus, Poisson Ratio, Tortional Stiffness, etc...), when the structure is subject to a moment **M** a tortional effect about its axies is experienced by and angle θ

3. Interial Function. The aerodynamic structure is characterized by its mass and geometry properties, that, all together, compose the inertial forces. Whenever the

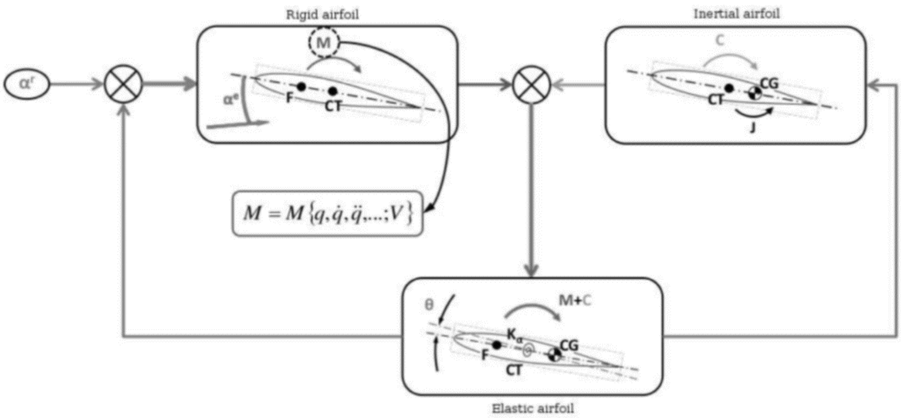

Figure 4.2: Flutter forces interaction diagram - [27]e

structure experiences an acceleration, the response is an inertial force/moment as an output.

It is worth mentioning that the cause-effect loops represented in Figure 4.2 take place at the same moment: inertial and aerodynamic forces excite the structure at the same time. The elastic response of the structure, on the other hand, changes the configuration of the profile, which means that the effet of the aerodynamic forces acting on the airfoil will have a different effect. These loop continuously repeat and by doinso they create a highly non-linear problem. This is the reason why the most complex models for Flutter analysis require a high computation power (as it will be seen through Section 4.4) and model simplifications are ofthen required.
Let us now consider the interaction between the fluid flow and the aerodynamic structure, provided that the geometric configuration of the structure has been fixed with an angle $\alpha = 0$. In this situation the aerodynamic forces acting on the airfoil mainly depend on the relative geometric configuration and on the velocoty of the fluid. The velocity V_{fluid}, in particular, is a key paramenter since it plays the role of the system critic parameter. Depending on its value, there may take place three different situations:

1. $V_{fluid} < V_{cr}$ any vibration is aerodynamically damped, which means that no aeroelastic instability occurs

2. $V_{fluid} = V_{cr}$ any vibration is aerodynamically sustained, meaning that an instability condition is set

3. $V_{fluid} > V_{cr}$ any vibration is aerodynamically amplified: the fluid enhances the vibration amplitde up to a point where the structure collapses

Let us now further investigate the instability model by taking into account the airfoil structure represented in Figure 4.2. This model features two DOFs, being the angular position θ and the vertical position h.

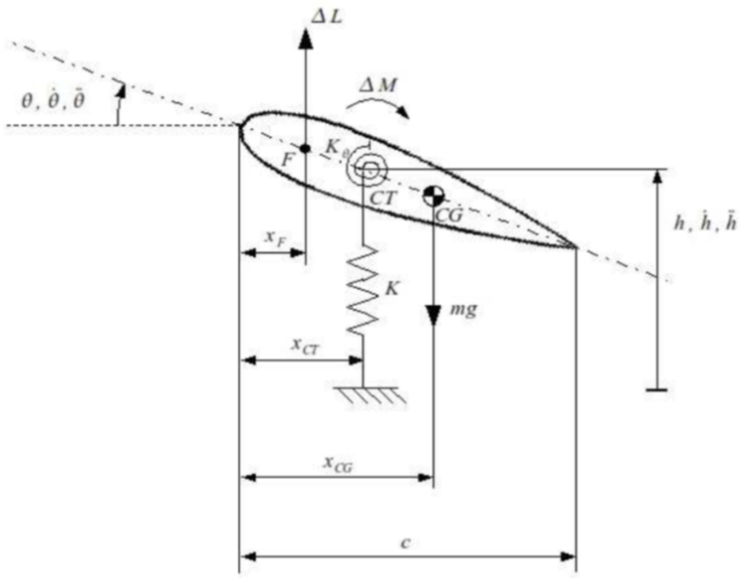

Figure 4.3: Schematic Representation of AF structure excited by aeroelastic forces [11]

By writing the balance equation for both DOFs, one obtains [11]:

$$\begin{cases} m\ddot{h} - S_\theta\ddot{\theta} + Kh = L \\ -S_\theta + I_\theta\ddot{\theta} + K_\theta = M \end{cases} \tag{4.1}$$

where we can define the first order static moment as:

$$\int_m (x - x_{CT})\,\mathrm{d}m \tag{4.2}$$

and the second order inertia moment as :

$$\int_m (x - x_{CT})^2\,\mathrm{d}m \tag{4.3}$$

Now let us consider a simplified aerodynamic model to express the lift force L. In this case the model can be defined as quasi-steady-state: in this model both the lift force L and M are taken as constant values, whereas the time dependant variable is represented by the stagger angle α [11]:

$$\alpha(t) = \alpha_0 + \theta(t) - \frac{h}{V_\infty} \tag{4.4}$$

By considering the parameter C_L and by recalling that the model is quasi-steady-state, we can write [11]:

$$C_L(t) = C_{L_\alpha}\alpha(t) \tag{4.5}$$

Now let us consider again eq. 4.1 by taking into account only excitation component, lift L and moment can be written as [11]:

$$\begin{cases} L(t) = q_\infty c C_{L_\alpha}\left(\theta - \frac{h}{V_\infty}\right) \\ M(t) = q_\infty c^2 C_{L_\alpha}\left(\theta - \frac{h}{V_\infty}\right)\left(\frac{x_{CT}}{c} - \frac{1}{4}\right) \end{cases} \tag{4.6}$$

. where:

- q_∞ is the dynamic pressure
- c is the airfoil chord length

Moreover we can act the followign replacement to obtain the adimensional coordinates of $x\tilde{_{CT}}$ [11]:

$$x\tilde{_{CT}} = \frac{x_{CT}}{c} \tag{4.7}$$

It is now possible to replace Eq. 4.6 into Eq. 4.1, and by writing the resulting equations in matricial form, we obtain [11]:

$$[M]\{\ddot{q}\} - [D_{AER}]\{\dot{q}\}([K] - [K_{AER}])\{q\} = \{0\} \tag{4.8}$$

where we can define:

$$[K_{AER}] = q_\infty c C_{L_\alpha}\begin{bmatrix} 0 & 1 \\ 0 & c\left(x\tilde{_{CT}} - \frac{1}{4}\right) \end{bmatrix} \tag{4.9}$$

By recalling what has been stated in Section 4.1, the fact that Eq. 4.8 is a homogeneous equation perfectly respects the nature of aeroelastic problems, where external exvitation are not taken into account.
If one was to solve the eigenproblem expressed with Eq. 4.8, a series of eigenvalues and eigenvectors can be found. The structures response vector, by taking into account a harmonic response, can be written as [11]:

$$\{q\} = \{\overline{q}\}e^{\omega t} \tag{4.10}$$

By parametrizing Eq. 4.10 by means of fluid velocity V_{fluid}, it is possible to derive the critical parameter V_{CR}, even called *Flutter Velocity*. By setting the osciallations period as T, we can define the log decrement δ as the ratio between the response amplitude at time (t) and the response amplitude at time (t+T) [11]:

$$\delta = \frac{\{q(t)\}}{\{q(t+T)\}} = \frac{\{q\}\, e^{(\omega_r + j\omega_i)t}}{\{q\}\, e^{(\omega_r + j\omega_i)(t+T)}} = -\omega_r T = -2\pi \frac{\omega_r}{\omega_i} \tag{4.11}$$

the parameter δ plays a crucial role in determining the presence of Flutter instability. The aeroelastic instability takes place whenever the real part of an eigenvalue changes sign. This eigenvalue sign change translates into a sign change in δ as well. Therefore, since δ is parametrized by means of the fluid velocity, the value of V_{fluid} that causes a sign change in δ is the critical velocity that causes the Flutter instability, or *Flutter Velocity*.

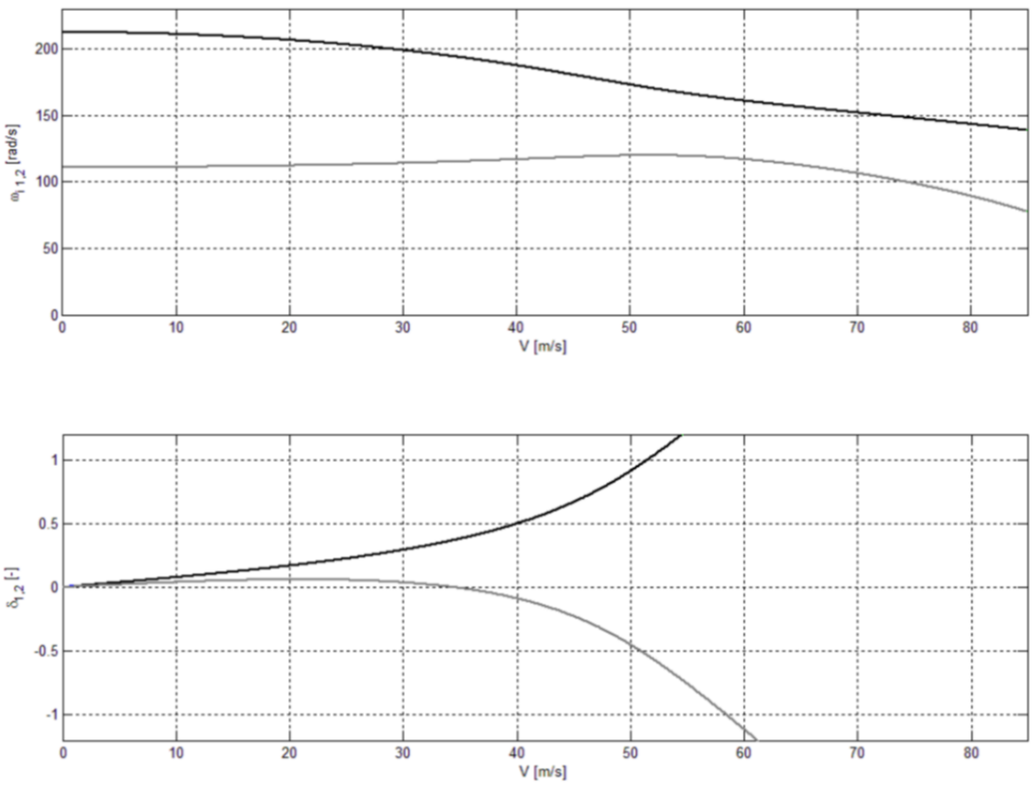

Figure 4.4: Flutter instability parameter depending on Fluid Velocity Source [11]

4.3 Flutter in Turbomachines

The case that has been taken into account through Section 4.2 is among the simplest models that can be used to describe the Flutter phenomenon. In spite the main physical meaning of the model remains valid, the same "simple structure" approach cannot be used for the aeroelastic study within turbomachines. Not only the beahvaiour of turbomachines is highly different from a simple aerodynamic structure [41], but there are various factors that turn the problem to highly non-linear. Among the most important reasons why the problem in the field of turbomachines is more complex is that the fluid flow is far from being developed in the blade sorrounding. The model that has been considered in Section 4.2 features a fluid flow with a fully developed velocity and pressure field in the sorroundings of the airfoil. However, the fluid fluid within aviation engines is highly perturbated due to the presence of adjacent blade within the same row (see Figure 4.3) and the adjacent rows within the turbine module, i.e. the different stages (see Figure 4.3).

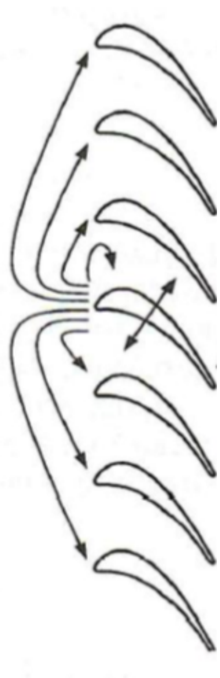

Figure 4.5: Aerodynamic Coupling due to adjacent blades presence [41]

The phenomenon where the fluid flow exciting the i-th blade is alterated by the presence of the adjacent blades and adjacent rows is called *Aerodynamic Coupling*. Both Figure 4.3 and Figure 4.3 give an insight of the Aerodynamic coupling effect within turbomachines.

The above described phenomenon adds high non-linearity effects to the Flutter problem, which would be hard to solve numerically. This is why a simplification is done in order to reduce the order of complexity of the problem. More specifically, the vibration modes of the blades are problem input data that are not affected by the aerodynamic

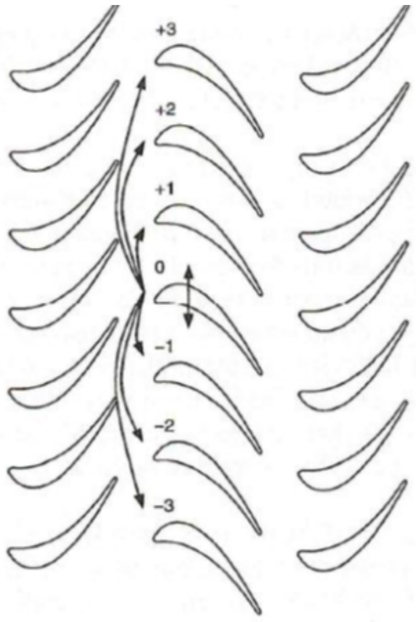

Figure 4.6: Aerodynamic Coupling due to adjacent rows presence [41]

loads on the profile. The eigenproblem is solved before the aeroelastic behaviour is considered and eigenvalues are considered to get a null effect from the aerodynamic perturbation. The aeroelastic problem, therefore, takes into account the aerodynamic perturbation vibration modes induce on the fluid flow. From this point, as it will be seen through Section 4.4, the purpose is computing the energy exchange between blade structure and fluid flow, represented by a coefficient being named as *Aerodamping*. By taking into account the latter, there may be two situations:

1. The energy exchange between fluid flow and blade structure is represented by a positive Aerodamping coefficient, which means that the blade loses energy towards the gas. In this case the fluid is able to damp the vibration modes and the Flutter condition is **Stable**.

2. The energy exchange between fluid flow and blade structure is represented by a negative Aerodamping coefficient, which means that the blade-fluid interaction allows the gain of energy from the blade's perspective. In this case the vibration is enahcned by the fluid flow. The oscillations amplitude increase and the condition is said to be Flutter **Unstable**.

Despite the aerodynamic coupling is among the most important factors that influence the aeroelastic instabilities within turbomachines, there are various others that should be taken into account. According to A.V. Srinivasan [41], there are at least 20 factors playing an important role in the aeromechanical problem within turbomachines. Among these, it is worth mentioning:

- shroud: it is capable of damping virbations thanks to friction effects.
- peak loads: they have a specific role on pressure fields in the LE and TE areas
- thermofluid-dynamic conditions at inlet-outlet cross sections
- reduced frequency: it is defined as "*ratio between the time it takes to a fluid particle to flow along the semi-chord and the time it takes to a blade profile to complete a vibration cycle*" [41]

  $$k = \frac{c\omega}{2V} \tag{4.12}$$

  High k values identify a quasi-steady-state fluid flow, which is likely to stabilize aeroelastic phenomena.
- IBPA: as it has been defined in Chapter 3, the IBPA has a key role in aeroelastic problem since it identifies the level of coupling between blades' vibration modes.
- mistuning: as it will be seen through Chapter 5, the presence of mass/stiffness asymmetry pattern has a high stabilizing effect on Flutter phenomena.

The approach that is used for the solution of the aeroelastic problem is the computation of the unsteady aerodynamic forces acting on the blades' profile. The problem is linearized since no effect of the fluid on the vibration modes is taken into account. Moreover, the behaviour of the blades is considered to be same but phase by the IBPA angle. This considerations reduces the complexity of the problem and allows an easier, but not less precise, solution to the Flutter analysis. The linear approach to the problem requires a deep understanding of the IBPA importance. By taking into account N_b blades, oscillating with the parameters coming from the eigenproblem solution, their effect on the fluid flow is linearly superposed. Each blade's response will be caused by its own effect on the fluid and by the effect of the adjacent blades, phased by the IBPA angle.

It is possible to better visualize the importance of the IPBA by looking at Figure 4.3. As highlighted by the first plot, the effect of blade 0 on itself is constant for any IBPA value, whereas the adjacent rows (see second and third picture) have a different effect on blade 0 according to the IBPA angle. It is clear that only the blade profiles being "close" to blade 0 have a relevant influence. This effect can be superposed and the result can be seen within an *Aeroplot*, where the Aerodamping coefficient is plotted against the various IBPA values, usually ranging from -180° to +180°. An example of Aeroplot is provided by Figure 4.3. Here, we may identify a Flutter instability (i.e. where the Aerodamping value is negative) fro IBPA values ranging from 150° to -30°.

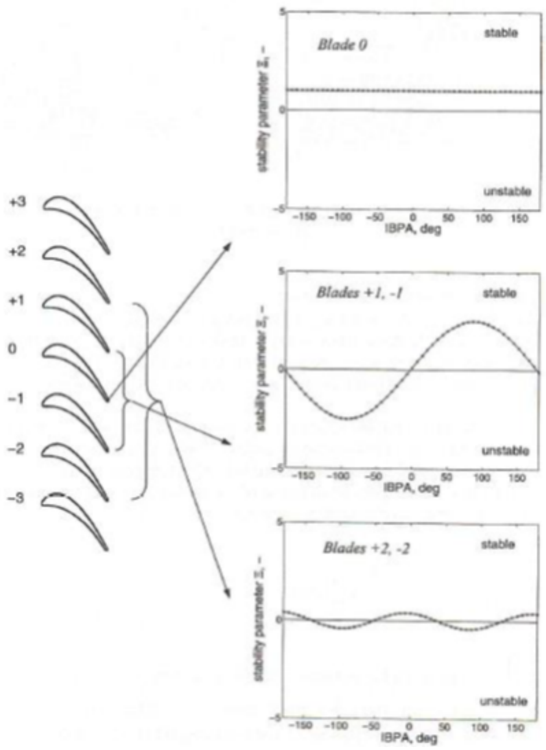

Figure 4.7: Influence of Adjacent rows on Blade 0, according to different IBPA values [41]

4.4 Autoflutter

The flutter analysis, whatever physical model is chosen, requires a high amount of complex equations to be solved both analytically and numerically. The complexity of the model is not only given by the interaction of a CFD with a FE modal analysis, but even by the high number of FE elements/nodes **BDs** are usually composed by. The first model simplification implies the deletion of all FE entities not being part of the aerodynamic profile, since there will not be any major fluid interaction in areas such as shank, disk, dovetail, etc...In spite of this major simplification that takes into account only the 2D "skin" mesh of the blade profile, usually turned back to first order to further reduce the complexity of the problem, aeroelastic computation still requires significant computation efforts. *Autoflutter3D* (herafter called only *Autoflutter* or *ATF*) is an in-house developed software tool capable of simulating the flutter conditions of LPT components. The tool, not only has been developed in with a specific coding structure that allows a significant saving in terms of computation time and power, but ensures significantly good precision of results, when these are compared with experimental tests.
Despite the tool is capable of performing analysis over both rotor and stator components

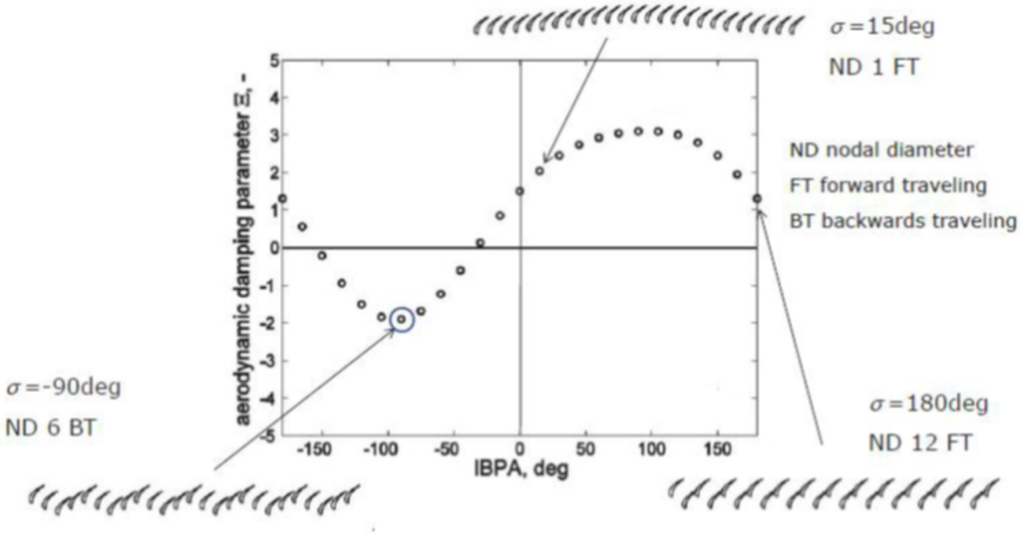

Figure 4.8: Example of Aeroplot, where Flutter instability occurs for $IBPA = [-50; -30]$ [11]

(i.e. complex or real vibration modes), the attention during the current section will focus on the complex section only.

The scheme shown in Figure 4.4 provides a general insight of how the tool works in consequential order and how the code is structured. Input files, required by the tool, are set on the left-hand side, while post-processing output files are listed on the right-hand side. It is worth that there is clear distinction among processes from an IT point of view: while the pre-processing and post-processing steps are usually run locally, the actual computation of aerodynamic and aeromechanical conditions is performed on HPC services, that provide higher computation power and thus allow significant time savings. The exchange of data between the locally run ATF software and HPC installed exe computation files is performed by means of .tar archives, where model data are stored. TAR archives are similar to .zip folders, but are usually specifically handled by UNIX OS run systems. In fact, despite most of the ATF code is based on simple exe files, the folder is handled in UNIX Bash Shell coding format, which allows a faster performance of basic file handling functions (copy, move, link, remove, cat, etc...)

The different parts of the software functioning process are accessible via a user-interface called *Shellassist*, represented in Figure 4.4. With the various buttons and input boxes in Shellassist, the user may either activate a specific software step or provide input during the computation. Despite the procedure of the software is currently undergoing a coding update to make it as automatic as possible, there are specific parts of the process

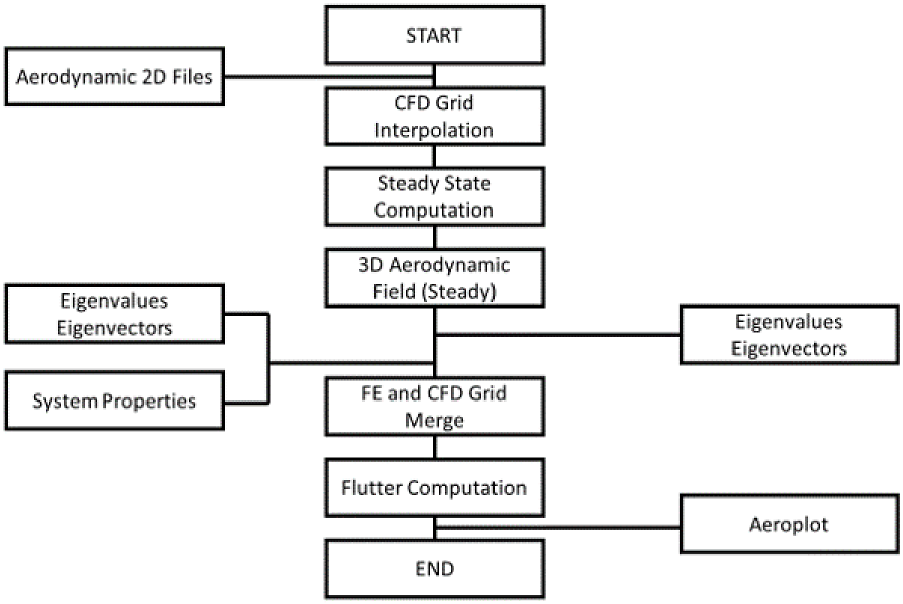

Figure 4.9: Flowchart showing ATF functioning structure

that still the user's action on the working folder. These actions are basically aiming at making the files' structure "recognizable" by the ATF code and can be done by manual transfer of files or files' renaming. In the following Subsections, a deeper insight of how the different parts of tool work will be provided.

4.4.1 Steady-State Conditions Computation

The first step of the tool computation process involves the definition of aerodynamic properties 3D field. The starting point of this part is a set of preliminary aerodynamic files, usually called *multirow* files, that provide all the information about the 2D profiles spanning from the lower fillet (Hub) of the blade's profile to its upper fillet (Tip). The profile is usually divided in 9 sections (airfois), even though a higher amount is possible. At each span thermo-fluid dynamic properties are defined, with specific attention to Inlet and Outlet Cross-sections.
The first action that ATF performs is the interpolation of geometric data of the different airfoils in order to create the CFD Grid. The following steps involves the matching of geometric information with thermo-fluid dynamic data contained in the relevant files. During this part the actual steady-state computation input files are prepared and compressed within a .tar archive, called **Steady.tar**. This file not only contains the relevant

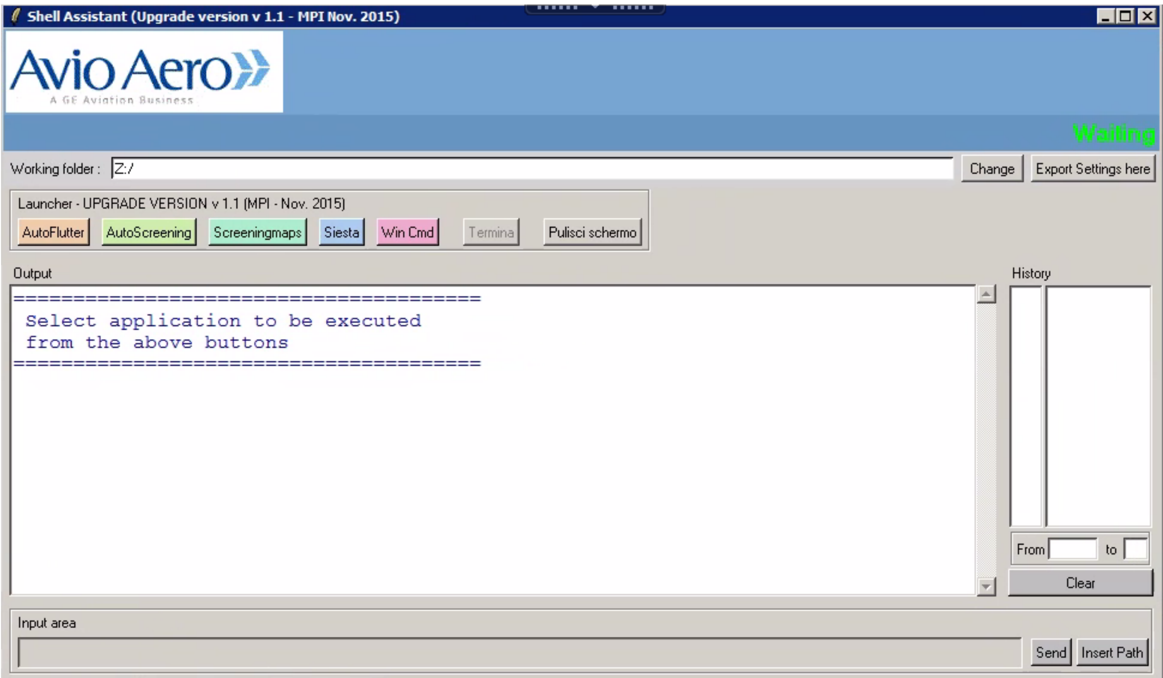

Figure 4.10: Autoflutter user interface, called *Shellassist*

data on the computation to be launched, but includes specific instruction files for HPC servers. These files are particularly important to activate the right processes on the online servers, with the launch of the specific computation exe files, required for the specific analysis.
After the HPC server performs the computation, a DONESteady.tar is generated and extracted in ATF working folder. Within this new archive the steady-state files are contained and can be post-processed by the specific ATF functions. Among the checks that are to perfomed by the user at this stage, the comparison between multi-stage and mono-stage results takes particular importance. It provides a good indication of aerodynamic results reliability.

For example, the results shown by Figure 4.4.1 shown that there is almost complete overlay between multi-row and single-row curves at all radial spans. The good results aproximation when only a single-row is considered makes the whole aeromechanical analysis computation reliable in terms of precision with respect to real engine conditions.

4.4.2 Unsteady Conditions Computation

The starting point of this section is the 3D fields of aerodynamic properties, whose computation has been described in Section 4.4.1. The main purpose of this section is the merging of FE and CFD grids in order to perform the aeroelastic simulation according

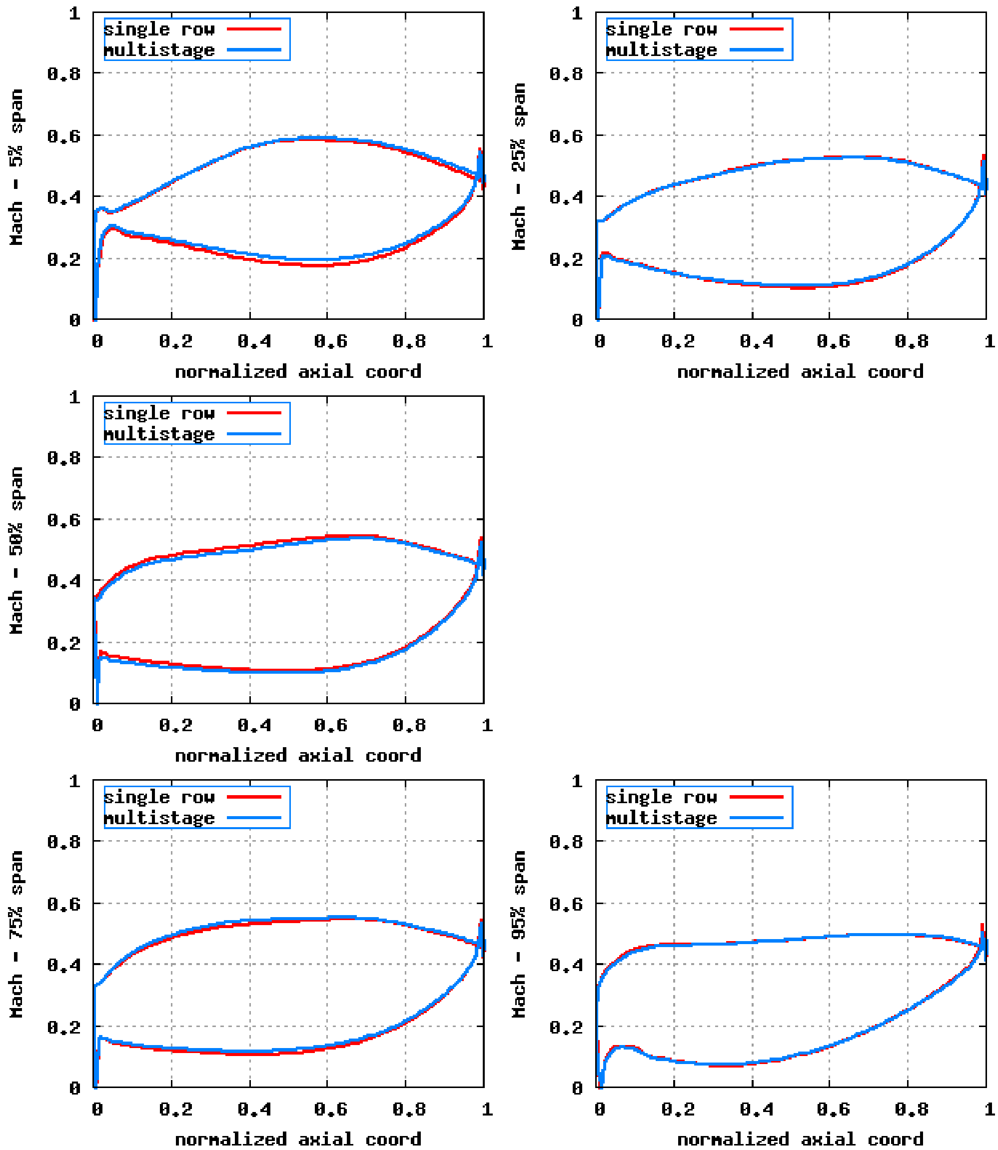

Figure 4.11: Example of Mach Results at different spans provided by Steady-State computation

to Figure 4.2.
Apart from the steady-state files, the input data of this part come from the modal analysis of the BD model. As mentioned in the previous sections, the reduction of entities is a key factor for an efficient computation: for this reason, the FE grid should be decreased to 1st order (tria3 elements) and only the external nodes belonging to the aerodynamic profile of the blade should be included in report files, since that is the only part where a

proper matching between FE and CFD grids is possible. The modal analysis report files are divided in three main categories:

- tmesh files: containing the information regarding how the mesh is structured (i.e. what nodes make the tria elements)
- bnlist files: containing the undeformed location of mesh nodes. This file should include two nodes in cyclic symmetry, that will be used to calculate the IBPA sign of vibration modes
- bXX file: containing the eigenvalues and eigenvectors of vibration modes, at different Nodal Diameter configurations. They include nodes in cyclic symmetry

With regards to the ND (harmonic index) the modal analysis should be based on, the choice is completely up to the user. However, a good choice would be selecting harmonic indeces able to equally span the IBPA from -180° to 180°. Usually, 13 different indeces are picked, by following the relation provided by Eq. 6.2.

$$ND = \frac{N_b \cdot IBPA}{360} \tag{4.13}$$

Further information with regards to the analysed system can be provided within he fem-reference.txt file: More in details, this files contains:

- Units FE model is based on
- Information regarding the orientation of coordinate frames
- Information regarding the direction of rotational speed
- ID of Nodes in cyclic symmetry
- Blade material properties

These data are used to act proper shiftin/rotating/scaling on the two grids in order to match their geometric coordinates. The goodness of this process can be checked by mean of neutral files that are generated by tool. These files contain geometric points location that can be added on the specific CAE software where modal simulations have been performed: the right location of these point with respect to blade's structure can be easily identified on display.
The following steps the unsteady part involves the computation of the IBPA sign for each mode at each ND configuration. This procedure is performed by specifically exe files, launched locally by ATF main code. It is always a good habit to check that the IBPA sign (and absolute value) respect what one can expect (see Chapter 3). After this part, the modeshapes.dat files are generated by relevant exe files, where vibration modes data

are stored in binary format. This allows a quicker handling of the information by HPC computation files. After the generation of modeshape.dat files, ATF starts the writing of various instruction files that are to be submitted online, together with summary files containing information regarding both the CFD and FE grids.
The whole set containing the model information and instruction commands is compressed in a Flutter.tar archive and submitted to HPC servers. After the computation is complete, results can be downloaded by means of DONEFlutter.tar, and relevant files extracted in ATF working folder. Post-processing of aeromechanical conditions is locally done directly by ATF. The final outcome of the tool procedure is generation of the relevant aeroplots, containing aerodamping values at the chosen IBPA (ND configuration). An example of Aeroplot generated by Autoflutter is shown in 4.4.2.

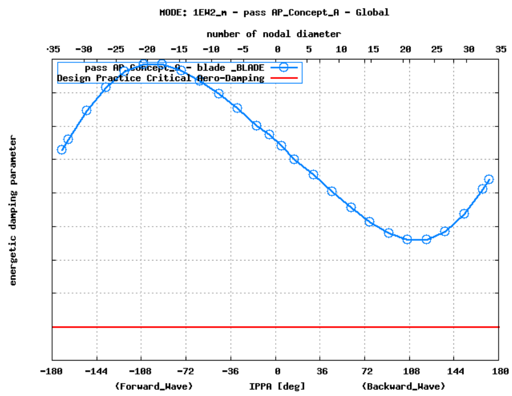

Figure 4.12: Example of Aeroplot generated during Autoflutter Post-Processing procedure

Chapter 5

Mistuning

Generally speaking, the word *Mistuning*, applied to turbomachinery, refers to the introduction of asymmetries in terms of mass and/or stiffness along the rotor that are able to produce a frequency shifting and splitting of vibration mode [14]. Recent studies have found that, when mistuning is intentionally applied according to specific mass and/or stiffness targets in terms of asymmetry value and asymmetry location, the vibrations modes that occur can cause a stabilizing effect over the Flutter phenomenon. The current chapter aims at providing not only an insight of how the various Mistuning studies have developed over the last decades, but even what is the mathematics between the stabilizing effect the technology introduction guarantees[16].

5.1 Effects of Mistuning

Generally speaking, despite the objective of this report is the description of the stabilizing effects of Mistuning over Flutter phenomenon, the technology introduction consequences cannot be considered either fully positive or fully negative. More specifically there are a series of parameters to be taken into account when one deals with mistuning. For example, despite the beneficial stabilization of modes will be proved, one cannot avoid considering the technology induces manufacturing and assembly complications, as well increases in the overall design and validation process Turbine rotors. As far as this report is concerned, the attention will be focused strictly on how intentional mistuning is capable of modifying the aeromechanical behaviour of engine rotors.

5.1.1 General Effects of Mistuing

The first evident effect of Mistuning introduction is a frequency shift of vibration modes. This shift have an influence on both the free response and on the forced response.

More in details what happens is that each natural frequency characterizing the all-tuned system gets divided in two different ω, which are similar in value, but different. This has an evident consequence on eigenvectors as well. The lack of perfect cyclic symmetry in the rotor system has a further effect: mistuned modeshapes are not perfectly described by the Nodal Diameter phenomenon (see Chapter 3). For each vibration mode taking place at a specific frequency values, there will an additional "disturbance" effect given by all the other modes. This disturbance takes effect by means of additional coefficients in the Fourier decomposition.

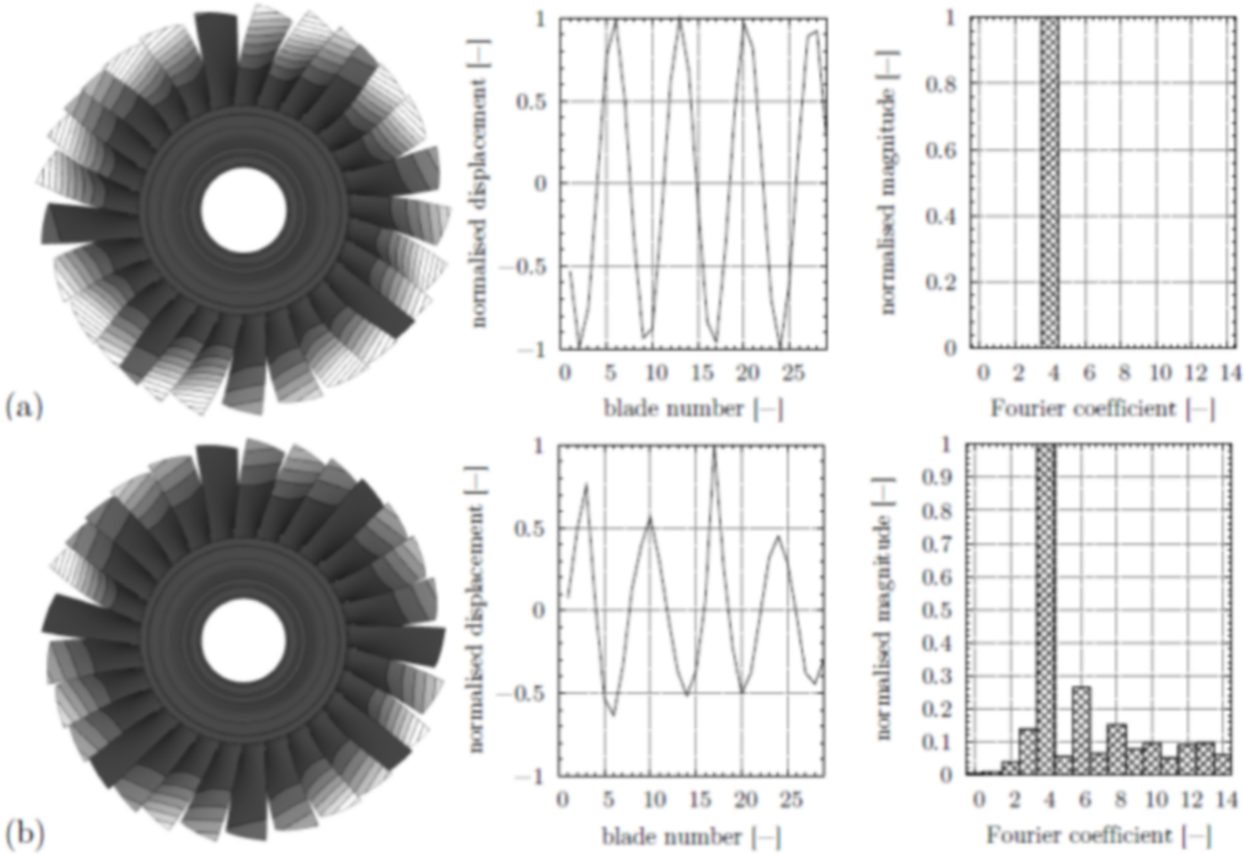

Figure 5.1: Generic Modeshape in an all-tuned (a) and mistuned (b) rotor [11]

By looking at Figure 5.1.1, the modal localisation effect (i.e. the vibration localisation referred to only a few blades) can be identified for the mistuned system. This effect is directly related to two parameters:

1. Interblade Coupling R

2. Mistuning Disorder Amount ϵ

$$localisation \propto \frac{\epsilon}{R^2} \tag{5.1}$$

The relation in Eq. 5.1 does not include the number of blades N_b, in spite several experimental tests conducted by Wei and Pierre [45], the effect is enhanced for a high N_b value.
The purely dynamic behaviour of the system is not the only affected one by the mistuning introduction. As a matter of fact, when the aerodynamic forces are taken into account to study the Flutter phenomenon in Turbomachines, mistuning induces several modifications even on the aerodamping parameter, expressing the actual energetic exchange between fluid and blade profile. Therefore, both real and imaginary eigenvalues (natural frequencies and aerodamping) are mistuning dependant, by means of both parameter R and parameter ϵ. By taking into account the eigenproblem for an all-tuned system and mistuned system with different ϵ grades, the results can be plotted, like in Figure 5.1.1, on the complex plane, reporting solution real part on the y-axis and solution imaginary part on the x-axis.

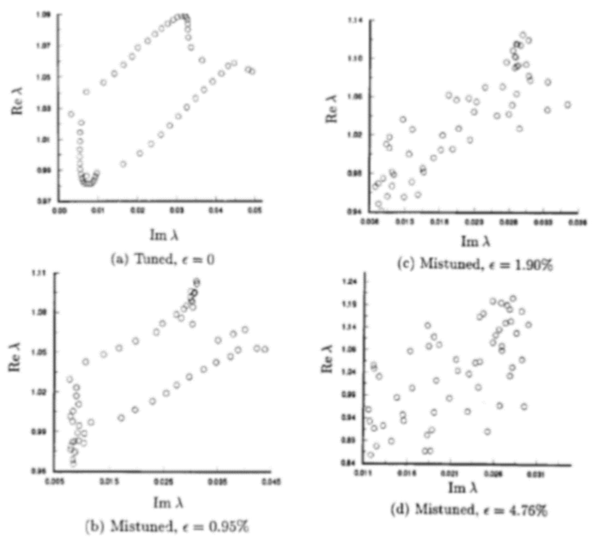

Figure 5.2: Eigenvalue Real and Imaginary part on the complex plain parametrized on the ϵ grade [11]

From Figure 5.1.1, one can notice the gradual appearance of a phenomenon called *loss of eigenstructure* [37]. While for the Tuned system (a), the eigenvalues seem to follow a well defined pattern, for increased ϵ grades, one can notice the gradual loss of the regularity, up to a point (d), where no specific regular trend can be identified.

Despite this phenomenon seems to be completely random and not following any specific rule, there is a clear feature that can be noticed, especially with reference to (c) and (d). On the one hand, real part of eigenvalues tend to diverge, with respect to case (a), while imaginary part of eigenvalues increasingly converges. This tendency is shown more clearly in Figure 5.1.1, where both real and imaginary parts of eigenvalues are plotted against the mistuning content ϵ.

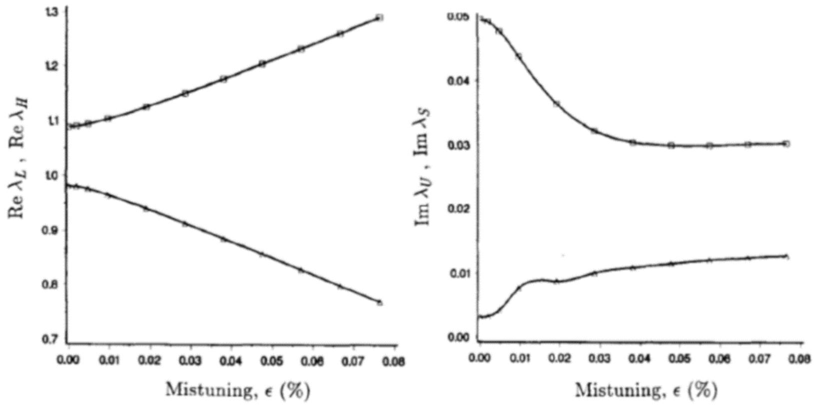

Figure 5.3: Trend of Real and Imaginary parts of Eigenvalues with respect to ϵ

5.1.2 Particular features of Alternate Intentional Mistuning

The considerations within 5.1.1 do not take into account the particular features that intentional mistuning technology cause. Despite several patterns have been studied in recent years, alternated mistuning constitutes one the most developed and studied way of introducing the technology within rotors [33] [42]. Not only this pattern minimizes costs and avoids the risk of mis-assembling, but it allows significant savings in computational power since only two blades are to be simulated in cyclic-symmetry. The sector that will be considered will therefore feature two different blade in a (0,1,0,1) pattern. The first effect of this configuration is the splitting of modeshapes in two different vibration modes: the first will refer to blade 0, while the second one will refer to blade 1. From a nomenclature point of view, a mode called **X** in an all-tuned system will split in:

- Mode **X**, referring to tuned blade 0
- Mode **X2**, referring to mistuned blade 1

The difference between the natural frequency of mode **X** and **X2** will be related to Δ in mass/stiffness. If referring Figure 5.1.1 or Figure 5.1.1, this will increase the rate of real part divergence and imaginary part convergence.

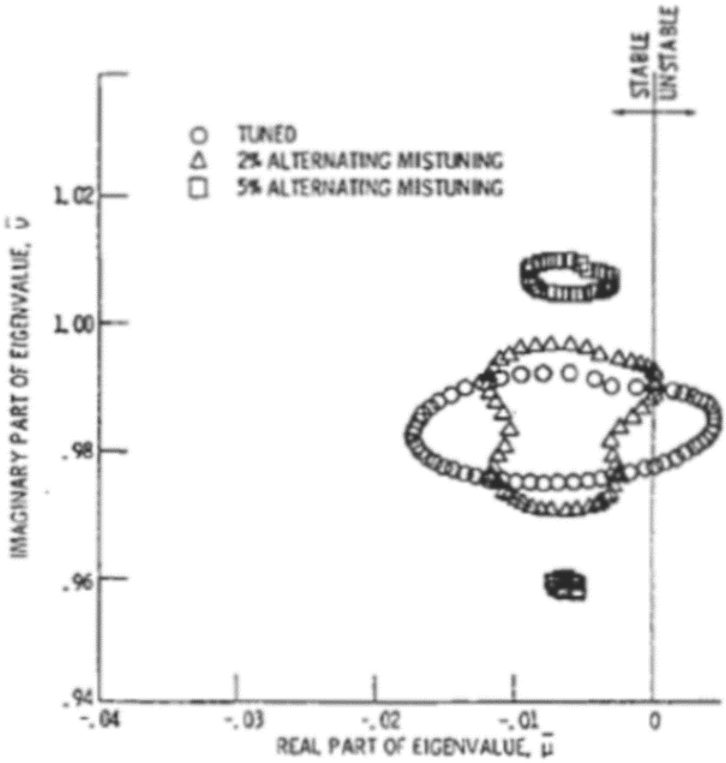

Figure 5.4: Eigenvalues on the complex plain parametrized over the alternate mistuning grade ϵ

As it will be seen in Section 5.4.1, the convergence of eigenvalues imaginary part leads to the stabilization of the unstable modes, on the one hand, and to a lower flutter stabilization of already stable modes, on the other hand. In other words, for increasing mistuning grades, the technology introduction will make the aerodamping values of two coupled modes tend to an aymptotic value, which may represent either a aeromechanical stable or aeromechanical unstable condition. From a more physical point of view, the stabilizing effect of this technology is caused by the coexistence of two vibration modes: when blades 0 vibrate, blades 1 are almost stationary (and viceversa). In this situation the displacements of vibrating blades (blades 0) constitute the only aerodynamic forces acting on stationary blades 1. These forces acting on the 0 modes have a stabilizing effect from an aeromechenical point of view [15].
By referring to the various analytical modesl that have been developed through the years [25], this report will focus its attention on AMM method, which is able to drastically reduce the number of DOFs through calculations, thus leading to considerable savings from computational power point of view. The AMM method, moreover, is considered

to be among the most precise analytical methods for systems characterized by alternate mistuning patterns [25].

5.2 AMM Method: Tuned System

Let us consider a rotor system being composed by N_b blades. The system will experience linear aerodynamic loads (L(x)), while the structural damping will be excluded since its effect is negligible with respect to the aerodynamic one. Let us now write the balance equation for the system [14] [31]:

$$M\ddot{x} + Kx = F_{aero}(t) \tag{5.2}$$

where $F_{aero}(t)$ represents the external aerodynamic forces acting on the blade, while the other terms have the same meaning that have described in Chapter 3.
The homogeneous eigenproblem can be written as[14]:

$$(K - \omega^2 M)X = 0 \tag{5.3}$$

By assuming a harmonic solution to Eq. 5.3, the modes can be written as[14][31]:

$$x = Xe^{j\omega t} + c.c. \tag{5.4}$$

where the notation c.c. indicates the complex conjugate. Now let us try to write in complete matricial form Eq. 5.3. It would read [14]:

$$\left(\begin{bmatrix} K & K_c & 0 & \cdots & K_c^T \\ K_c^T & K & K_c & \cdots & 0 \\ & \vdots & & \ddots & \\ K_c & 0 & 0 & \cdots & K \end{bmatrix} - \omega^2 \begin{bmatrix} M & M_c & 0 & \cdots & M_c^T \\ M_c^T & M & M_c & \cdots & 0 \\ & \vdots & & \ddots & \\ M_c & 0 & 0 & \cdots & M \end{bmatrix} \right) \begin{bmatrix} X_1 \\ X_2 \\ \vdots \\ X_N \end{bmatrix} = \begin{bmatrix} 0 \\ 0 \\ \vdots \\ 0 \end{bmatrix} \tag{5.5}$$

Each of the the terms composing the matrices present in EQ. 5.5 is a sub-matrix. Submatrices K and M are symmteric matrices being with dimension m x m, where m stands for the number of DOFs that each i-th sector, among the N_b sectors, features. On the other hand, sub-matrices M_c and K_c represent the coupling terms between different sectors. In case the anslysis would be dealt with in cyclic symmetry, it is possible to write the eigenvector in its complex solution, that would read[14]:

$$\begin{bmatrix} X_1 \\ \vdots \\ X_i \\ \vdots \\ X_N \end{bmatrix} = \begin{bmatrix} Z_k e^{j(2\pi k/N_b)_1} \\ \vdots \\ Z_k e^{j(2\pi k/N_b)_i} \\ \vdots \\ Z_k e^{j(2\pi k/N_b)_{N_b}} \end{bmatrix} k = 1 \ldots N_b \tag{5.6}$$

The vector Z_k present in Eq. 5.6 features the vibrations modes of the rotor sectors, that are characterized by a phase shift by $\frac{2\pi}{N}$. The whole system be hence expressed as a set of N_b equation, uncoupled among them and featuring dimension m, that would read as follows[14]:

$$\left(\left(K_c - \omega^2 M_c\right) e^{j(2\pi k/N_b)} + \left(K_c - \omega^2 M_c\right)^T e^{-j(2\pi k/N_b} + K - \omega^2 M\right) Z_k = 0withk = 1 \ldots N_b \tag{5.7}$$

By the set of equations being expressed in Eq. 5.7 one can obtain m eigenvalues for each of the k-th nodal diameter configuration.
Let us now define matrix P_k as follows:

$$P_k = \begin{bmatrix} Z_{k1} & Z_{k2} & \cdots & Z_{km} \end{bmatrix} \tag{5.8}$$

The use of matrix P_k, defined in Eq. 5.8 can be done to normalize mass matrices M. Let us now take into account the forcing term that had been identified in Eq. 5.2 with $F_{aero}(t)$. It represents the vector of aerodynamic loads acting on the blade and it is function of time. This load can be expressed as complex vector and can be described as a travelling wave with EO r and frequency Ω. Therefore, it would read:

$$F_{aero}(t) = Fe^{j\omega t} + c.c. = \begin{bmatrix} Fe^{j(\Omega t + (2\pi r/N_b)_1)} \\ \vdots \\ Fe^{j(\Omega t + (2\pi r/N_b)_i)} \\ \vdots \\ Fe^{j(\Omega t + (2\pi r/N_b)_{N_b})} \end{bmatrix} + c.c. \tag{5.9}$$

It is now possible to identify the complete system response with the generic form $\mathbf{X} = \mathbf{PA}$ where the terms $\mathbf{P}$ [14]and $\mathbf{A}$ [14] can be defined as follows:

$$A = \begin{bmatrix} A_1 \\ \vdots \\ A_i \\ \vdots \\ A_{N_b} \end{bmatrix} \tag{5.10}$$

$$P = \frac{1}{\sqrt{N_b}} \begin{bmatrix} P_1 e^{j(2\pi 1/N_b)_1} & \cdots & P_1 e^{j(2\pi N_b/N_b)_1} \\ \vdots & & \vdots \\ P_i e^{j(2\pi 1/N_b)_i} & \cdots & P_1 e^{j(2\pi N_b/N_b)_i} \\ \vdots & & \vdots \\ P_{N_b} e^{j(2\pi 1/N_b)_{N_b}} & \cdots & P_1 e^{j(2\pi N_b/N_b)_{N_b}} \end{bmatrix} \tag{5.11}$$

It is now important to describe the meaning both matrix A and matrix P_k hold. While the terms composing matrix P_k, defined in Eq. 5.8 express the vibration modes of the modal analysis conducted in cyclic symmetry (see Eq. 5.6), matrix A, defined in Eq. 5.10 defined the amplitude of the eigenvectors.
The forced problem can be expressed with the following eigenproblem expression:

$$(K - \omega^2 M)X = F_{aero}(\omega)X \tag{5.12}$$

or in its complete form[14]:

$$\begin{bmatrix} \Omega_1^2 - \Omega^2 I & \cdots & 0 \\ \vdots & \ddots & \vdots \\ 0 & \cdots & \Omega_N^2 - \omega^2 I \end{bmatrix} \begin{bmatrix} A_1 \\ \vdots \\ A_i \\ \vdots \\ A_{N_b} \end{bmatrix} = P^H F_{aero} P \begin{bmatrix} A_1 \\ \vdots \\ A_i \\ \vdots \\ A_{N_b} \end{bmatrix} \tag{5.13}$$

where $P^H F_{aero} P$ represents the diagonal matrix with the aerodynamic contribution. This aerodynamic correction matrix induces small effects on the merely structural natural frequencies. Let us take into account the i-th mode having eigenvalue ω_{ik} in the k-th Nodal Diameter configuration. If considering the aerodynamic correction, the new natural frequency ω would read[14]:

$$\omega = \omega_{ik}\left(1 - \frac{|M_k(\omega_i k)|_{ii}}{2\omega_{ik}^2} + \cdots\right) \tag{5.14}$$

where $|M_k(\omega_i k)|_{ii}$ represents the energy exchanged between exciting fluid and the blades. The expression in Eq. 5.14 is only valid under the following assumptions:

- Modes with different Nodal Diameter configuration are uncoupled and hence do not play any intereference role in the natural freqeuncy correction
- Terms $|M_k(\omega_i k)|_{ii}$ and $(\omega_{ik}^2 - \omega^2)$ are small and ω_{ik} is close to ω.
- The aerodynamic correction does not cause any correction of the eigenvectors

It is possible to explicitly write the energy exhange between fluid flow and blades in the generic form[14]:

$$|M_k(\omega_i k)|_{ii} = -2\omega_{ik}^2(\eta + 2j\xi) \tag{5.15}$$

By looking at Eq. 5.15 it possible to identify the aerodamping coefficient ξ, whose sign needs to be computed for each i-th mode in each k-th Nodal Diameter configuration in order to evaluate the flutter (in)stability condition of the rotor. In Section 5.3 the same approach will be used to analyse the *Mistuned* system, where a small Δ in mass and stiffness is introduced.

5.3 AMM Method: Mistuned System

The model that has been described through Section 5.2 can be developed in the case of a Mistuned sector, where the two Δ terms referring to the mass, ΔM, and stiffness ΔK are to be added to the balance equation expressed in Eq. 5.2. The whole problem solution can be derived by following a similar approach to the one used in Section 5.2 and by taking advantage of correction terms, where needed. By starting from the dynamic balance, the equation of motion would read as:

$$\Big((K + \Delta K) - \omega^2 \left(M + \Delta M\right)\Big)\, X = F_{aero}(t) \tag{5.16}$$

The two new matrices, ΔM and ΔM, appearing in Eq. 5.16 express the variation in mass and stiffness due to to the mistuning pattern. They are diagaonal matrices and can be expressed in their complete form as[14]:

$$\Delta M = \begin{bmatrix} \Delta M_1 & \cdots & 0 \\ \vdots & \ddots & \vdots \\ 0 & \cdots & \Delta M_{N_b} \end{bmatrix} \tag{5.17}$$

$$\Delta K = \begin{bmatrix} \Delta K_1 & \cdots & 0 \\ \vdots & \ddots & \vdots \\ 0 & \cdots & \Delta K_{N_b} \end{bmatrix} \tag{5.18}$$

In the development of the model the following assumptions will be made, without compromising a good precision of the results:

- $$\sum_{i=0}^{N_b} \Delta K_i = 0 \tag{5.19}$$

- $$\sum_{i=0}^{N_b} \Delta M_i = 0 \tag{5.20}$$

- $$\Delta K_i = \Delta K_i^T fori = 1 \ldots N_b \tag{5.21}$$

- $$\Delta M_i = \Delta M_i^T fori = 1 \ldots N_b \tag{5.22}$$

It is now possible to express Eq. 5.13 with regards to the mistuned model[14]:

$$\left(\begin{bmatrix} \Omega_1^2 - \Omega^2 I & \cdots & 0 \\ \vdots & \ddots & \vdots \\ 0 & \cdots & \Omega_N^2 - \omega^2 I \end{bmatrix} \begin{bmatrix} A_1 \\ \vdots \\ A_i \\ \vdots \\ A_{N_b} \end{bmatrix} + \Delta \right) = \begin{bmatrix} 0 \\ \vdots \\ P_r^H F \\ \vdots \\ 0 \end{bmatrix} \tag{5.23}$$

where Δ represents the correction matrix term caused by the mistnuning presence in the system. It can be expressed as[14]:

$$\Delta = P^H \left(\Delta K - \omega^2 \Delta M \right) P \tag{5.24}$$

It is possible to differentiate the term described in Eq. 5.24 in the component representing the one concerning the mass and the one concerning the stiffness with the Fourier series:

$$\Delta K_j = \sum_{k=1}^{N} \Delta K_k^F e^{j(2\pi k/N_b} i with j = 1 \ldots N_b \tag{5.25}$$

$$\Delta M_j = \sum_{k=1}^{N} \Delta M_k^F e^{j(2\pi k/N_b} i with j = 1 \ldots N_b \tag{5.26}$$

Let us now apply the conditions stated in Eq. 5.19, 5.20, 5.21,5.22 to Eq. 5.18 and 5.17. The formulation of Δ matrix would become:

$$\Delta = \begin{bmatrix} 0 & \Delta_{12} & \cdots \Delta_{1N} & \\ \Delta_{21} & 0 & \cdots \Delta_{2N} & \\ \vdots & \vdots & \ddots & \vdots \\ \Delta_{N1} & \Delta_{N2} & \cdots 0 & \end{bmatrix} \tag{5.27}$$

The submatrices contained in Eq.5.27 are linked to the definition provided throught the Fourier series by mean of the following expression:

$$\Delta_{ki} = P_k^H \left(\Delta K_{k-i}^F - \omega^2 \Delta M_{k-i}^F \right) P_i \tag{5.28}$$

It is worth mentioning that the matrix expressed in Eq. 5.27 contains off-diagonal terms. This means that the effects of mistuning are present only by taking into account the coupling of different Nodal Diameter configurations. This coupling between the waves having Nodal diameter configuration i and k, respectively, occurs only with the terms of the Fourier series having harmonic index k-i.
Let us now consider a forcing term $f(t)$ whose frequency is identified with ω_0. The value ω_0 is considered to be "far" from the natural frequency of a mode identified by the tuned

system. In this case, the correction, terms due to the mistuning presence will not have any significant impact on the whole system response.
One the other hand, when the natural frequency of the tuned system is close enough to ω_0, the terms related to the mistuning introduction cannot be neglected. The modes are said to be the *active* modes From Eq. 5.23 it follows[14]:

$$\left(\omega_a^2 - \omega^2 + 2j\zeta\omega\omega_a\right) A_a + \sum_{a' \neq a} \delta_{aa'} A_{a'} = F_a \tag{5.29}$$

where:

- A_a is the active mode amplitude
- ω_a is the natural frequency of the modes in the tuned system

Let us now express the coupling coefficients δ as follows[14]:

$$\delta_{aa'} = Z_a^H \left(\Delta K_{aa'}^F - \omega^2 \Delta M_{aa'}^F\right) Z_{a'} \tag{5.30}$$

where Z_a and $Z_{a'}$ are the eigenvectors of modes with amplitude A_a and $A_{a'}$ and Nodal Diameter configuration a and a'. The natural frequency of these active modes, again, is considered to be close to ω_0.
Finally, it is possible to introduce the frequency correction term $\omega = \overline{\omega}(1 + \Delta\omega)$ where $\overline{\omega}$ is the natural frequency up to the only structural problem, and $\Delta\omega$ is the frequency correction with ($|\Delta\omega| \ll 1$). By doing this, Eq. 5.29 can be written in a more convenient way[14]:

$$\left((\omega_a^2 - \omega^2) - 2\overline{\omega}^2\Delta\omega\right) A_a = -2\omega_a^2(\eta_a + 2j\xi)A_a - \sum_{a' \neq a} \delta_{aa'} A_{a'} \tag{5.31}$$

5.4 AMM Application

The introduction of intentional mistuning within the rotor system is performed with a target frequency *shift*. The asymmetries make the mistuned sectors vibrate with their own natural frequency. By modally simulating the dynamic behaviour of the mistuned rotor, it is possible to identify two different type of "close" vibrating modes, when their frequency is referenced to the mistuning frequency shift:

- Two modes are *isolated* when their natural frequency difference is higher then the frequency shift introduced through mistuning application
- Two modes are *clustered* when their natural frequency falls within the range of the mistuning frequency shift

5.4.1 Isolated Modes

In this case the two vibrating modes are only described by means of two counter-rotating waves (identified with symbols "+" and "-") in nodal diameter configuration $\pm k_0$. According to AMM method, these two modes are the only active modes. It is possible to identify these two modes as follows[14]:

$$-2\omega_0^2 \Delta\omega A_+ = -2\omega_0^2(\eta_+ + j2\zeta_+)A_+ - \delta_- \tag{5.32}$$

$$-2\omega_0^2 \Delta\omega A_- = -2\omega_0^2(\eta_- + j2\zeta_+)A_- - \delta_+ \tag{5.33}$$

where, for each $k\pm$ Nodal Diameter configuration:

- $A\pm$ represents the mode amplitude
- $\eta\pm$ represents the aerodynamic correction
- $\zeta\pm$ represents the modes damping

The off-diagonal terms that refer to the mistuning introduction can be written as[14]:

$$\delta = Z_{k0}^H \left(\Delta K_{2k0}^F - \omega_0^2 \Delta M_{2k0}^F\right) \overline{Z_{k0}} \tag{5.34}$$

It is possible to notice, by looking at Eq. 5.34, that the only harmonic index taking active part in the Fourier series is the one having value $2k_0$.
It is now possible to explicitly write the solution of the eigneproblem descried by either Eq. 5.32 or Eq. 5.33, with reference to eigenvalue $\Delta\omega_0$ [14]:

$$\Delta\omega_0 = \frac{(\eta_+ + \eta_-) + 2j(\xi_+ + \xi_-)}{2} \pm \sqrt{\left(\frac{(\eta_+ + \eta_-) + 2j(\xi_+ + \xi_-)}{2}\right) + \frac{|\delta^2|}{4\omega_0^4}} \tag{5.35}$$

The expression of eigenvalue $\Delta\omega$ expressed in Eq. 5.35 can be written in the generico form $\Delta\omega = \eta + 2j\xi$. In this generci expression what is most interesting from the flutter stabilization point of view is the term ξ that represents the aerodynamic damping (or aerodamping) coefficient. As expressed in Chapter 4, whenever the value of ξ (+ or -) is negative, an aeromechanical instability is taking place. The purpose of mistuning is turning both ξ_+ and ξ_- positive, so that the rotor system can operate in an aeromechanically stable condition. It is possible to explicitly write ξ with reference to the mistuning correction terms. It would read [14]:

$$\xi = \frac{\xi_+ + \xi_-}{2} \pm \frac{1}{2}\sqrt{\frac{\sqrt{a^2 + b^2} - a}{2}} \tag{5.36}$$

where:

- $$a = \frac{\eta_+ + \eta_-}{4} - (\xi_+ + \xi_-)^2 + \frac{|\delta^2|}{4\omega_0^4} \quad (5.37)$$

- $$b = (\eta_+ + \eta_-)(\xi_+ + \xi_-) \quad (5.38)$$

The term representing the mistuning amplitude is $\frac{|\delta^2|}{4\omega_0^4}$. It is possible to plot (see Figure 5.4.1) the value of ξ against the mistuning amplitude. In this way, it possible to visualize the point where the aerodamping value switches from negative to positive, identifying the mistuning pattern that stabilizes the rotor against the flutter instabilities: It can

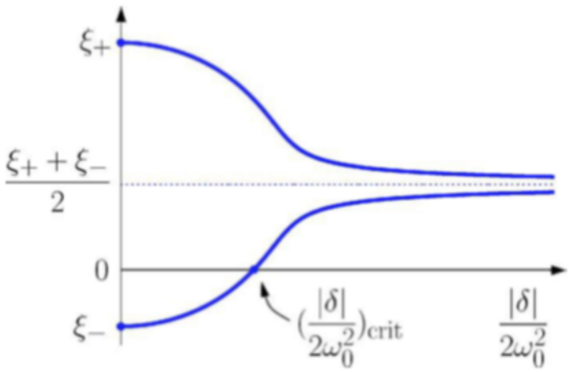

Figure 5.5: Aerodamping ξ_+ and ξ_- against mistuning amplitude - Source [14]

be seen from Figure 5.4.1 that fro a null value of $\frac{|\delta^2|}{4\omega_0^4}$ rotor is unstable. By increasing the mistuning amplitude a critical value, i.e. $\left(\frac{|\delta^2|}{4\omega_0^4}\right)_{cr}$, is reached. Fro this point of the flutter condition is stabilized. From increased values of mistuning amplitude the two ξ asimptotically tend to the average value at null mistuning. It is worth mentioning, by looking at the graph, that while the initially unstable modes tend to stabilize when mistuning is introduced, the opposite occurs for initially stable modes. By looking at the ξ_+ value, it can be noticed that it reaches less stable conditions at increasing mistuning amplitude values. In the case represented in Figure 5.4.1, the asymptotic value is anyhow positive, but this situation implies that the aeromechanical condition of initially stable modes should be always checked after the mistuning introduction in the rotor design.
The term $\left(\frac{|\delta^2|}{4\omega_0^4}\right)_{cr}$ plays a crucially important role in the work that is being presented in this report. As it will be seen during Chapter 6, this value represents the target Δ in mass that is to be added in the design process of the rotor.

5.4.2 Clustered Modes

The complex dynamic behaviour of an aircraft engine turbine rotor implies that some two subsequent modes may be fetauring a frequency difference that falls into the freqeuncy shift mistuning introduces. This is more common when modes high-density intervals are found. In this case, modes are classified as *clustered* and, according to AMM method, they play a less active role in the flutter stabilization due to mistuning presence. The effect when the rotor is excited within this interval can be considered as an average effect of all the modes within the interval. It is possible to write[14]:

$$\begin{bmatrix} d_k & & & & \\ & d_{k+1} & \Delta & & \\ & & \ddots & & \\ & \Delta^H & d_{k+1}^- & d_k^- & \end{bmatrix} \begin{bmatrix} A_k \\ A_{k+1} \\ \vdots \\ A_{k+1}^- \\ A_k^- \end{bmatrix} = [0] \tag{5.39}$$

With reference to Eq. 5.39, it possible to explicitly write the diagonal terms as:

$$d_i = \left(\omega_i^2 - \omega_B^2\right) - 2\omega_i^2\left(\eta_i + j2\xi_i\right) - 2\omega_B^2\Delta\omega \tag{5.40}$$

while the off-diagonal ones would read:

$$\delta_{kk'} = Z_k^H\left(\Delta K_{k-k'}^F - \omega_B^F \Delta M_{k-k'}^F\right) Z_{k'} \tag{5.41}$$

In Eq. 5.40 and in Eq. 5.41, the term ω_B is the average natural frequency active modes. The eigenproblem can be solved by looking at the value of $\Delta\omega$, that can be written in its general form as $\Delta\omega = \eta + 2j\xi$. Similarly to what has been stated in Section 5.4.1, the flutter stabilization problem aims at finding the mistuning amplitude values that turn the ξ term positive. The difference between the isolated modes case and the clustered modes case is that an average should be done when clustered modes are taken into account.

Chapter 6

Mistuning Stabilization of Flutter Unstable Rotor

The methodology explained through Chapter 5 has been applied to a real case study whose development is being described in the current Chapter. By starting from a geometry model representing a real engine rotor row, several preliminary analysis have been performed to benchmark the starting point of the project work. The analysis haven not been limited to the only flutter field, but aimed at providing a complete background of the structural behaviour of the engine. This benchmarking results to be very important in the moment introduces modifications to the geometry and a new validation process needs to started over. Results referring to the mistuned model can be thus compared to the ones obtained in the preliminary work, in order to point out the goodness of the CAD modelling, or highlighting what further studies are necessary to validate the process.
The model the project has started from will be identified with the name *Baseline*, or *BS*. Once the several simulation with regards to the BS models are performed, several methodologies of introducing Mistuning will be talked over by looking at design and manufacturing factors and two different Mistuned Sectors will be concepted in order to stabilize the Flutter occurrence at Baseline level. It is important to notice at this point that, due to the high amount of sensible data this project has dealt with, some of the results will be presented with a sanitation process been acted.

6.1 Definition of Baseline Model

6.1.1 Geometry

The starting point of the project is the definition of the geometry model that is to be benchmarked. The rotor row that is to be simulated represents the first stage Bladed Disk of an in-house developed engine module.

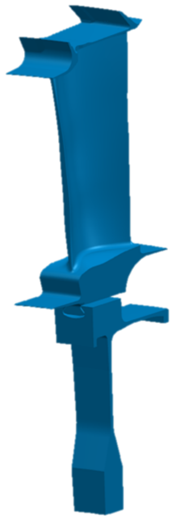

Figure 6.1: Geometric Model of Baseline Bladed Disk

It is worth mentioning that this model has a few important geometric features whose consequences can be noticed in its dynamic behaviour:

- As it will be seen in the following Sections Veering areas between system modes are common. This highlights the importance to perform a cautious Modal classification when creating either a FREND diagram or a Campbell Diagram, since a Frequency based classification may mix up modeshapes, with the result of obtaining non-precise results.

- The presence of these features sets difficulties in the meshing process of the model. More specifically, cavities are hard to mesh through automatic meshing tools. Especially when dealing when Static analysis, the importance of the meshing quality covers an important role. Therefore, Engine Blades usually require an increased attention to the meshing process that automatic meshing tools struggle to provide. This is why a manual meshing process has been adopted for this model, thus making sure results, particularly in Static analysis, will not suffer any problems due to bad meshing quality in high-stress areas.

6.1.2 Finite Elements Model

After the correct setting of CAD constraint definition and reference frame orientation (z axis aligned with engine axis), it is important to define the FE model by means of a meshing process. With reference to what has been described in Section 6.1.1, the meshing process has been performed manually. Hereafter, the most important meshing criteria that have been followed to obtain a good BD mesh are itemized:

- Mesh elements average sizing should be decreased in all areas where high stresses are expected. In this set of areas we may include:

  1. Dovetail Curvatures

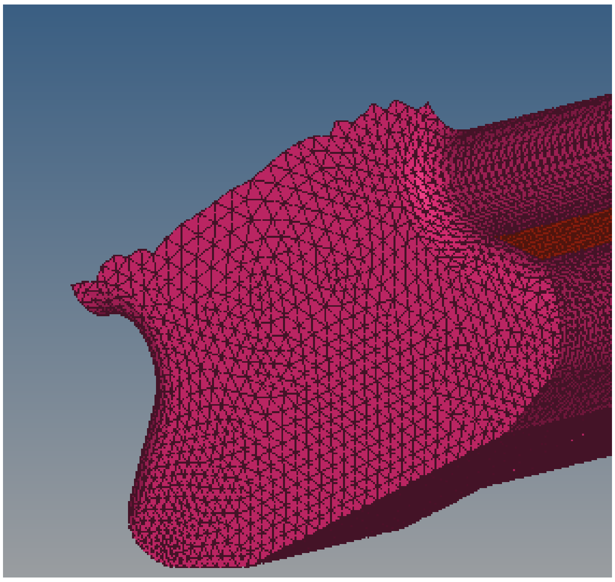

Figure 6.2: Example of FE model with reference to Dovetail area

  2. Shank Pockets Curvatures
  3. Shank Pockets Borders
  4. AF fillets
  5. AF Leading Edge
  6. AF Trailing Edge
  7. Contact Area

- in order to reduce the overall number of FE entities, several areas are allowed to be described with a coarser mesh sizing, without compromising the precision of results, neither in Dynamic nor in Static analysis:

  1. Disk component
  2. Shroud stiffness bar
  3. Shroud Finns and Cutters
  4. Lips
  5. Angel Wings

6. AF cental areas

- Blends are to be described by R-tria elements. In case of 2nd order elements every blade should be described by at least 5 trias in the main curvature direction
- The use of Biasing meshing tool, that enhances the sizing gradient in large surface areas, is to be preferred whenever the number of entities is to be kept low but a good definition is required at the surface borders

Due to the high amount of sensible data the geometry model holds, the overall result of the meshing process cannot be shown.

6.2 Baseline Dynamic Analysis

After the definition of the FE model through the mesh generation, the benchmark analysis can be launched in order to understand the dynamic and static behaviour of the model. The definition of the system loads and constraints constitutes a very important part of the simulation pre-processing. The model, to be computed with ®Nastran commercial code, will feature the following mechanical constraints:

1. Explicit SPC, locking all three-axes displacement, to be defined at the LE area of the Disk highlights in Figure 1

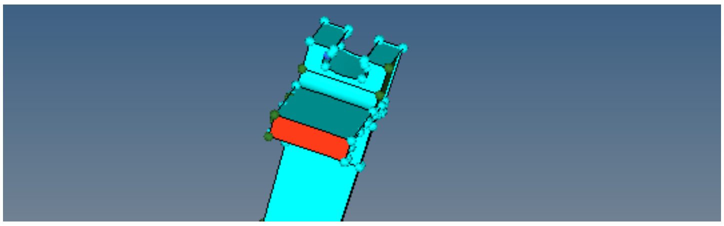

Figure 6.3: Area where the locking SPC will be defined, highlighted in orange

2. Cyclic Symmetry MPC to be defined on the lateral areas the disk, representing the cyclic symmetry condition that allows the run of a single blade sector (Figure 2)
3. Cyclic symmetry MPC to be defined on the interlock area to simulate the kind of contact between adjacent blades at the Shroud level.
4. Explicit Symmetry MPC between contact areas of Disk an Blade, locking all three-axes displacement DOFs

With reference to the loads applied to the model, the Bladed Disk will experience:

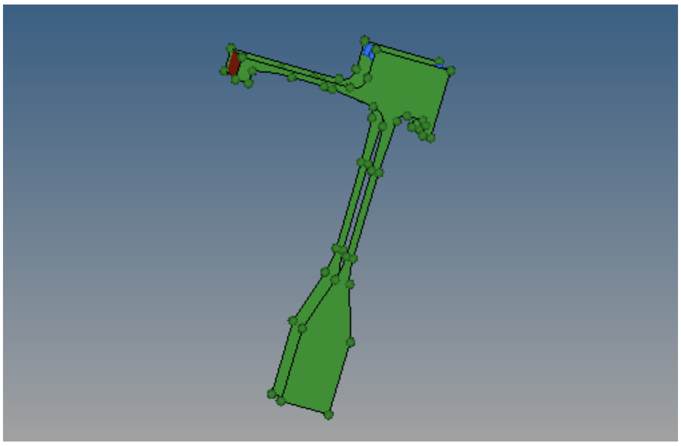

Figure 6.4: Area where the Cyclic Symmetry MPC is defined, in green

1. Centrifugal Load due to the rotational velocity about the engine axis (identified with Z).

2. Temperature Load in the form of a T spatial-field. Each node will be assigned with a specific temperature value depending on its radial coordinate. In the case of Dynamic Analysis, no thermal stresses are considered to take place (this effect will be taken into account only through Static Analysis). The temperature will only cause the change of Thermal-dependant material properties, such are density, elasticity, etc...

6.2.1 Considerations on the Interloking Conditions

Among the mechanical constrains that are to be defined for a BD model the interlocking model covers a fundamental role. Not only it highly affects the eigenvalues of the modal simulations, but it has a high impact on the modeshapes, their development at different Nodal Diameter configurations, and the presence of veering areas.
The model that has been chosen for this project has been designed to be working in fully interlocked conditions (identified, hereafter, with **TH**). However, the high temperatures the system experiences and the need of a long-lasting component life-cycle, where wear may be occurring to a high extend, forces the consideration of not-interlocked conditions as a possible scenario in the operative life of the engine. The not-interlocked conditions, identified with **TF**, enable the setting of more dangerous modeshapes. These modes, as it will be seen in Section 6.4, are more likely to cause aeromechanical instabilities' setting. For this reason, not only TF conditions are part of the analysis, but are where the most attention is to be paid.

Conditions	**Rotational Velocity n** [Hz]	**Temperaure T**
Cold (COLD)	ω_{CO}	T_{CO}
Cruise(CR)	ω_{CR}	$T_{CR_{min}} \div T_{CR_{max}}$
Take-Off(TO)	ω_{TO}	$T_{TO_{min}} \div T_{TO_{max}}$

Table 6.1: Simulated Engine Operative Conditions

6.2.2 Operative Conditions

In order to obtain a Campbell Diagram, several crossings between modes and EOs are required. The more harmonics and operative conditions are analysed the more the Campbell diagram will feature smooth curves and precise crossing values. However, since the FE model requires high computation power to obtain the results of a modal analysis, the simulation is restricted to the following conditions:

- Take-Off (TO) Conditions
- Cruise (CR) Conditions
- Cold (COLD) Conditions

The above conditions will feature the loads highlighted in Table 6.2.2:

6.2.3 EOs of Interest

As mentioned in Section 6.2.2, the precision of a Campbell is higher when a good amount of harmonics are analysed. The simulation of various harmonics/EOs allows the description of the dynamic behaviour of the rotor according to multiple Nodal Diameter configurations, resulting in a more complete dynamic behaviour description. The choice of Engine Order of interest is always performed by looking at the overall engine/module architecture: since the forcing term is often associated to the exciting action of a specific engine component, it is common to simulate the corresponding harmonic index to determine the effect on the BD model. Engine Orders are usually classified in three major sections:

- Primary Engine Orders, identified in Pink, represent the most critical exciting confitions for the Rotor. They include the LEO (Low Engine Orders, i.e. 1-2-3).
- Secondary Engine Orders, identified in Blue, represent less dangerous excitations
- Special Engine Orders, identified in Grey, are usually related to specific excitations whose concern comes from design guidelines or experimental tests

6.3 Dynamic Analysis Results

The modal analysis run is run by using ®Nastran computation code. A pre-stressed modal system is used to simulate the BD response to an initial excitation. As explained in Section 6.2.1, the analysis is to be run in a dual interlocking condition (i.e. TH and TF). In the current section the results are shown by means of both Campbell and FREND Diagrams.

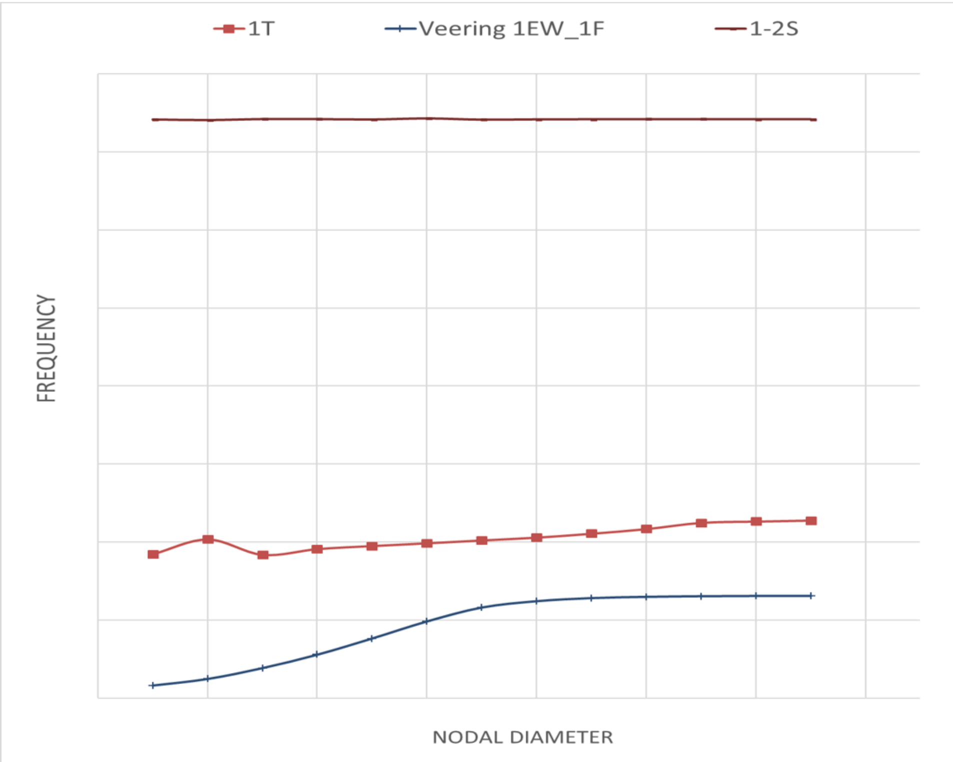

Figure 6.5: FREND Diagram - TH Take Off Conditions

By looking at Figure 6.3 one can notice the particular trend modeshapes tend to have in fully interlocked conditions. By looking at the development modes feature according to increasing Nodal Diameter configurations, TH BC usually causes an evident veering effect between 1EW and 1F modeshapes. The resulting veered mode has been visualized in the FREND diagrams: it is hard to obtain a fully determined 1F or 1EW mode along all the ND configurations. Despite veering effect is possible for any modeshape, it is hard to identify it within the engine operative range: 1EW and 1F are the among the most common modes to feature this phenomenon, while other modal families experience veering in conditions that are not physically possible for an aircraft engine (very high speed). As the 1-2S mode is concerned, it usually occurs at very high frequency values, and features a great stability at all ND configurations.

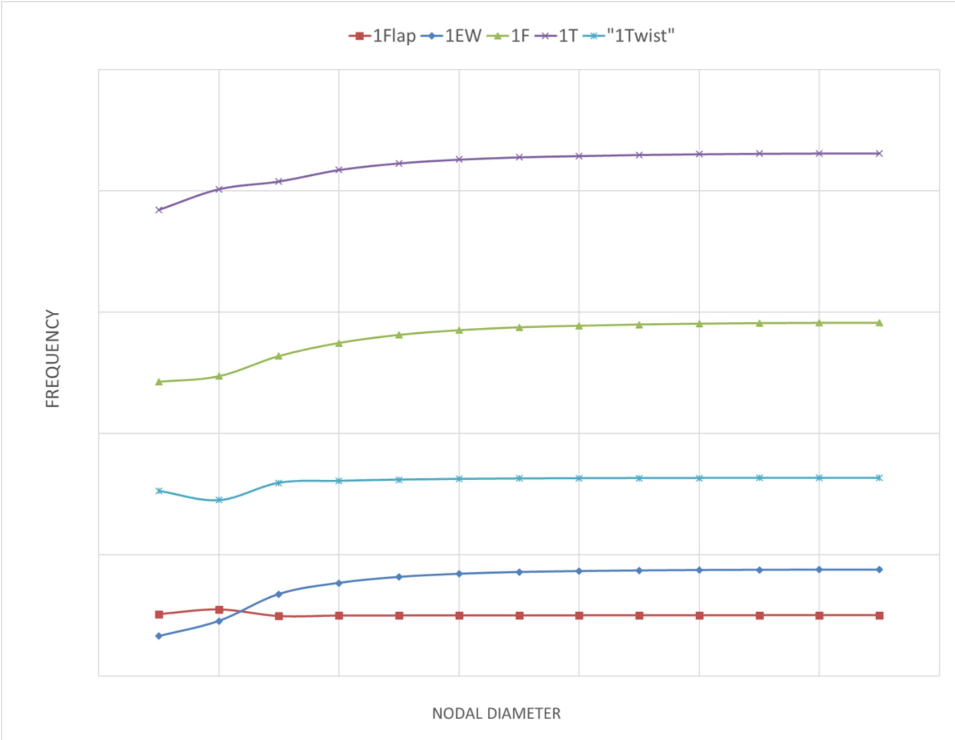

Figure 6.6: FREND Diagram - TF Take Off Conditions

When dealing with Figure 6.3, there are various differences that can be seen from the TH case. As a matter of fact, the 1Twist modal family is not present in rotor systems being fully interlocked. On the other hand, the lack of a mechanical constraint at the shroud level in TF conditions allows the 1Twist mode to occur. The same thing can be said when talking about 1Flap modeshape. The latter, considered to be a system modeshape of BD systems, is among the most dangerous modes from an aeromechanical point of view. More specifically, it will be sees during the following parts of the report that 1Flap mode constitutes the objective of the flutter stabilization that is to be achieved through the introduction of intentional mistuning technology. Still talking about 1Flap mode, one can see that at low ND configurations it features a veering phenomenon, together with an other system mode, i.e. 1EW mode. As it has been explained in Chapter 3, the veering effect can be seen on FREND diagrams only when modal classification is performed based on modeshapes, rather than frequency. At the stage when the project as been conducted, no automatic tool is providing a reliable and efficient way to create FREND/Campbell diagrams through mode-based modal classification (various tools offer a good reliability for frequency based classification). For this reason it is often convenient to act a manual modeshape-based classification when LPT blades are involved. In fact, veering effect between 1EW and 1Flap modes is common when modal analysis

is performed on blade model being characterized by internal cavities.
Similar considerations on the dynamic behaviour of the rotor can done by looking at the Campbell diagrams.

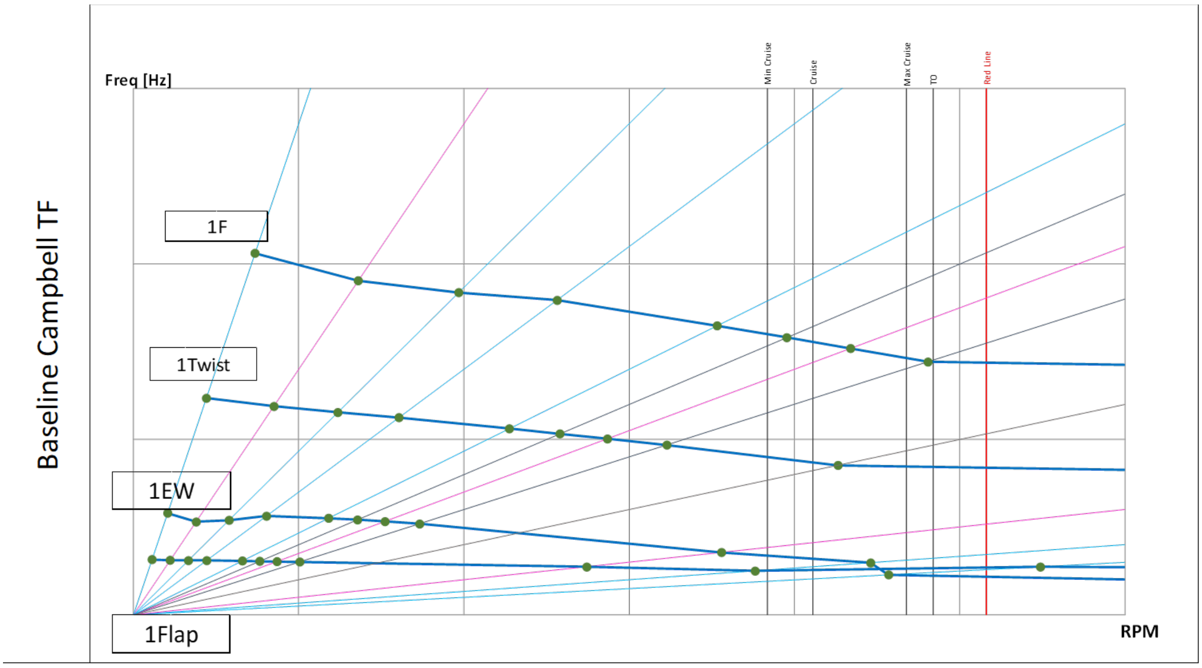

Figure 6.7: Campbell Diagram of Baseline Model in Tip Free Conditions

By referring to 6.3, where Tip Free conditions are reported, one can see that the modal-family based classification, the veering phenomenon between 1EW and 1Flap modes can be noticed. When looking at the diagram, particular attention should be paid on mode crossings. More specifically, the further validation process is to be undergone when crossings between modes and EOs falls within the operative range, namely between Min. Cruise speed and Red Line speed. Various classifications of crossing can be done based on the Engine Order, thanks to the design and validation experience. The major crossings providing more probability of failure are reported in Table 6.3: these ones are required to be deeply analysed and their low effect for a failure failure needs to be validated.

Figure 6.3 reports, on the other hand, the Campbell Diagram in Interlocked Boundary Conditions. The veering effect between 1EW and 1F mode is more than visible by looking at the "S-shaped" curve. As far as the major crossings are concerned, they are listed in Table 6.3.

Crossing #	Mode	EO Type
1	1EW	Secondary
2	1EW	Secondary
3	1Twist	Special
4	1F	Special
5	1F	Primary
6	1F	Special

Table 6.2: List of Major Campbell Crossings in TF BCs

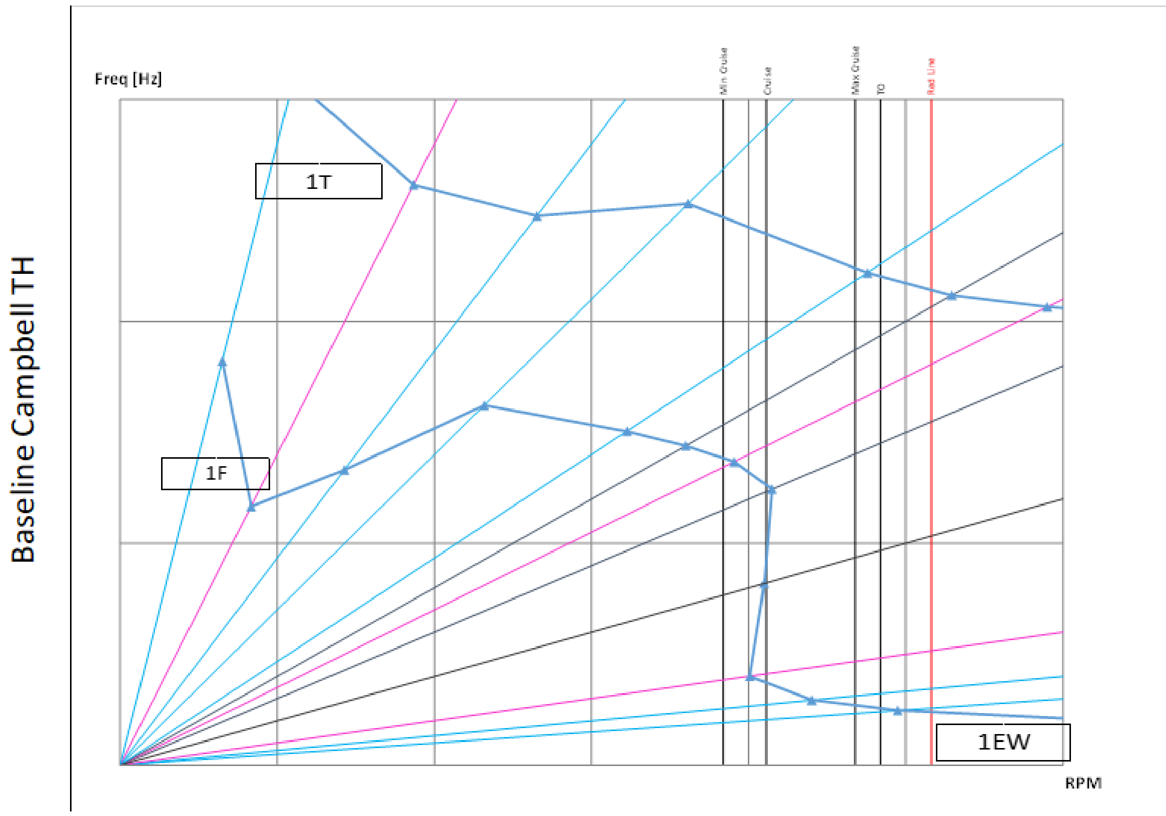

Figure 6.8: Campbell Diagram of Baseline Model in Interlocked Conditions

6.4 Aeromechanical Instability Analysis

The current section will analyse the presence of Flutter instabilities within the BD system in case the interlocking condition is lost during the engine life-cycle. The analysis, explained in Chapter 4, will be merging input files coming from both aerodynamic and modal simulations. As far as the operating conditions are concerned, both Take

Crossing #	**Mode**	**EO Type**
1	1EW-1F	Sedondary
2	1EW-1F	Secondary
3	1EW-1F	Primary
4	1EW-1F	Special
5	1EW-1F	Special
6	1EW-1F	Primary
7	1T	Secondary

Table 6.3: List of Major Campbell Crossings in Interlocked BCs

Off and Cruise conditions have been simulated: Take-Off conditions provide the most severe conditions for flutter setting. The mistuning application aims at reducing such instabilities at TO, and by doing so the stabilizing effect will propagate to CR conditions as well. By company experience data, coming from both experimental and numerical tests, the most critical mode from an aeromechanical point of view is the 1Flap mode, despite in rare case even 1F and 1EW modes may be dangerous. In the current work, all three modeshapes have been simulated, despite the most of the attention has been paid on 1Flap, which features the lowest aerodamping values.

6.4.1 Pre-Processing of Flutter Analysis

Despite various numerical methods and approaches are possible to conduct a Flutter analysis over a Turbine bladed system, the company Design Practice suggests the use of Autoflutter tool that, as explained in Chapter 4, ensures a good precision of results with respect to experimental ones, without requiring a high computation power. As explained in the relevant section, the pre-processing of the analysis is performed on the locally installed packages of the tool.
As far as the aerodynamic field properties computation in steady state conditions, the profile of the blade is divided in 21 different sections. Despite the normal practice suggest the division of the profile into only 9 sections, the use of a higher number (i.e. 21) allows a higher precision for the creation of the CFD grid when interpolating data from one section to the adjacent one. The analysis is hence performed with the Cluster computation of the 3D aerodynamic properties field starting from the 2D values coming from the preliminary studies. This operation is performed both for he Cruise operating conditions and the Take-Off operating conditions.
Once this part of the analysis is complete the modal anlaysis reports can submitted to the pre-processing tool in order to have the merging of the modal simulation with the CFD simulation. As far as the modal analysis is concerned, it is important to pick a set of Nodal Diameters configurations to be simulated, spanning up to the maximum value

Set Number	**IBPA**	**Harmonic/ND**
# 1	0	1
# 2	15	6
# 3	30	12
# 4	45	18
# 5	60	24
# 6	75	30
# 7	90	36
# 8	105	41
# 9	120	47
# 10	135	53
# 11	150	59
# 12	165	65
# 13	180	70

Table 6.4: Values of ND configurations based on 13 sets

given by Eq. 6.1:

$$ND_{max} = \frac{N_b}{2} \tag{6.1}$$

The choice of the ND values (or harmonic index values) will produce a subsequent effect on the IBPA values. Based on past experience, good results are obtained when the IBPA range is divided into 13 sets. Hence, the 13 different harmonic indeces are to be simulated during the Modal analysis, whose values are shown in Table 6.4.1.

The choice of ND follows the already relation contained in 6.2

$$ND = \frac{N_b \cdot IBPA}{360} \tag{6.2}$$

Since the CFD grid is valid only where the fluid flow is present (i.e. along the aerodynamic profile), there is no need to generate report files of the different modal displacement for nodes that are not belonging to the external mesh of the AF (e.g Shank, Shroud, Dovetail, Disk, etc..). This allows for an enormous saving of computational power since the software is not required to hand a high amount of Node displacement data where there is no need to do so. This saving in terms of computational power is increased since the modal reports contain only results referring to corner nodes of mesh tria elements.

6.4.2 Flutter Analysis Results

The results of the aeromechanical simulation performed through Autoflutter on the Tip-Free Baseline model can be shown with the aeroplot diagrams. As explained in

Chapter 4, they show the tred of aerodamping value at different IBPA (ND) values. One difference that should be mentioned between the company design practice and the theory physical models is that the critical ξ is not zero, but rather a little lower value. Due to the compliance restrictions, the value of the critical aerodamping cannot be shown in the reported graphs. The results are herein reported.

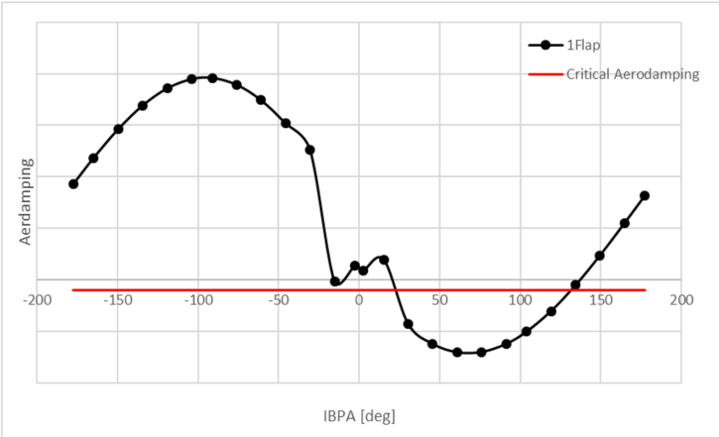

Figure 6.9: Aeroplot of 1Flap mode in Take-Off operative conditions

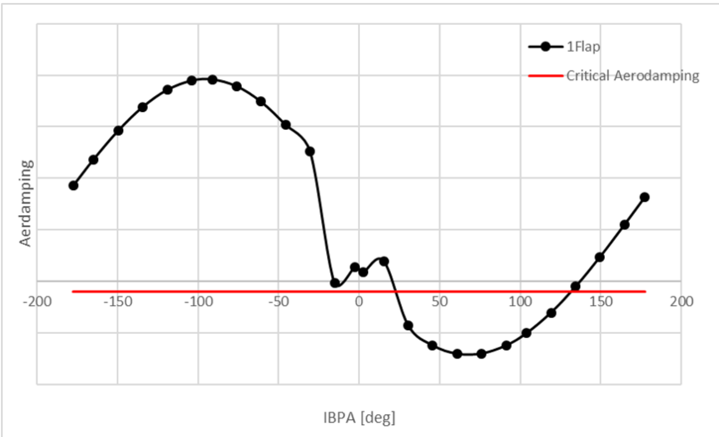

Figure 6.10: Aeroplot of 1Flap mode in Cruise operative conditions

As far as the 1Flap is concerned, the aeroplots shown in Figure 6.4.2 and Figure 6.4.2 highlight the instability from an aeromechanical point of view. In spite both the CR and TO conditions lead to Flutter setting, the Take-Off graph shows a much higher situation, with a ξ well below the critical threshold. The value highlights the importance of a stabilization through Mistuning technology since the setting of TF conditions in the life-cycle of the component may lead to dangerous unexpected failure.

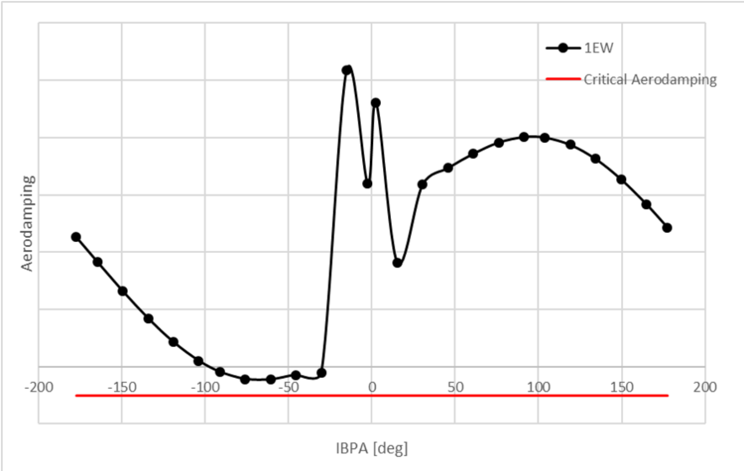

Figure 6.11: Aeroplot of 1EW mode in Take-Off operative conditions

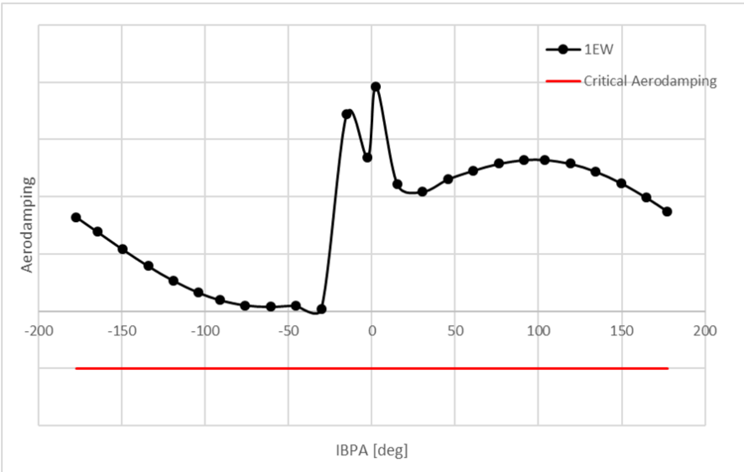

Figure 6.12: Aeroplot of 1EW mode in Cruise operative conditions

Talking about the 1EW mode, whose aeropolots are shown in Figure 6.4.2 and Figure 6.4.2, only the TO conditions shows a situation where the mode is slightly stable. Despite the instability is not as enhanced as the one highlighted in 1Flap mode, the lack of a full positive aerodamping value imposes to pay attention to any changing in the relative aeroplot in the mistuned model, since any shift to lower values of the ξ values immediately turns into a dangerous instability.

Finally, as it is shown in Figure 6.4.2 and 6.4.2, the 1F mode does not highlight any aeromechanical condition to be particularly concerned about.

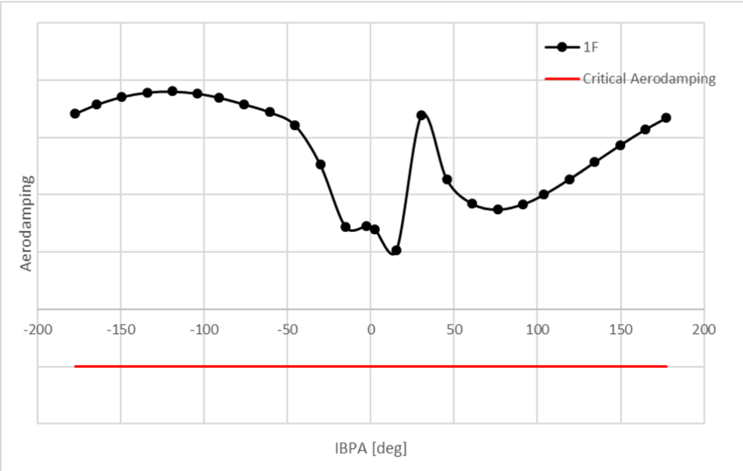

Figure 6.13: Aeroplot of 1F mode in Take-Off operative conditions

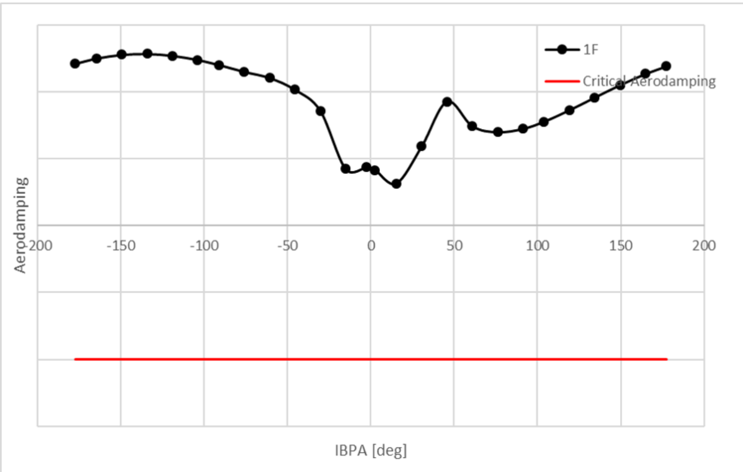

Figure 6.14: Aeroplot of 1F mode in Cruise operative conditions

6.5 Alternate Mistuning Application on Basline Model

The results shown within Section 6.4.2, with particular reference to the aeroplot shown in Figure 6.4.2, have demonstrated the importance of applying a stabilization technique in order to avoid the occurrence of Flutter in case the BD starts working in Tip Free BCs. The data concerning the ξ value at each ND configuration can be submitted to a company in-house tool called AMMIS. The tool is a specifically developed software whose aim is to compute the necessary Δ in either mass or stiffness capable of turning the aerodamping values positive (and thus stable) at the chosen ND configurations. The tool is provided with the relevant Aerodamping and Aerostiffness (computed by means of specific CFD simulations) vectors, the eigenvectors of the unstable mode and the location of nodes where mistuning is to be applied (i.e. in what specific component feature). The outcome of the computation is graph shown the mass/stiffness Δ that is to be applied in order to produce the frequency shift $\Delta\omega$ the designer wants to cause in the rotor model. However, the use of this tool is useful only after a detailed definition of how the mistuning technology is to be applied, i.e. through what specific manufacturing technology, and in what particular area of the model. With reference to the latter point, several studies have proved that the higher the radial component of the application region, the more effective mistuning will be on 1Flap modes. Therefore, application of either ΔM or ΔK is to be preferred on the blade's Shroud.

6.5.1 Definition of Mistuning Application methods

The definition of the specific mistuning application methods is a part of the project, since it is able to prove the wide panorama of the possible options the technology introduction may offer. Not only this part of the study has the objective of reducing he actual costs of technology introduction, but it aims at minimize the impact on other design and validation engineering fields, such as aerodynamics, aeroacoustics, manufacturing, etc... The brainstorming activity that has been conducted within the team has come up with four different methods for mistuning introduction, translated into four different mistuned concepts.

Concept ID	**Concept Definition**
A	Interlocked
B	Plain Shroud
C	AM Shroud
D	AF Fillets

Table 6.5: Mistuned Concepts Definition

- Concept A: This model is to be realized by applying only ΔM on the Shroud features. This is to be obtained by means of slight changes to casting and machining dimensions during the manufacturing process. The method aims at keeping the interlocked structure of the blades.

- Concept B: The aim of this application method is to revolutionize the interlocking structure by avoiding the Z-notched shaped features at the Shroud. No contact is hence designed by adjacent blades, whose mechanical conditions turn into fully Tip Free by design. The ΔM aims at ensuring a Flutter stability for both system modes, i.e. 1Flap and 1EW.

- Concept C: This model aims at obtaining the ΔM by means of a different material density between adjacent blades. The different density may be accounting to either only the Shroud or the whole blade. This application is possible by manufacturing the lighter blade with additive manufacturing (AM). The AM technology would create a lighter structure in the desired areas, thus producing a different material density from the casted component.

- Concept D: This is the only concept taking into account a ΔK. This model stiffness changes is to be obtained by dimensioning the AF lower/upper fillets with different radii.

6.5.2 Critical to Quality Factors Analysis

Subsequent to the brainstorming activity that has lead to the definition to four different mistuned concepts, it is important to analyse these technology introduction methods, in order to better concentrate efforts on the mistuned concepts with more efficient introduction outcomes. This part of study focuses the attention on all the the design, manufacturing and economic factors that are to be considered for the mistuning introduction, since it involves changes to already tested and validated engine components. The analysis of each factor tries to answer a few questions by providing a weight and a relevant score to each concept ID. Consequentially weighted scores are summed and concepts are laddered.

1. How much is mistuning introduction affecting the overall weight of the bladed-disk sector? And by considering N_b blades in a 0,1,0,1 layout, how much is the stage affected in terms of mass? Does this affect the overall performance?

2. Is the introduction of this kind of mistuning expensive in terms of manufacturing shift from one process to an other? Am I asking for a complete casting process revision or am I asking for simple machining modifications?

3. By not taking into account the introduction itself, is the technology expensive if seen from a series-production point of view? Will my unit-cost be affected by introduction of this kind of mistuning?

4. Besides costs in the introduction and in the mass-production, is the technology that the mistuning introduction requires available? If not, how much time will take to have it ready to go?

5. Are the mistuning modifications anyhow affecting the flow-path, not only by means of a Airfoil modification?

6. Is the introduction of mistuning anyhow requiring a modification of the Airfoil or the interpolation of AF segments among them?

7. With reference to the above mentioned factor, is the change in the assembly process of the stage/LPT module affecting the assembly costs as a whole? If so, is the rise in costs acceptable?

8. After the manufacturing process of the blade, how is the mistuning implementation affecting the assembly of the stage/LPT Module? Are the different clearances/interferences playing a role in making the assembly process harder or simpler (stacking-up..)

9. Is the mistuning introduction requiring the use of a different material? If so, is it available? At what cost?

10. Is the mistuning changing the radial gap layout between shroud and carter? Will this modification to shroud geometry affect the performance due to changes of a different behaviour of radial-gap flow? Will this gap-change lead to any interference/loss of required clearance?

11. Similar considerations may be applied to tangential gaps as well, especially when considering the interlocking conditions. How about the twist when blade gets operational?

12. Has the suggested concept already undergone any previous test campaign from a numerical point of view? How about similar concepts in different engines?

13. Based on previous experience on mistuning applications, is this technology likely to affect the flutter instabilities? Is the likely flutter stabilization effect compliant with the aim of the work?

14. Is the modification likely to affect the behaviour of the stage from an acoustic point of view? Are the modifications allowing a different interaction with the air that may cause vibrations/noise?

15. Are the modification likely to affect the nominal interference at the interlock?

16. Is the suggested concept needing numerical analysis only from a dynamic point of view, or does the aerothermal behaviour have to be tested again? Is there a good literature for the suggested changes implementation?

17. Is this approach likely to increase the wear rate at the interlocking level? Could this impact the overall life-cycle management of the blade component?

Factor ID	Factor	Score Weight
1	Overall Weight	2
2	Technology Introduction Costs	3
3	Long Run Manufacturing Costs	3
4	Manufacturing Availability	3
5	Affecting Flow Path	3
6	Modification of AF	3
7	Assembly Easyness	1
8	Assembly Process Change Costs	1
9	Material Availability	3
10	Radial Gap	1
11	Tangential Gap	1
12	Concept Already Tested	1
13	Flutter Stabilization	3
14	Acoustics	1
15	Interlocking Interference	1
16	Analysis needs	1
17	Interlocking Wear Issues	2

Table 6.6: CTQ factors meaning and relevant score weight

The score weight ranges from 1 (least important, easiest issue to solve) to 3 (highest impact or hardest issue to overcome). Each concept is consequentially provided with a score with reference to each factor, by replying to the questions reported in Table 6.5.2.

The scores reported in Table 6.5.2 have been assigned with a detailed analysis of all the aspects that a new technology introduction involves, with the help of long-experiences company engineers. With the subsequential computaion of the weighted sums, the final scores are reported and laddered in Table 6.5.2:

Given the total results provided in Table 6.5.2, and after its review with company supervisors, the project has focused its attention on the development of Concept A Mistuned Sector.

6.6 Concept A Development

The development of a mistuned sectors starts from a series of preliminary studies to be executed on the Baseline model. Apart from CTQ analysis, which provides a good insight of all the pros and cons that the specific method of introduction may lead to from an economic and manufacturing point of view, specific engineering design considerations should be made in order to obtain a model that can likely experience numerical and experimental validation.

Factor ID	**Concept A**	**Concept B**	**Concept C**	**Concept C**
1	3	3	3	1
2	3	2	1	1
3	3	3	1	3
4	3	3	3	1
5	3	3	3	1
6	1	2	3	3
7	2	1	3	3
8	3	2	3	3
9	3	2	3	3
10	3	3	1	3
11	3	3	1	3
12	3	2	1	2
13	3	3	3	1
14	3	3	3	3
15	3	1	3	2
16	3	3	1	1
17	2	2	3	3

Table 6.7: CTQ Score for each concept

Concept ID	**Weighted Total Score**	**Ladder N.**
A	2.85	1
B	2.60	2
C	2.18	4
D	2.03	5

Table 6.8: CTQ Analysis total weighted scores for mistuned concepts

6.6.1 AMMIS Analysis

AMMIS is an in-house developed software tool specifically coded to compute the ΔM and ΔK during the AMM method application for misutuned sector modeling. The tool aims at providing the amount of stiffness/mass to be added (or removed) to (or from) the Baseline model, in order to achieve a mode frequency shift capable of stabilizing flutter unstable modes. The input required by the tool are:

- Aerodamping values at different IBPA/ND configurations
- Aerostiffness values at different IBPA/ND configurations
- Mode Eigenvectors and Eigenvalues at different IBPA/ND configurations

- Location of mesh nodes where mistuning is to be applied. In this case, Shroud nodes are involved

The tool is then required to be set with a frequency shift, decided by the user. As far as this analysis is concerned, several iterative attempts have been conducted, by starting from both literature studies and company simulations on similar geometric models. The frequency shift has been finally set to $\Delta\omega = 8\%$, if compared to the 1Flap baseline model.

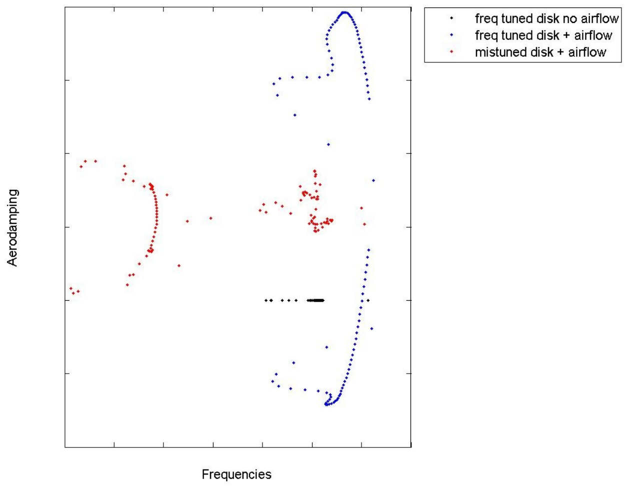

Figure 6.15: Aerodamping vs 1Flap Frequency

The outcome of the tool computation is summed up in two graphs, reported in Figure 6.6.1 and Figure 6.6.1. Particular attention should paid about the meaning of Figure 6.6.1, which recalls the Isolated Modes analysis in Chapter 5. This plot reports the function of ξ with respect to the mistuning content (represented i ΔM. It can noticed that, for a given amount of mass difference, the aerodamping value switches sign from negative to positive, thus turning the model from 1Flap flutter unstable to 1Flap flutter stable. Therefore, the effort of the work will be modelling a mistuned blade with a mass target being $\Delta M = 3.5\%$.

6.6.2 Concept Definition Constraints

By starting from the target ΔM value provided by Figure 6.6.1, the concept definition has focused the attention on the geometry generation with CAD modeling tools. However, the mass difference target constitutes only one of the main objectives when attempting the realisation of a mistuned sector. It is worth recalling that the purpose

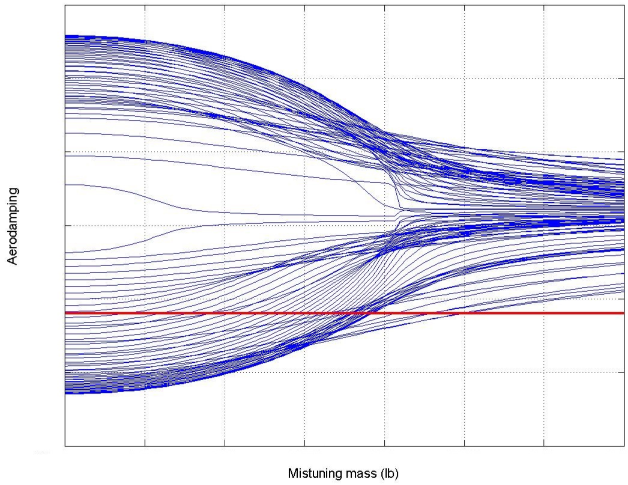

Figure 6.16: Aerodamping vs Mistuning ΔM

of the work is not proving the stabilizing effects that mistuning technology creates on Flutter phenomenon, but rather demonstrating that this method can be fully integrated in real aviation engine LPT module, by not compromising crucial engine components and functionalities. This said, the design work has been conducted by considering a series of constraints coming from multiple engineering fields: this constraint analysis has been performed in strong collaboration with design engineers of the specific LPT module, whose information have been crucial to determine the feasibility of the technology within the system. Therefore, a set of constraints have been defined as follows:

- Casting Angles: Since the majority of the component features in a BD system are realized with casting technology (despite new technologies are being used in the latest years), attention should be kept on the draft angles, that are key factors to avoid good manufacturing results within the accepted tolerance range. The values of the BS model are to be kept constant in order to avoid the repetition of the casting validation process.

- Interlocking Surface Area: despite the interlocking and stiffness bar region constitute a wide region where mass can be added/removed, the dimensions are to be kept constant in order to avoid peak contact stress between adjacent blades and the modification of tortional stiffness

- Radial and Axial Clearance: during its most critical operative conditions, such as Take-Off, turbine blades geometry configuration is different from the one that can seen at Cold conditions. The high centrifugal loads, together with the pressure airflow acts on the profile, lead to strong static deformation. This is why axial and radial clearance handling is amoing the top prorities when designing engine components. In order to avoid any modifications to adjacent engine components (Vanes, honeycomb, etc..), a series of geometry boundaries have been defined:

   - Finns: radial dimension to be kept constant.
   - Finn cutters: only axial dimension can be modified
   - Main Shroud thickness: radial clearance can be decreased
   - Lips: Axail dimension changes are allowed to a low extent, while the radial dimension can be freely adapted to design needs

- Tangential Gaps: they are to be kept constant in order to avoid flow spills on one side and interference stress on the other side.

- Main Shroud thickness: its radial overall dimension cannot be decreased since the machining process would hardly reach the required geometric and dimensional tolerance target (small thickness features are harder to machine).

- AF Fillets radii: these dimensions can be decreased by 10 %, as a max difference, since a higher ΔR would determine the affection of aerodynamic profile performance.

The relevant geometry modelling work has been conducted by keeping in mind the above constraints, and the overall outcome is reported in Section 6.6.3

6.6.3 Mistuned Sector Geometry

The CAD generation process has followed an iterative approach, aiming at obtaining the $\Delta M = 3.5\%$ on one side, and acting the lowest possible Center of Mass modifications, on the other side. The modelling approach has been performed by creating a parametric CAD file and by exploiting synchronous modelling tools, embedded in commercial CAD software ®Siemens NX. The modifications on the BS blade have aimed at modifying:

- Forward Lip: axial dimension has been increased, together with the overall radial thickness

- Aft Lip: radial thickness has been increased

- Shroud blends: increased the blend radii in the lips area and finns areas

- Main Shroud thickness: radial dimension has been increased, by keeping the overall curvature

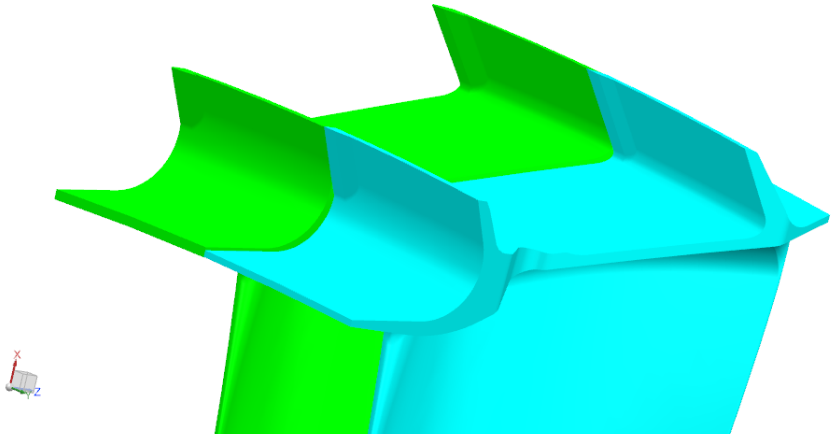

Figure 6.17: Concept A Mistuned Sector Geometry layout. Baseline is light blue, Mistuned is green

The outcome of the geometry modelling process is shown in Figure 6.6.3, where the mistuned sector in (0,1,0,1) configuration has been plotted.

As mentioned above, the procedure aimed at keeping the Center of mass location as similar as possible to the one that characterizes BS model. This not only avoids stress concentration due to dynamic and static unbalance (especially at the AF lower fillet), but ensures that the Baseline Disk model can be adopted for the mistuned Blade as well, since no a low shift in center of mass allows for an equilibrated distribution of contact stress at the contact region. The shift in both center of mass location and second order moments of inertia are reported in Table 6.6.3

Shift	**Shift Value**
X_c (radial)	0.169 [in]
Y_c (tangential)	0.008 [in]
Z_c (axial)	0.0001 [in]
I_{xx} (radial)	17.27 $[in^4]$
I_{yy} (tangential)	42.97 $[in^4]$
I_{zz} (axial)	25.71 $[in^4]$
I_{sp} (spherical)	0.29 $[in^4]$

Table 6.9: Center of Mass and Moments of Intertia Shifts

6.7 Concept A Analysis

After the definition of the geometry model, the mistuned concept needs to undergo various simulation processed in order to validate its effectiveness against Flutter phenomenon, on the one hand, and its dynamic stability, on the other hand. Despite the complete validation process of a new system configuration would require a series of more complex validation simulations, as highlighted in Chapter 3, the current report will focus its attention on the dynamic and aeromechanical analysis, in order to better underline the differences with Baseline tuned rotor, described in Section 6.3 and Section 6.4.2.
One key difference that needs to mentioned when dealing with mistuned sectors with respect to all-tuned sectors is that the cyclic symmetry constraint works slightly differently to how it has been seen in Chapter 3, and more specifically within Section 6.2. More specifically, in having a Blade 0 that is remarkably different to mistuned Blade 1, the cyclic symmetry properties can be only applied to a double-sector being characterized by the couple of blades. Not only this fact requires higher computational power during the computation of the simulation, but shows evident differences in the modal behaviour of the system as well: each eigenvalue/eigenvector, taken singularly, refers to only one of the two blades. This means that in double-blade sector each modeshape will be referring more specifically to Blade 0, with first eigenvalue, and Blade 1, with the second eigenvalue. As nomenclature is concerned, the modes that will be analysed will hence be:

- Flapwise
    1. 1Flap
    2. 1Flap2
- Edgewise
    1. 1EW
    2. 1EW2

Both Aeroplots and Campbell/FREND diagrams will show the two modes referring to the two blades, respectively.

6.7.1 Mistuned Dynamic Results

A similar approach to the one followed in Section 6.3 should be herein undertaken. It is important to recall that the purpose of dynamic behaviour analysis for the mistuned sector is mainly making a comparison with the Baseline model, and more specifically

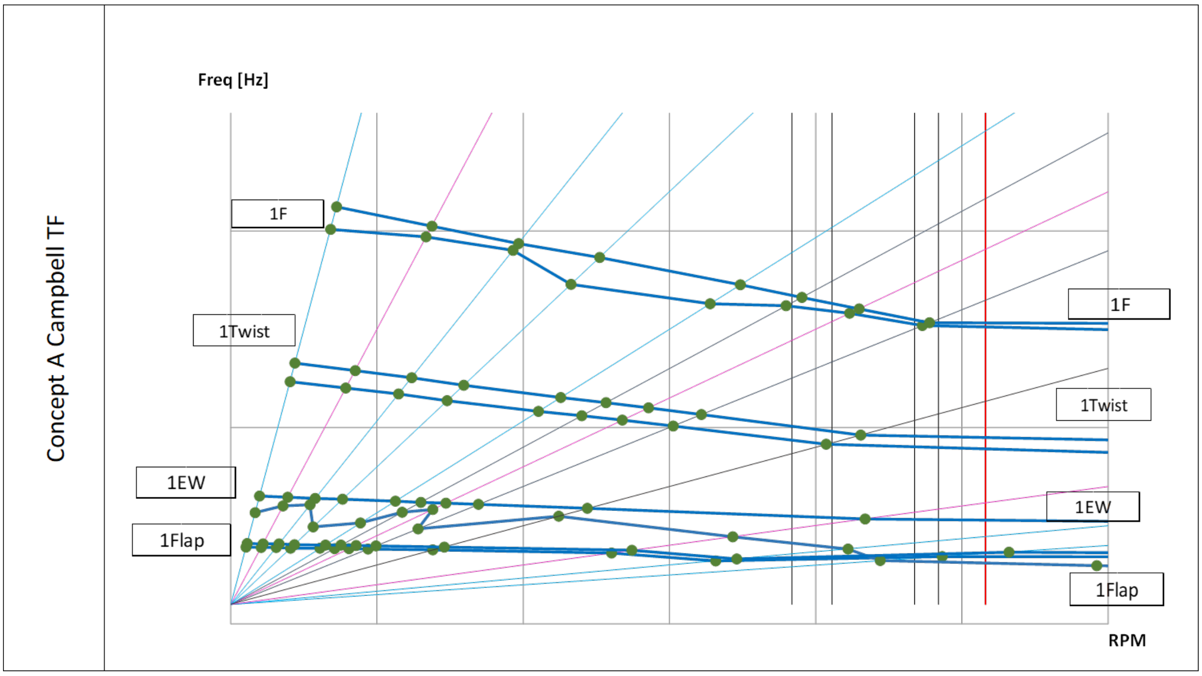

Figure 6.18: Campbell Diagram of Mistuned Sector in Tip Free Conditions

with the aim of checking the presence of further (or less) crossings between modes and EOs on the Campbell diagram.

By looking at Figure 6.7.1, and by comparing the results with the ones reported in Figure 6.3, one can notice that an additional crossing appears between 1Flap mode and a secondary EO. On the other hand, all the other modeshapes, i.e. 1F, 1EW, 1Twist and 1F, present exactly the same crossings with EOs of interest. One more feature of the dynamic behaviour that can be noticed is the dynamic stability, from a frequency point of view, of Edgewise mode 1EW2, referred to Blade 1. As it can be seen, it keeps almost constant frequency values for different operative conditions and Nodal Diameter configurations.
Very interesting considerations can be done by looking at the TF FREND diagram as well.

In Figure 6.7.1, obtained in Take-Off operative conditions, 1Flap mode trend is reported for both Baseline and Mistuned models. Apart from having similar graphic trend, the eigenvalue shift respects what has been predicted by AMMIS. In Section 6.6.1, the $\Delta\omega = 8\%$ has been defined as the frequency shift target. By looking at the FREND reported in Figure 6.7.1, one can notice that there is a $\Delta\omega$ by 6 %. This result, despite not exactly matching the expectations, mainly due to the non-linearity effects caused by temperature-dependant material properties, demonstrates the overall good reliability of

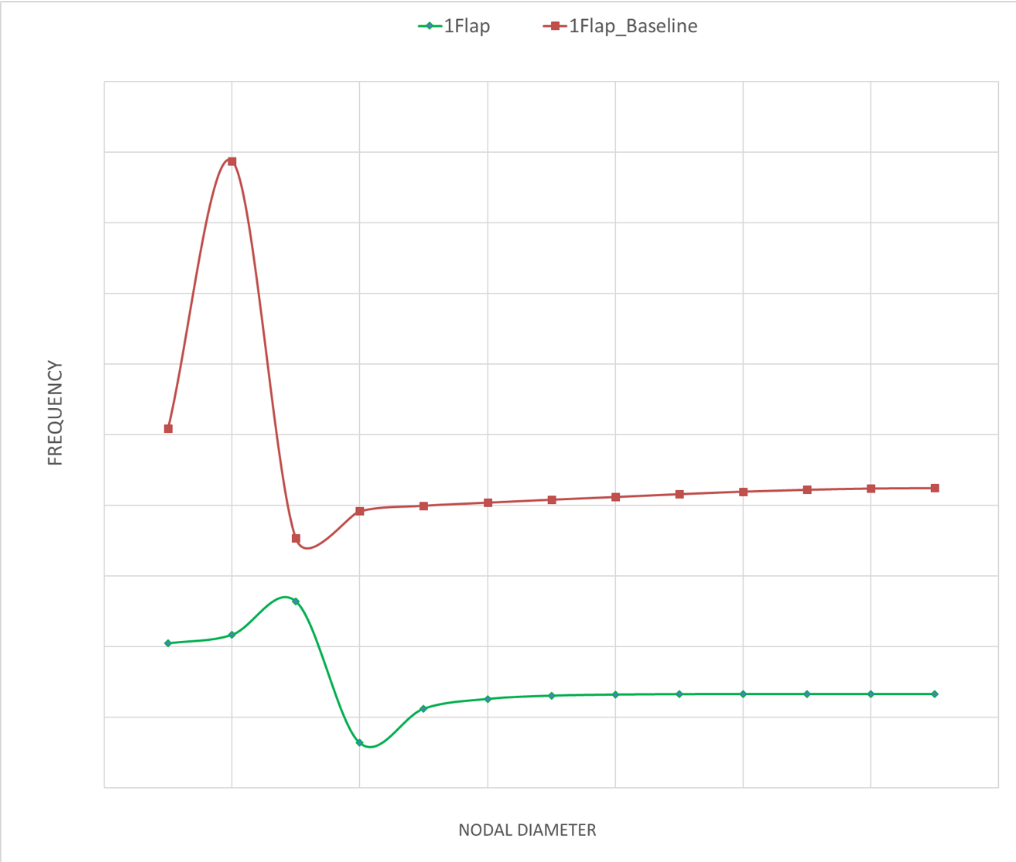

Figure 6.19: FREND Diagram of 1Flap mode, compared between Baseline and Mistuned model

AMM method and, by consequence, of AMMIS in-house tool.

6.7.2 Mistuned Flutter Results

The use of Autoflutter software tool allows the integration of analytical methods seen in Chapter 4 within a user-friendly interface that is currently in use for all company aeromechanical simulations. In fact, there is a specific section of the software dedicate to mistuned sectors analysis, that can be run with a very similar procedure with respect to the compex all-tuned section. The only differences form a user point of view are to be accounted to the complete distinction of files between tuned blade 0 and mistuned blade 1:

- Eigenvalues for Blade 0 and Blade 1
- Eigenvectors for Blade 0 and Blade 1

- Nodal Files for Blade 0 and Blade 1
- Mesh report files for Blade 0 and Blade 1
- CFD-FEM conversion files for Blade 0 and Blade 1

The rest of the process follows the same approach that has been described in Chapter 4. From a post-processing point of view, the aerdoamping value computation is performed for both the Blade 0 and Blade 1 separately. This allows the identification of aeromechanical instabilities on specific part numbers, rather than the overall system, which can be very useful to better investigate why results outcome is not the expected one (in case of residual instabilities for a single component). In spite the single blade aerodamping value constitutes a very useful simulation parameter, the whole system Flutter phenomenon is better described by a single variable. For this reason, the tool applies the superposition effect between Blade 0 and Blade 1 in order to compute the overall aeroplot.
The results of the mistuned sector simulation, performed in Take-Off Conditions, are herein shown.

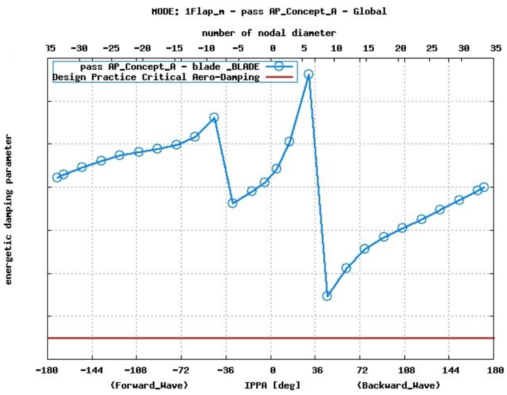

Figure 6.20: Overall Aeroplot of 1Flap mode for Mistuned sector in TO Conditions

Figure 6.7.2 and Figure 6.7.2 shows the aeromechanical analysis results for mode 1Flap, which constitutes the most important objective of this project. By comparing the values shown in Figure 6.7.2 and Figure 6.7.2 and the ones reported for the BS model in Figure 6.4.2, one can notice that the minimum aerodamping value has shift to the upper zone with respect to the threshold, which proves that the mistuning technology introduction has effectively stabilized mode 1Flap from Flutter phenomenon occurrence.

As far as the 1EW and 1EW2 modes are concerned, it is important to highlight the mode has stayed stable with respect to the results shown in Figure 6.4.2. This means that, even though the project developed has focused more its attention on Flapwise mode, the Edgewise has not undergone any decrease in aerodamping values from Baseline to

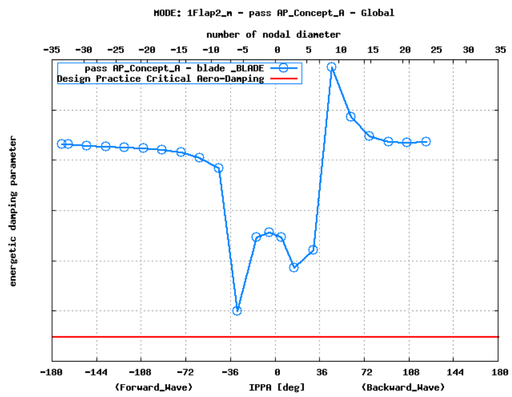

Figure 6.21: Overall Aeroplot of 1Flap2 mode for Mistuned sector in TO Conditions

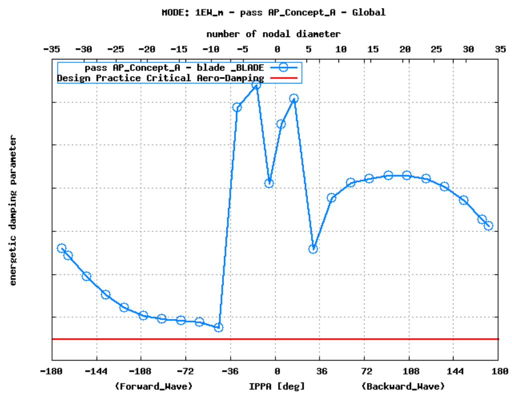

Figure 6.22: Overall Aeroplot of 1EW mode for Mistuned sector in TO Conditions

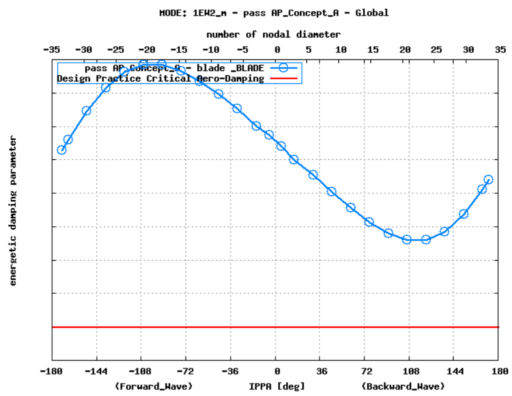

Figure 6.23: Overall Aeroplot of 1EW2 mode for Mistuned sector in TO Conditions

Mistuned system. This fact proves the increased reliability of AMM method: even though this does not constitute a general rule, the improvement of the aeroelastic conditions on one modal family has not worsened the stability of other modeshapes.

Chapter 7

Conclusions

Thw work that has been presented within this report has highlighted the great potentialities of the mistuning technology in the aerospace field, and more specifically in the design of Low Pressure Turbine Modules. Nevertheless, it is important to keep in mind the major goals of this work to have a better understanding of the provided results. Despite both literature studies [45] [15] [16] [24] [14] [26] and company directed studies [11] [20] [28] have proved the reliabile befeficial effects of mistuning against aeromechanical instability, this project aimed at a complete integration between the need providing a ΔM and the various mechanical design constraints being part of the general turbofan turbines' features. The work has not only confirmed the results that had been shown in past company studies [11] [20], but there a great possibilities for a complete use of the technology in the aeronautics field. Since the goal of the aviation industry is the continuous savings in terms of fuel consumption and polluting emissions, the mistuning technology may be very helpful in keep instabilities low while attempting an overall components mass reduction, which is among the main causes of flutter phenomena.
On the other hand, it is important to highlight that the method has various limits, hence reducing its widespread application. First of all, the goodness of results has been based on initial data that are representative of the engine taken into account. The eigenvectors, together with aerodynamic field properties, change stage by stage, module by module, engine by engine. This great variety and unpredictable nature of factors make the mistuning technology difficult to be applied in all aviation engines. Moreover, one of the key strength of the work herein presented is the handling of Shrouded blades: Shroud features in Bladed components, despite having a very specific role within the engine functioning, are separated from the gas flow. Therefore, the possibility of modifying dimensions in areas that are not concerned by the flow-path incredibly reduces the non-linearity of the design problem: adding mass on the tip of the blade hardly impacts the aerodynamic performance of the profile since the Airfoils are not involved in the modification process. This leads to a very important consideration when attempting the introduction of this technology within other engine modules. Various engine bladed components are, in

fact, un-shrouded components. This design characteristics is more than common within Compressor (both LPC and HPC) as well as HPT modules. The lack of a component feature at high radial location leads to great difficulties in case system modes (such as 1Flap or 1EW) were to be stabilized by means of mistuning. Two options, both difficult to apply, would be possible:

1. Modifying Airfoil profiles in order to increase/reduce mass according to a mistuning pattern. This solution adds great non-linearity components to the design procedure since the aerodynamic performance would be impacted by this approach and the process would have to be started over up to a point where performance and mistuning stabilization reach convergence

2. Adding/removing mass at the hub level of the component. System modes are much more sensible to mass increase/reduction at high radial locations. This is why the stabilization of system modes by means of mass additions/removal at the hub would lead to an unacceptable increase in the overall engine mass, which would highly impact the global efficiency of the system.

By going back to the work that has been conducted, it is important to underline that the overall validation process is far to be over. Any change in dimensions, when aeronautical components are concerned, requires a big effort to reach validation according to aviation rules. This is why the mistuned component that has been designed would require a set of simulations in order to cover the validation process. Therefore, the first step of future works would be further investigate the impact of mistuning from a fatigue point of view up to the generation of Goodman tools. It is worth mentioning that the calculations performed on the BS model would have very limited validity, especially when aeronautical components are taken into account. For example, by loooking at the Campbell Diagram of both BS and Mistuned model, one can notice that a further crossing (between 1Flap and a secondary EO) is present in the Mistuned model. It would be necessary, as well as interesting, investigating the impact of this crossing in the fatigue validation of the component.
As manufacturing technologies continue to develop (e.g. by looking at the Additive Manufacturing improvements), it will be interesting to understand how these may influence the easyness of introducing mistuning within engine module. For example, among the various methods that have been analysed during the work (see Chapter 6), Concept C is among the ones that sets the most interest, since it allows the perfect integration of ΔM needs with various mechanical constraints. Besides, although due to time limitation this work has not included the analysis of further concepts, it will be interesting to simulate the aeromechanical behaviour of the multiple concepts that have been suggested within Chapter 6. Together with the repetition of aeromechanical simulations for different models, further studies require the definition of new assembly procedures in order to make sure the designed pattern is respected. Among the techniques to avoid

mis-assembling, great attention can be focused on the creation of a *Murphy Proof*, i.e. a specific feature embedded in the blade components that would make the assembly of a wrong pattern impossible. Together with the development of new manufacturing and assembly strategies, the integration of the technology in the aviation market cannot lack the development of specific experimental methodologies that can investigate the dynamic behaviour of mistuned sectors. Since the experimental test campaign is a key part of the validation process, especially when aviation engines are concerned, it is important to set specifically developed procedures for mistuned rotors, similarly to what has been done for the analytical simulations with the Mistuning section within Autoflutter.
The mistuning technology introduction can be easily compared to puzzle game that the aviation industry is currently playing. At the current stage, despite a lot needs to be done, significant steps have been completed to allow its integration within engines, and its future development can be a key factor to allow further mass decrease and efficiency improvement in the aviation propulsion field, thus allowing the sustainable growth of the aviation market.

Bibliography

[1] Boeing finishes tests fopr genx engine.

[2] Development of aviation technology.

[3] Fuel economy in aircraft.

[4] How does an engine work.

[5] Lift(force).

[6] Turbofan.

[7] Turbojet.

[8] Turbprop.

[9] Barry Bangert and Ralph Hawkins. Aircraft engine reliability business model, November 4 2003. US Patent 6,643,570.

[10] Fabio Bellacicco. Stabilizzazione di uno stadio di lpt bladed-disk in presenza della condizione di instabilità a flutter mediante mistuning intenzionale, 2016.

[11] Fabio Bellacicco. Stabilizzazione di uno stadio di lpt bladed-disk in presenza della condizione di instabilità a flutter mediante mistuning intenzionale, 2016.

[12] Ernesto Benini and Stefano Giacometti. Design, manufacturing and operation of a small turbojet-engine for research purposes. *Applied Energy*, 84(11):1102–1116, 2007.

[13] Andrea Bray. Interazione fluido-struttura in turbine aeronautiche di bassa pressione, 2018.

[14] MS Campobasso and MB Giles. Flutter and forced response of mistuned turbomachinery. Technical report, Unspecified, 2000.

[15] MS Campobasso and MB Giles. Flutter and forced response of mistuned turbomachinery. Technical report, Unspecified, 2000.

[16] Matthew P Castanier and Christophe Pierre. Modeling and analysis of mistuned bladed disk vibration: current status and emerging directions. *Journal of Propulsion and Power*, 22(2):384–396, 2006.

[17] Lee Chapman. Transport and climate change: a review. *Journal of transport geography*, 15(5):354–367, 2007.

[18] Lingen Chen, Ning Ni, Gang Cheng, Fengrui Sun, and Chih Wu. Performance analysis for a real closed regenerated brayton cycle via methods of finite-time thermodynamics. *International journal of ambient energy*, 20(2):95–104, 1999.

[19] Lingen Chen, Fengrui Sun, Chih Wu, and RL Kiang. Theoretical analysis of the performance of a regenerative closed brayton cycle with internal irreversibilities. *Energy Conversion and Management*, 38(9):871–877, 1997.

[20] Marco Ciferri. Riduzione modale applicata alla tecnica del mistuning intenzionale per stabilizzare i rotori di turbina in presenza di flutter, 2015.

[21] AR Collar. The expanding domain of aeroelasticity. *The Aeronautical Journal*, 50(428):613–636, 1946.

[22] BD Coller and PA Chamara. Structural non-linearities and the nature of the classic flutter instability. *Journal of Sound and Vibration*, 277(4-5):711–739, 2004.

[23] Simone Concas. Static analysis of low pressure turbine stages:tool development, 2018.

[24] Roque Corral and Carlos Martel. Mistuning effects on flutter margin. 2012.

[25] Dimitri Franz et al. Master thesis: Mistuned flutter analysis of strongly coupled bladed disks in conjunction with reduced order modeling. 2017.

[26] Zhi Zhong Fu and Yan Rong Wang. Mistuning and structural coupling effects on flutter of turbomachinery blades. In *Structural Engineering, Vibration and Aerospace Engineering*, volume 482 of *Applied Mechanics and Materials*, pages 311–314. Trans Tech Publications, 3 2014.

[27] Yuan Cheng Fung. *An introduction to the theory of aeroelasticity*. Courier Dover Publications, 2008.

[28] Matteo Furfaro. Stabilizzazione di rotori in presenza di fenomeni aeroelastici critici per mezzo del mistuning intenzionale, 2014.

[29] Clive Hart. *The prehistory of flight*. University of California Press Berkeley, 1985.

[30] Sighard F Hoerner and Henry V Borst. Fluid-dynamic lift, practical information on aerodynamic and hydrodynamic lift. Technical report, BORST (HENRY V) AND ASSOCIATES WAYNE PA, 1975.

[31] Walter C Hurty. Dynamic analysis of structural systems using component modes. *AIAA journal*, 3(4):678–685, 1965.

[32] Gerhard Kahl. Aeroelastic effects of mistuning and coupling in turbomachinery bladings. 2002.

[33] Robert E Kielb, Drew M Feiner, Jerry H Griffin, and Tomokazu Miyakozawa. Flutter of mistuned bladed disks and blisks with aerodynamic and fmm structural coupling. In *ASME Turbo Expo 2004: Power for Land, Sea, and Air*, pages 573–579. American Society of Mechanical Engineers, 2004.

[34] Feng Liu and William A Sirignano. Turbojet and turbofan engine performance increases through turbine burners. *Journal of propulsion and power*, 17(3):695–705, 2001.

[35] Jack D Mattingly, William H Heiser, and David T Pratt. *Aircraft engine design*. American Institute of Aeronautics and Astronautics, 2002.

[36] Marija Nikolic. *New insights into the blade mistuning problem*. PhD thesis, University of London, 2007.

[37] Christophe Pierre and Durbha V Murthy. Aeroelastic modal characteristics of mistuned blade assemblies-mode localization and loss of eigenstructure. *AIAA journal*, 30(10):2483–2496, 1992.

[38] Davide Prino. Automatic preliminary assessment of the mechanical response of lpt stages, 2018.

[39] Amedeo Ramieri. Analisi e comparazione di diversi modelli di contatto all'interlocking per rotori di turbine di bassa pressione, 2017.

[40] Jan Christopher Schilling. Turbofan engine assembly and method of assembling same, February 8 2011. US Patent 7,882,693.

[41] AV Srinivasan. Flutter and resonant vibration characteristics of engine blades. *Journal of engineering for gas turbines and power*, 119(4):742–775, 1997.

[42] S Tatzko, L Panning Von Scheidt, and J Wallaschek. Forced response of turbine bladings with alternating mistuning and friction damper coupling. In *M07 Colloque EUROMECH Coupling and Nonlinear interactions in Rotating Machinery*. AFM, Association Française de Mécanique, 2015.

[43] Egbert Torenbeek. *Synthesis of subsonic airplane design: an introduction to the preliminary design of subsonic general aviation and transport aircraft, with emphasis on layout, aerodynamic design, propulsion and performance*. Springer Science & Business Media, 2013.

[44] Irwin E Treager and Irwin E Treagan. *Aircraft gas turbine engine technology*, volume 1995. McGraw-Hill New York, USA, 1979.

[45] S-T Wei and C Pierre. Localization phenomena in mistuned assemblies with cyclic symmetry part i: free vibrations. *Journal of Vibration, Acoustics, Stress, and Reliability in Design*, 110(4):429–438, 1988.

[46] Terry A Weisshaar. Aeroelasticity, an introduction to fundamental problems-with an historical perspective, examples and homework problems, 2012.

[47] RA Zimbrick and JL Colehour. Investigation of very high bypass ratio engines for subsonic transports. *Journal of Propulsion and Power*, 6(4):490–496, 1990.